ENHANCED RESERVOIR MANAGEMENT WITH MULTIPLE REALIZATIONS

by

George de Barros

A thesis submitted in partial fulfillment of the requirements for the degree of

Doctor of Philosophy

in

Mining Engineering

Department of Civil and Environmental Engineering

University of Alberta

Abstract

A numerical reservoir model is the result of studies whose main objective is to describe the dynamic behaviour of a hydrocarbon reservoir for predicting its future performance under different development and production strategies. Reservoir models are built with uncertain parameters. The available data are widely spaced, at large scale and contain error. Thus, predictions based on these models are also uncertain. Understanding the uncertainties related to the reservoir is crucial for making development and management decisions throughout the lifetime of reservoir production.

Conventionally, decisions in hydrocarbon field development are based on a single reference case. The reference case represents the best model with the appropriate set of input parameters for predicting future reservoir performance. However, this model is only one outcome of a large ensemble of possible models describing the reservoir. Making decisions based on one reference case disregards the geological uncertainty. The complexity of many response variables requires managing multiple realizations to improve the consistency and accuracy of reservoir models.

A methodology to facilitate the transfer of subsurface uncertainty through reservoir management is developed and demonstrated in this thesis, reaching up to 5% of improvement in the economic performance of projects. The ensemble of realizations must be used in the calculation of measures of performance and in optimization, helping the reservoir team make decisions for maximizing the value of the reservoir project.

The number of realizations could be large and the analysis of results is largely automated; however, human inspection is still necessary for quality control. Tools are required for processing and analyzing the ensemble of realizations qualitatively and productively. Since all realizations should be considered in reservoir management, a visualization methodology is developed to facilitate the understanding of the space of uncertainty. Methods combining the distance between realizations and animations are considered.

The computational requirements for history matching and flow simulation is an often mentioned reason to avoid dealing with all realizations all the time. Computational performance has grown exponentially over the past 30 years through faster processors, multiple cores, parallelism, and GPUs, supporting the premise of managing multiple realizations. Moreover, developments in ensemble-based history matching techniques encourage the use of a large number of reservoir models. An alternative approach to integrating production data into the geological modeling workflow is also developed. The geological consistency is preserved through an ensemble of reservoir models conditioned to the available static and dynamic data.

The impact of considering all realizations in the decision-making process is demonstrated with a realistic case study. The improvement of the production revenue considering all realizations is significant, reaching more than $100 million, and supports the statement of this research.

To the memory of my parents, ***Geraldo*** *and* ***Lucia****. Their memories continue to regulate my life.*

To my beloved wife, ***Maria Anisia****, for her support and unconditional love*

and

Moustache

Acknowledgements

I would like to express my gratitude to my supervisor Dr. Clayton V. Deutsch for his guidance, patience, and invaluable advice in my research. This thesis would not have been possible without his constant support and encouragement throughout the dissertation journey.

I would like to acknowledge the Petrobras for providing financial and technical support for this research at the University of Alberta, especially my manager José Fernando Rosalba. My special thanks to the operational support of Vera Lucia de Oliveira Silva and her coworkers during my life in Canada.

I am extremely grateful to Alice da Silva for all support given to students at the University of Alberta. In addition, I would like to thanks all CCG colleagues for providing an enjoyable research environment and expanding my geostatistical knowledge beyond the classroom.

Acknowledgement is also due to Marcelo da Costa Monteiro for our initial discussions about reservoir uncertainty analysis. I am extremely grateful to my Petrobras coworkers for the helpful discussions, especially Paulo Paraízo, Emílio Coutinho and Alexandre Emerick. I would also like to thank to my friends at Cenpes, in especial to Alexandre Augusto, Camila Faria, Eduardo Roemers, Eldues Martins, Marcia Fillardi and Thais Empinotti.

I would like to thank my brother Marcelo for his support and patience. During the last four years, he has been my helper in Brazil, solving the daily life troubles.

My special thanks to all great new Brazilian friends made in Canada: Felipe Pinto and Cintia, Diogo and Marina, Dhaniel and Ana, Felipe Saliba and Gabi, Dudu and Leila, Victor and Daniele, Rafael and Kadija, Felipe Cestari. You people have made us to feel like at home during these last four long years.

Finally, this challenging adventure would not have been possible without the love and support of my wife Maria Anisia. In joy and in sorrow, in sickness and health, in good and bad times, as well as in warm and cold, we always will walk side by side!

Table of Contents

List of Tables

List of Figures

List of Abbreviations

Abbreviation	Description
AHM	assisted history matching
BHP	bottom-hole pressure
DKM	distance kernel method
DoE	design of experiments
ED	experimental design
EnKF	ensemble Kalman filter
FLOPS	floating-point operations per second
FMM	fast-marching method
GPU	graphic processing unit
GSLIB	geostatistical software library
HCPV	hydrocarbon pore volume
HCPVo	hydrocarbon pore volume for oil
HM	history matching
IRR	internal rate of return
MCMC	Markov chain Monte Carlo
MDS	multidimensional scaling
NPV	net present value
NTG	net-to-gross
OOIP	original oil in place
PR	production revenue

RI	relative improvement
RML	randomized maximum likelihood
RQP	reservoir quality property
RSM	response surface model
SA	simulated annealing
SGS	sequential Gaussian simulation
SIS	sequential indicator simulation
VOI	value of information
WTA	well-test analysis

Chapter 1

Introduction

Hydrocarbon projects are capital intensive. The combination of large investment and high uncertainty makes these projects high risk, requiring the analysis and evaluation of production and economic scenarios.

The geological processes that generate the petrophysical properties of a reservoir are relatively well understood. However, despite the fact that geological phenomena are not random, reservoir conditions could never be predicted exactly due to limited available data and no access to initial or boundary conditions. Numerical models are created in an attempt to reproduce the reservoir conditions and to provide important input to planning and decision-making.

Well tests, production data, seismic data, and geological knowledge are all used to complement direct well log and core measurements, to build accurate reservoir models and to characterize the uncertainty. Understanding the uncertainties related to the reservoir is crucial for making development and management decisions through the lifetime of the reservoir production. The suitability of the reservoir models is validated by their ability to accurately predict future flow performance under different conditions (Pyrcz and Deutsch, 2014).

Geostatistics is commonly used to predict rock properties away from known well data. Geostatistical techniques quantify the uncertainty through a probabilistic approach. Multiple equally probable realizations are generated by geostatistical simulation techniques in order to characterize the geological heterogeneity and uncertainty. The response of these realizations could be combined into a model of uncertainty. Dealing with multiple realizations provides an assessment of the space of uncertainty to be used in the decision-making processes.

Models can be used to obtain long-term development plans. The selection of appropriate model or combination of models is fundamental for the optimal depletion strategy for a given reservoir asset.

1.1 – Managing Uncertainty in Reservoir Forecasting

There is a need to determine how much hydrocarbon can be extracted from a reservoir to determine the most profitable path forward. After starting production, the reservoir team must analyze the production development in order to maintain maximal oil recovery and profitability.

Reservoir flow simulation is a tool for the management of hydrocarbon reservoirs that can aid understanding of flow and the recovery process for a particular reservoir. This is useful for sensitivity and uncertainty assessments, to predict reservoir performance under different operating conditions, and for optimizing reservoir performance (Cardoso, 2009).

In order to improve the reliability of reservoir predictions, the information available from historical field production data (e.g. pressures and production rates) should be incorporated into the reservoir models, in a process called history matching (HM). Since HM is an optimization problem, hundreds or possibly thousands of flow simulations may be required to find a match (Thiele et al., 2010).

Flow simulation and history matching processes may be very time consuming. The detailed 3-D reservoir simulation models can have a large number of cells, multi segmented wells, local grid refinements causing the simulation of a single model to take hours of CPU time.

A common approach is to apply a less expensive transfer function on all realizations, ranking them according their responses, then selecting a few realizations to be processed through the flow simulator. There is no unique ranking method considering geological models and multiple response variables. However, a simple and widely used ranking measure is the original oil in place (OOIP) for each realization (Corre et al., 2000; Steagall and Schiozer, 2001; Campozana et al., 2007; Gross and Honarkhah, 2011).

This well-established approach usually selects one model with a low response, one model with an average response and one model with a high response, corresponding to the so-called

P10, P50 and P90 models. Instead of considering all realizations, these three models are submitted through the flow simulator.

1.2 – Problem Statement

According to Sharifi et al (2014) and Gorbovskaia (2017), selecting few realizations based on some properties, such as OOIP, does not adequately reflect the influence of uncertain geological parameters on production rate and recovery factor. According to Pyrcz and Deutsch (2014) and Deutsch (2015), those methodologies that use a reduced number of realizations yield an incomplete assessment of uncertainty. This leads to inaccurate reservoir production forecasts and the resources may be underestimated or overestimated (Figure 1.1).

Given the imperfections of ranking, three realizations (P10, P50 and P90) will not span the uncertainty model after the transfer function (Pyrcz and Deutsch, 2014). Ranking should be applied more carefully to select models. A P10 realization may have P90 values at some locations, P50 at others and so on. The P-value of a realization must be considered as a global parameter with little local meaning. Since the relationship between the response of the simple function and the full simulation is not linear, selecting too few realizations from the reservoir model may result in misleading forecasts.

Ballin (1992) recommends that flow simulation must be run for a large number of reservoir realizations in order to transfer geological uncertainty to reservoir performance evaluation. da Cruz (2000) presents the same idea; each geostatistical realization must be submitted to the flow simulator for a robust approach of transferring geological uncertainty to the production forecast. However, one of the main reasons to avoid managing multiple realizations in flow simulation is the excessive computational requirements for performing history matching for each reservoir model.

With recent advances in computer science and hardware, the use of multiple geostatistical models to improve production forecasts should be more popular in reservoir engineering (Figure 1.2). Reservoir simulation on massively parallel computers can reduce simulation times over three orders of magnitude (Beckner et al., 2015). The magnitude of the real time speedup is

impressive with parallel computing. Multithreaded shared memory architecture allows flexibility in parallelizing various algorithms in different ways (Lu et al., 2008). As multi-core CPUs for computers become common, parallel computing provides a viable and flexible option to handle complex reservoir simulation models with significant run time reductions.

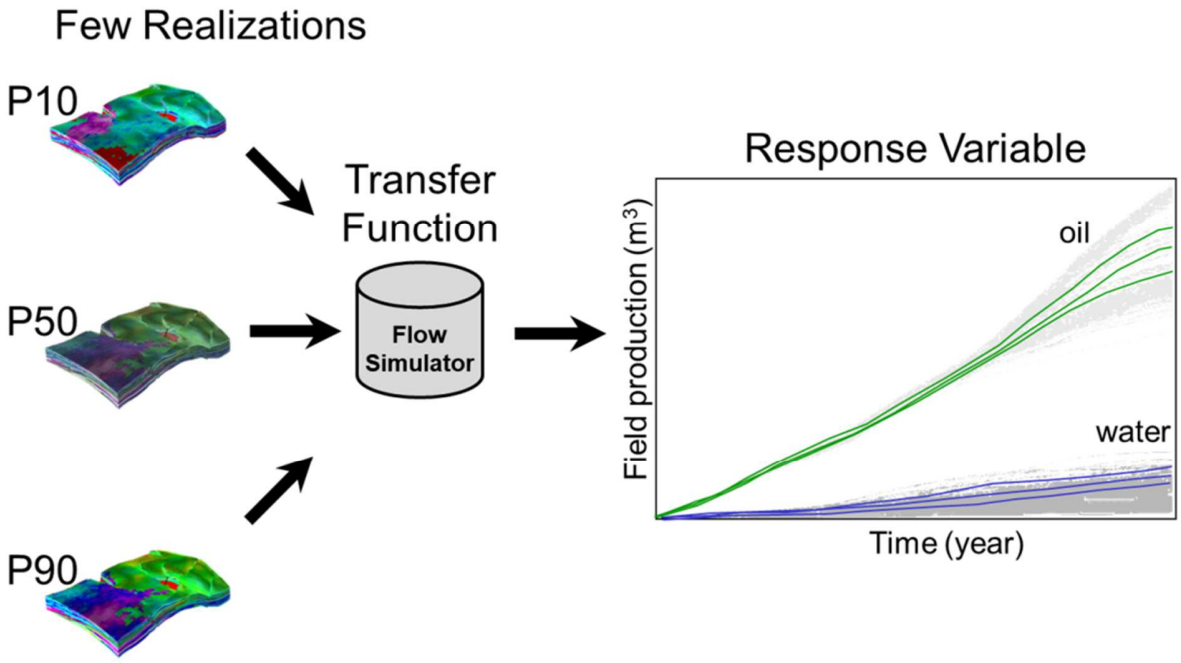

Figure 1.1: Reservoir responses based on just a few realizations may correspond to unrealistic production forecasts.

1.3 – Thesis Statement

Development of methodologies to facilitate the transfer of subsurface uncertainty through reservoir management will improve the consistency and accuracy of reservoir models and their ability to reliably forecast reservoir performance.

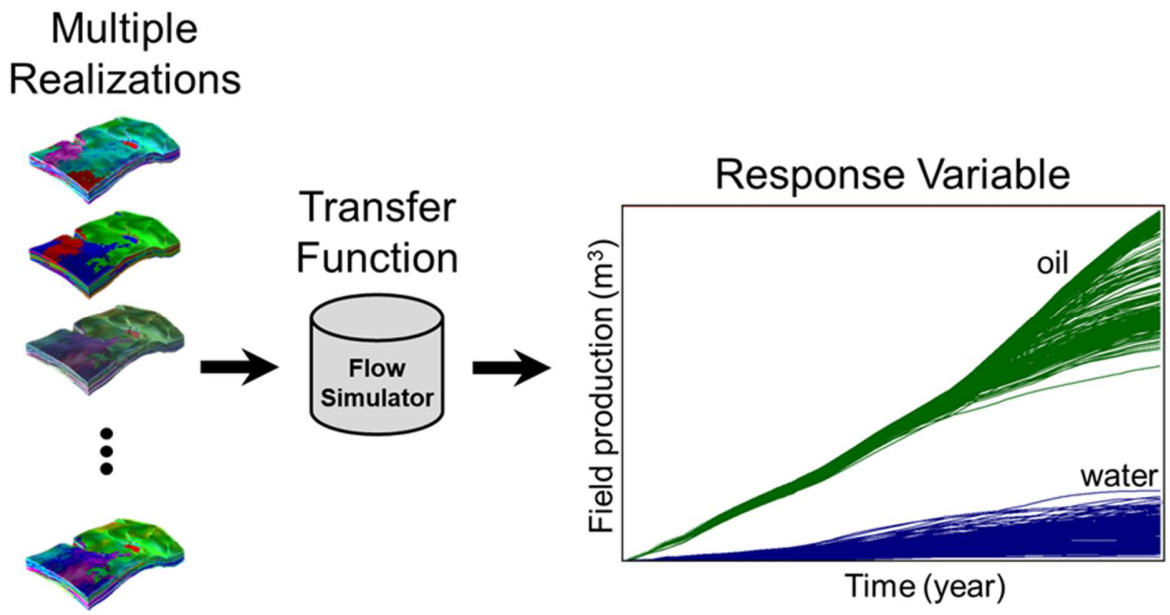

Figure 1.2: Multiple geostatistical realizations provide an assessment of geological uncertainty in reservoir modeling.

1.4 – Dissertation Outline

This thesis focuses on understanding and managing the uncertainty throughout the lifecycle of a reservoir. The goal is to improve the consistency of reservoir models and the reliability of reservoir predictions by transferring the complete geological uncertainty through reservoir management. Eight chapters are presented to address this goal: **Chapter 1** presents an overview of the problem setting with a brief description of the current state of geological uncertainty assessment in reservoir management. The motivations and the thesis statement are also provided in this chapter. **Chapter 2** provides a background for the developments of this thesis as well as a literature review. **Chapter 3** describes the methodology, discussing the correct paradigm for uncertainty management. **Chapter 4** presents a reasoned view to the correct management of multiple realizations, in terms of response evaluation and visualization. **Chapter 5** presents a discussion about computational resources required for managing multiple realizations as well as the historical perspective and the computational trends in reservoir characterization. **Chapter 6** presents methodologies for how multiple realizations can be processed through history

matching, presenting a data integration in geostatistical simulation by rejection sampling. The proposed methodology is validated by a real case study in **Chapter 7**. The goal is to evaluate the performance of the proposed model relative to the conventional approach. The last **Chapter 8** wraps up the thesis with conclusions and future work. A detailed description of well test analysis is provided in **Appendix A**. A description of developed codes is provided in **Appendix B**.

Chapter 2

Background and Literature Review

The reservoir model is the result of studies whose main objective is to understand and describe the dynamic behavior of a hydrocarbon reservoir in order to predict its future performance under different development and production strategies. Geostatistical reservoir modeling is used for creating detailed numerical 3-D geological models. These models simultaneously integrate available geological, geophysical and engineering data with varying degrees of resolution, quality and certainty (Pyrcz and Deutsch, 2014).

A fundamental principle of geostatistical simulation is to generate multiple realizations in order to cover a large set of cases and capture a reasonable measure of uncertainty in model parameters. The main sources of uncertainty in reservoir characterization are related to: 1) subsurface structures - such as stratigraphic surfaces and faults; 2) geological properties - such as facies including horizontal barriers and conduits; 3) petrophysical properties, such as porosity, permeability, water saturation and shale volume; and 4) dynamic properties, such as temperature, pressure and production rate data.

Although many realizations should be generated to provide a stable assessment of uncertainty, the high computational cost of running flow simulation and the iterative nature of history matching restricts the number of simulation models that can be used for production predictions. Processing all realizations through a flow simulation may take a very long computational time. The common approach used in industry is, according to some criteria, select a few realizations from the initial realizations and then perform flow simulation on these few realizations (Ballin et al., 1992; Idrobo et al., 2000; Ani et al., 2016; Thiele and Batycky, 2016; Meira et al., 2017).

2.1 – Literature Review

Geostatistical simulation plays an important role in geostatistical modeling. The technique is used to build models that reproduce the characteristics of the spatial variable of interest as represented by the conditioning data (Rossi and Deutsch, 2013). Multiple alternative and equiprobable models (realizations) are generated by geostatistical simulation in order to provide an assessment of the space of uncertainty. Simulation is well established and widely used for petroleum reservoir modeling (Journel, 1986, 1989; Isaaks and Srivastava, 1989; Goovaerts, 1997; Deutsch and Journel, 1998; Caers, 2011; Chiles and Delfiner, 2012; Pyrcz and Deutsch, 2014).

A fundamental principle of simulation is to consider many realizations (Deutsch, 2015). In reservoir modeling, multiple realizations are simulated in order to cover a large set of cases and capture the uncertainty of the model parameters, such as expected mean values, variance, spatial dependence of each geological attribute and interdependence among the attributes (da Cruz, 2000).

Considering uncertainty in the input parameters may be important. Parameter uncertainty is assessed by simulating realizations of all of the modeling parameters, including gross volume uncertainty, facies proportion uncertainty, histogram uncertainty, variogram uncertainty and multivariate relationship uncertainty (Deutsch, 2015).

2.2 – Ranking Realizations

Different approaches have been used to handle multiple realizations (da Cruz, 2000; Pyrcz and Deutsch, 2014). Ballin et al (1992) proposed the concept of ranking for the first time. The authors presented an approach to analyze the problem of transferring uncertainty in the geological model through the flow simulation model. Each reservoir realization is ranked using what they called a Fast Simulation, which is coarsening simple simulations, rather than Comprehensive Flow Simulations.

Many ranking methods have been proposed in the literature considering static and dynamic approaches. Static-based ranking methods are those methods that rank realizations on basis of

the static properties of the underlying realization such as porosity or permeability. Static ranking measures include OOIP, average petrophysical properties, and effective connected pore volume. Dynamic-based ranking methods are those methods that are based on fluid flow.

2.2.1 – Static-based ranking methods

Alabert and Modot (1992) point out the importance of comparing models by measuring connectivity. Gomez-Hernandez and Carrera (1994) proposed a linear approximation of the flow equation to rank realizations. According to the authors, a better approach would be to rank the realizations of the parameters controlling fluid flow and then solve the flow equation.

Hird and Durbrule (1995) present an approach of connectivity calculation by incorporating dynamic data. Ranking reservoir realizations according to the corresponding reservoir characteristics are developed as an application of their technique.

Deutsch and Srinivasan (1996) review the methods of ranking geostatistical reservoir models. The use of loss functions is presented as well as the expected loss to measure the value of ranking realizations. According to the authors, there is no unique ranking index since there are multiple flow response variables. Moreover, the use of fast simulation techniques, like streamline simulation could be used as a ranking method.

Saad et al (1996) introduce ranking of geostatistical models based on tracer production data. Their results indicate that ranking based on tracer breakthrough time and ranking based on cumulative oil recovery are not correlated.

Sandsdalen et al (1996) quantify the effect of the uncertainty given by the variability of the observed petrophysics and facies data on the dynamic behavior of the reservoir. A higher hierarchical model with two individual levels of uncertainty is used in order to generate equiprobable realizations.

Idrobo et al (2000) present a connectivity criterion based on streamline time-of-flight for ranking geostatistical realizations. The proposed approach provides a method for computing volumetric sweep efficiency for arbitrary heterogeneity and well configuration. According to the

author, this method can be applied for ranking stochastic reservoir models since there is a strong correlation between the connectivity criterion and waterflood recovery.

da Cruz et al (2004) introduce the concept of a quality map, a representation of the reservoir responses and their uncertainties of each stochastic realization. The quality maps of all realizations provide a distribution of quality values and for each cell of the grid. The quality concept may be applied to compare reservoirs, to rank realizations and to incorporate reservoir characterization uncertainty into decision-making with fewer full-field simulation runs.

Connectivity measures for ranking and selecting reservoir realizations is also presented in McLennan and Deutsch (2005). The authors describe static connectivity measures tailored to heavy oil recovery processes. Flow simulation is performed on many geostatistical realizations to calibrate the ranking measures to production response, allowing an inference in reservoir areas where it is not possible to perform many flow simulations. Yazdi and Jensen (2014) present a static measure based on average harmonic permeability to help rank realizations. The methodology is applied in a steam-assisted gravity drainage (SAGD) model, reaching good correlations with thermal simulation results.

2.2.2 – Dynamic-based ranking methods

Static-based methods may not truly represent the ranking based on actual performance of the reservoir. For example, a reservoir which contains large OOIP but is not well connected will ultimately produce less oil than a reservoir that is well connected but contains less OOIP. Static-based ranking does not guarantee that the selected models will represent the range of uncertainty of the true dynamic performance of the reservoir. A better ranking criterion would be use a method that captures the dynamic connectivity and present a good relationship to oil recovery (Kelkar et al., 2014).

The use of streamline simulation for ranking realizations is presented in Ates et al (2005). The volumetric sweep efficiency parameter is used as a quantitative indicator of connectivity, in order to rank reservoir models and for selecting a few realizations for further processing. The volumetric sweep is a simple performance measure that quantifies the interactions between the uncertainties in the static model with the dynamic flow conditions. The authors combine both

sweep efficiency and OOIP in the process to rank different scenarios. High sweep and high OOIP represent the optimistic scenario, whereas low sweep and low OOIP represent the pessimistic scenario. The most likely scenario presents a medium sweep efficiency and OOIP.

Scheidt and Caers (2009) introduce a technique to select reservoir stochastic models to be evaluated by flow simulation, called the distance kernel method (DKM). The authors propose the concept of dissimilarity distance between reservoir models, which indicates how dissimilar any two models are in terms of their associated response of interest. Flow response models are grouped based on their distances and a few representative realizations per group are selected for full-field simulation, prediction and history-matching purposes.

The ranking method proposed by Sharifi et al (2014) uses the fast-marching method (FMM) to determine the dynamically connected reservoir volume to a given well. A radius of investigation can be calculated as a function of time without running any flow simulation. Comparing with ranking from flow simulation, a larger number of reservoir models can be ranked in order to span the range of dynamic uncertainty.

Recently, Fei et al. (2016) discuss a novel way to choose optimal models from multiple realizations. A two-way cluster analysis is presented for quantitatively evaluating a grid cell by cell throughout each of the realizations. A connectivity analysis ranks the volume of connected geobodies and a statistical analysis quantitatively identifies the optimal realizations.

Although dynamic ranking shows better correlation with the production responses (Kelkar et al., 2014; Sharifi et al., 2014; Fei et al., 2016), selecting a limited number of models for history matching still leads to the problem of how the uncertainty in dynamic performance are properly captured.

2.2.3 – Experimental design approach

Alternatively to the ranking methods, Experimental Design (ED), also often referred to as Design of Experiments (DoE), has been used in multiple approaches to significantly reduce the number of geological models that must be built and flow simulated to evaluate the reservoir

performance. The principle of the method consists of running a few reservoir simulations by varying all the uncertain parameters simultaneously. The simulation results are then used to fit a simple polynomial Response Surface Model (RSM). The specific response (e.g. cumulative oil production) will then be predicted by RSM to replace the time-consuming fluid flow simulator.

The theory behind experimental design was developed in the 1920s for agricultural applications. An early reference of the technique in petroleum industry is presented by Sawyer et al. (1974), initially using physical experiments. However, there were no further published examples of the methods in oil/gas studies until the end of the 1980s. Computational experiments provide an economical and straightforward method of experimentation (Gupta et al., 2012).

Damsleth et al. (1992) apply the basic concepts of ED to a case study from the North Sea. The basic sensitivities obtained with a minimum number of simulations. The results from the analysis also were used as input to a Monte Carlo simulation. This approach is widely used to propagate uncertainty in input parameters through a performance model (Jensen et al., 2000).

Jones et al. (1997) present an approach to evaluate waterflood development options and to understand the impact of uncertainties in reservoir description. The methodology has been selected the combination of input parameters in order to provide accurate estimates of the effects of individual factors. Based on ED techniques, 800 simulation runs have been reduced to a set of 144, allowing prediction of recovery for any combination of factor settings.

Dejean and Blanc (1999) integrate ED, RSM and Monte Carlo methods to build a simplified model of a process and to estimate the uncertainties on response predictions. The results quantified uncertainties on the reservoir production forecasts conditioned on uncertainties on the reservoir modelling parameters, reducing the computational costs.

Kloosterman et al (2007) apply ED to provide a quantified decision-based plan for minimizing risk in oil reservoirs. ED has been used to eliminate scenarios with negative impact on project economics, to select those that added net present value, and to optimize development plan of reservoir.

Fetel and Caumon (2008) develop a methodology combining ED and RSM, which associates results of both conventional and alternative flow simulations. Although these alternative

simulations do not predict exactly the flow performance, they can rank the reservoir models according to some given criterion, with reduced computational cost. This approach improves the modelling of non-linearities in the reservoir flow response, which are not usually captured while using standard ED and RSM.

Lisboa and Duarte (2010) present a methodology based on ED and RSM including HM. Besides a cumulative production response surface, another one is generated to represent the quality of the HM. Only cases with a good HM are selected as input to the Monte Carlo simulation. Becerra et al (2012) also integrate HM with ED to select representative scenarios, reducing the range of possible models taking into account observed.

2.3 – Current Trends in Reservoir Characterization

The increase in computational power has made it possible routinely running reservoir simulations with millions of grid blocks (Lie et al., 2016).

Up to this point, managing multiple geostatistical models for improving production reservoir forecasts is still a challenge in the petroleum industry due to the computational demands to perform flow simulation and history matching.

However, considering all realizations simultaneously is possible due to the recent advances in computer science. The performance of the computers has been increased five orders of magnitude in the last 20 years (de Barros and Deutsch, 2016; Cao, 2002; Watts, 1997). Computers are more than 100 times faster than they were about ten years ago. Moreover, during the last few years, the emergence of massively parallel computing platforms, such as the GPU architecture, has opened new pathways to efficient parallel processing.

2.3.1 – Parallel Processing

Parallel processing means running a computational process that has been divided into several smaller sections into several processors simultaneously to reduce the computation runtime. The main calculation is divided into several smaller sections that are run separately and simultaneously through a set of threads, or processors, instead of doing the computation using only one CPU. Afterwards, the intermediate results are joined to produce the outcome. The most

important reason for the use of parallel processing in comparison with conventional or serial processing is to increase the solution speed (Mattson 2003).

Figure 2.1 illustrates the differences between serial and parallel computing. In serial computing, a problem is broken into a series of instructions that are executed sequentially, one after another, by a single processor. Only one instruction may execute at any moment in time. In parallel computing, a problem is broken into some parts that can be solved concurrently. Each part is further broken down into a series of instructions that can be executed simultaneously on different processors.

The popularity of parallel reservoir simulation has increased in recent years due to the availability of multicore CPUs and the opportunity for runtime reduction, especially in complex and fractured reservoir models that include large amounts of data (Mohajeri et al., 2018).

The development of shared memory and distributed memory machines in the 1980s intensified the research on parallel reservoir simulation. Scott et al. (1987) present a reservoir simulation approach using parallel computers. Chien et al. (1987) investigate the parallel processing on shared memory computers. They developed a general-purpose reservoir simulator in a multiple vector processor machine, creating several independent tasks in a shared memory environment.

In the early 1990s, black oil and compositional simulators have been developed considering multiprocessors machines (Killough and Bhogosvera, 1991; Killough and Wheller, 1991; Rutledge et al., 1991). Reservoir models over 2 million cells could be run on machines with 65,536 processors, reaching computational speeds in the order of 1 Gigaflops. (Dogru et al., 1999).

Simulators on distributed memory machines gradually moved from research to real field applications using massively parallel simulators in the mid-late 1990s (Shiralkar et al., 1997; Chien et al., 1997; Kilough et al., 1997; Praetor et al., 1997). Problems using one million grid points could be solved in a few minutes of computer time (Kaarstad et al., 1995).

A new generation of reservoir simulator has been developed in the 2000s, using massively parallel computing techniques (Ma and Chen, 2004; Fjerstad et al., 2005; Lu et al., 2008; Batycky et al., 2010).

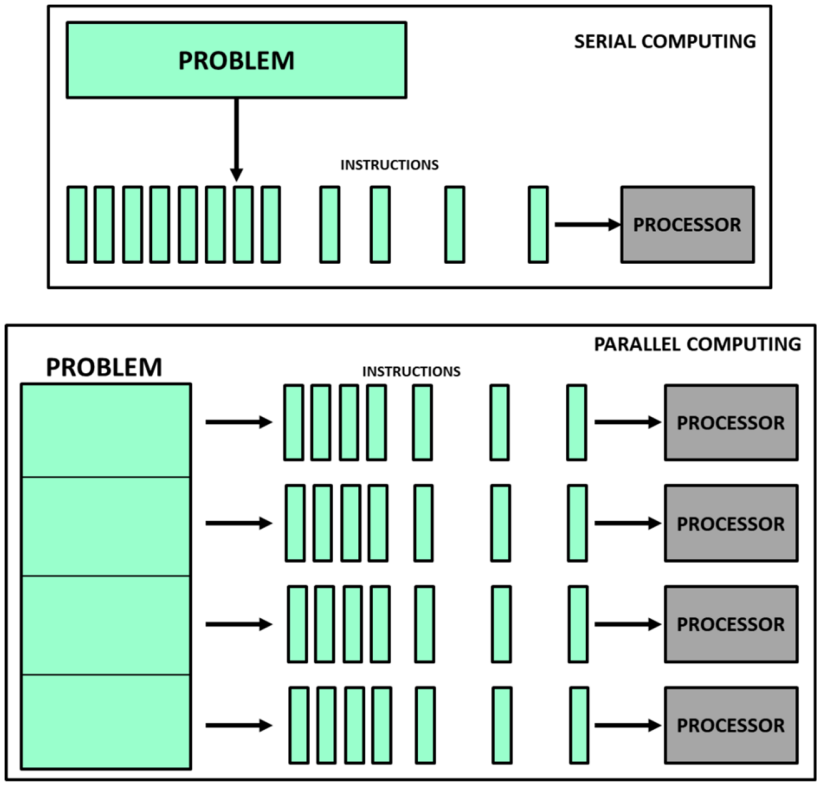

Figure 2.1: Serial and parallel computing differences.

Current studies investigated parallel processing for numerical flow simulation large-scale fields (Tleukhabyluly et al., 2016; Mohajeri et al., 2018); fractured reservoirs (Mesbah et al., 2019) and assisted history matching (Al-Samhan et al., 2017). These recent studies have been achieved speedup ratios up to five times relating to the reference simulations, preserving the accuracy of production responses.

Reservoir simulation on massively parallel computers can reduce simulation times over 3-4 orders of magnitude. The magnitude of the real-time speedup is impressive. Huge gains in the reduction of reservoir management study times are possible. More alternative reservoir management scenarios can be considered, including considering all geological realizations, since computational time is a bottleneck for dealing with multiple reservoir models. Parallelism offers a solution to make computationally intensive methods practical to apply to routine field studies.

2.3.2 – GPU Architecture

Reservoir simulation has evolved together with scientific computer hardware. Advances in reservoir simulation performance have been first limited by the memory of CPU based computer systems (Telishev et al., 2017). Then, simulators have been endowed with the capability to distribute computational processes using multicore architectures. Simulators have been redesigned to share computations between multiple threads, keeping coarse-grained parallelism approach (Zhou et al., 2013).

Graphic processing units (GPU) have been developed as a new scientific computing hardware architecture, exploiting fine-grained parallelism (Khait and Voskov, 2017). GPUs have been used for many parallel applications in addition to their originally intended purpose of graphics processing algorithms (Hawick et al., 2010).

Originally designed to accelerate graphics, GPUs are increasingly used to deal with computationally intensive algorithms. From an architectural perspective, GPUs are very different from traditional CPUs (Figure 2.2). They are devices equipped with hundreds of cores able to handle thousands of threads simultaneously so that a very high level of parallelism can be reached. In addition to the number of cores, GPUs also have significantly greater memory bandwidth.

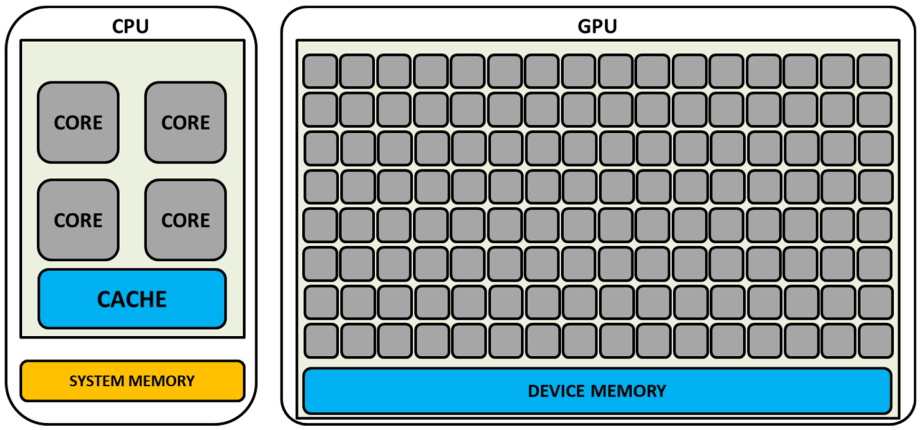

Figure 2.2: CPU and GPU architectures.

The main disadvantage of using GPUs is related with the effort required to code algorithms. Algorithms must be coded to reflect the architecture of these hardware accelerators. Incorporating GPU support into existing codes is difficult and typically requires significant changes in the code and the algorithm (Själander et al., 2014).

The efforts in reservoir simulation are mainly concentrated with employing GPUs to accelerate the solution of linear systems (Esler et al., 2014; Khait and Voskov, 2017). Manea (2015) presents a literature survey concerning to parallel computing and GPU architecture in the context of reservoir simulation. Klie et al. (2011) discuss the application of GPU accelerated computation in reservoir simulation. Esler et al. (2011) report a speedup up to 100 times compared to a single CPU implementation, using a parallel implementation of algebraic multigrid on the GPU architecture as a preconditioner in solving the pressure equation. Bayat and Killough (2013) report GPU speedups ranging from 25 (50,000 grid blocks) to 45 (2 million grid blocks) in reservoir simulation. Recently, GPU architecture has achieved speedups up to 3 times compared to multicore implementation for a 16 million grid blocks model (Manea and Tchelepi, 2017).

Implementation of multicores and GPU architecture in reservoir simulation is relatively recent. Such technologies present great potential for achieving computational speedups making full use of the computational power of the massively parallel architecture. GPU architectures are evolving rapidly compared to the traditional CPU architectures.

2.4 – Summary

- Static-based ranking methods are fast but may not truly represent the performance of the reservoir;
- Dynamic-based ranking methods present a higher correlation with reservoir performance than static-based ranking methods;
- Regardless the methodology, ranking and selecting one or a limited number of models does not span the reservoir uncertainty;
- The novel computer architectures and the recent computational performance allow the industry to consider all realizations simultaneously instead of ranking and selecting a few models.

Chapter 3

Correct Paradigm for Uncertainty Management

Development decisions need to be taken despite an imperfect knowledge of the subsurface. Methodologies to understand and quantify reservoir uncertainties will likely lead to improved production. In addition to the static subsurface uncertainties, there are significant uncertainties in flow parameters (relative permeabilities, fluid properties, original fluid in place distributions, initial reservoir pressure, etc.) and economic parameters (oil price, production/injection costs, etc.).

Uncertainty quantification is not synonymous with decision-making (Bickel and Bratvold, 2007). Making a good decision often requires the assessment of uncertainty. Incorporation of uncertainty analysis is intended to improve the quality of decisions taken to explore and develop hydrocarbon fields.

The single model approach for forecasting remains popular in the industry, despite extensive work on uncertainty, partly because there is a belief that a single best model could be found by adding more physics, increasing the grid resolution, finding a better geological description, or some other improvement (McVay and Dossary, 2014). The search for the best model can lead to excessively long development times and ultimately forcing decisions to be taken without the full benefit of the modeling work (Thiele and Batycky, 2016).

The single-model paradigm cannot be used to quantify uncertainty in the reservoir forecast. A single model is assumed correct because inconsistencies are minimized through post-processing techniques, such as histogram corrections and history matching. The single model approach leads to a danger of overconfidence associated with forecasting and decision-making (Brashear et al, 2001).

This chapter is focused on the importance of uncertainty management in reservoir development planning considering multiple realizations.

3.1 – Uncertainty Reservoir Management

Projects on hydrocarbon fields are capital intensive. They are considered high risk since they are a combination of large capital and high uncertainty. Risk cannot be eliminated due to inherent uncertainties in the reservoir models used to generate production forecasts of the hydrocarbon fields. There is a need to make the best decisions with the appropriate level of technical analysis considering all available data and the inevitable uncertainty.

Understanding the uncertainties related to reservoir production is crucial for making development and management decisions through the lifetime of the reservoir. Deterministic methods produce a single response, with no understanding of uncertainty in reservoir production forecasts. Uncertainties must be evaluated through a probabilistic approach.

The development of a hydrocarbon field has a high degree of uncertainty due to the lack of complete knowledge in required geological, engineering and economic parameters. The oil price forecast is one of the biggest sources of economic uncertainty, but it affects projects equally. The spatial distribution of rock properties such as porosity depends on each reservoir. The values at the well locations are better known while values at the inter-well locations are estimated with some uncertainty.

The major sources of uncertainty in reservoir modeling are associated to the geological properties, such as facies, porosity and permeability; and flow properties, such as fluid composition, saturation and pressure.

Considering reservoir engineering, the uncertainties arising from the lack of complete knowledge about the important variables for the project, such as the number of wells and production units, imply additional costs for its development. This increased cost is often understood using the concept of a loss function. Any underestimation or overestimation produces costs that reduce the return. If there is an underestimation of the true reserves, the increase in costs will be linked to changes not foreseen in the initial project or the incomplete exploitation of the deposit. If the project is based on underestimated production, with the

development of production it will be necessary to make changes in the original project to recover the unplanned volumes. In an extreme case, for example, it may be necessary to employ a new production unit since the original planned unit does not contain the necessary number of producing wells and other necessary facilities. If the correct volume had been initially predicted, a single unit could have been designed with the required number of wells, lowering the final cost.

If, on the other hand, there is an overestimation of the reserves, the increased cost will be due to expenses arising from unnecessary investments. Using the same example, if the expected oil volume is greater than the actual recoverable volume, a larger more expensive unit than required (with a larger number of wells and other facilities) may be employed, reducing the effective project return.

For these reasons, uncertainties are important in all phases of the development of a hydrocarbon field. It is necessary to quantify the uncertainty to understand possible variations around the estimated values for each project.

This thesis is restricted to geological aspects of reservoir characterization and uncertainty management. The degree of uncertainty depends essentially on three factors: 1) the degree of knowledge of analogous models to the studied reservoir (conceptual model); 2) the existing sampling for each relevant property considered; 3) the degree of variability in structural framework and reservoir properties, including facies, porosity and permeability. These factors interact since the characterization of homogeneous reservoirs needs smaller amounts of data than heterogeneous and complex reservoirs.

The geological properties associated with a newly discovered reservoir likely have high uncertainty, mainly due to limited sampling. This is particularly critical since the economic viability is analyzed and the development strategy is designed in this stage. In the later stages of development, uncertainty is also present, especially when drilling costs are very high. This is especially true in deep water offshore reservoirs, located in basins along the continental shelf. Although it is difficult to reduce these uncertainties, they should be quantified and understood through reservoir simulation and economic analysis.

A commonly used reservoir modeling methodology consists of (1) modeling of facies, porosity and permeability for each block of a three-dimensional grid. The fluids contained in the

reservoir are also characterized through PVT analysis (pressure, volume and temperature), relative permeability, capillary pressure, etc.; (2) history matching, when flow simulation results are matched to field observations from the beginning of production to the current date. In this phase, the pressures and rates from the simulation are compared with observed values, both for the whole reservoir and for each active well. When there are differences between the simulation and the observed behavior of the reservoir, local adjustments are made in the reservoir and fluid properties, in order to minimize these differences; and (3) prediction of reservoir behavior, where future hydrocarbon production is forecast together with tuning of the production development plan.

The purpose of reservoir modeling and history matching is not limited to building a model that is consistent with the production data currently available, but one that gives good predictions of its future behavior. Understanding the uncertainties related to reservoir production is crucial for making development and management decisions through the lifetime of the reservoir.

The assessment of uncertainty is based on the probability distributions of all the major reservoir properties. Multiple equiprobable reservoir models are generated by geostatistical simulation techniques in order to characterize the geological heterogeneity and uncertainty. Dealing with multiple realizations provides an assessment of the space of uncertainty to be used in the decision-making processes.

Common current practice in the hydrocarbon industry is applying a simple and fast transfer function over the ensemble of models and ranking them according to the responses (Corre et al., 2000; Campozana et al., 2007; Gross and Honarkhah, 2011). Although there is no unique ranking method, the original oil in place (OOIP) is the most widely used ranking measure (Pyrcz and Deutsch, 2014).

Based on the responses of the transfer function, some of reservoir models are selected and passed to history matching and flow simulation, where new uncertain variables are considered. These uncertain variables are related to the properties of reservoir fluids (uncertainty regarding fluid type, saturation distribution, pressures, viscosity, fluid composition, etc.) and the characteristics of the production system (number of wells, drainage mesh configuration, special

wells - horizontal, multilateral, etc.). At the end of the flow simulation phase, the production forecast curves over the life of the reservoir for each of the simulated models are obtained. The value of the accumulated 10 to 30 year production forecast is brought to the present through the calculation of net present value (NPV).

The NPV for each of the models are obtained combining geological, economic and developmental uncertainties. Each production alternative has a distribution of NPV as well as production results, such as total volume produced of each fluid.

The most reliable predictions are based on flow simulation with realistic 3-D models of reservoir properties (Ballin, 1992; da Cruz, 2000). However, all predictions involve uncertainties, since reservoir models are built with uncertain parameters.

3.2 – The Single Model Paradigm

Decisions in reservoir management are often based on a single reference case (Ani et al., 2018; Shirangi and Durlofsky, 2016; Hegstad and Saetrom, 2014). These predictions are uncertain. There are many different parameter values that are consistent with the data and geological knowledge. Any single reference case reservoir model is only one outcome out of an ensemble of possible models describing the unknown reservoir. Considering an ensemble of reservoir models is a better basis for decision support instead of only one or a few 3-D models. Risk and uncertainty are managed and optimized.

Making decisions based on a single reference case disregards geological uncertainty. Multiple realizations of the model are generated in order to capture some of the uncertainties associated with the model.

Several approaches for ranking and selecting a single case are presented in Chapter 2. The appropriate selection method may be different in different contexts. Normally, the optimal realization is considered the realization that matches the real reservoir data the closest (Ani et al, 2018). However, with the aim of selecting the reference model from a set of multiple realizations, results from the selected model may not represent the response from the full set of models. The main idea of setting a single reference case is to find the best model with the

appropriate set of input parameters for matching the history of production data, and thus, predict the future reservoir performance better. However, different realizations are able to match history equally well.

The influence of uncertain geological parameters is not adequately reflected in the reservoir production responses when just a few models are selected. Reservoir forecasts are inaccurate when incorrect or suboptimal decisions are made with a reduced number of realizations.

Multiple realizations should be generated to provide a stable assessment of uncertainty by geostatistical simulation. However, the high computational cost of running flow simulation and the iterative nature of history matching restrict the number of simulation models that can be used for production predictions. Processing all realizations through a flow simulation may take a very long computational time. A detailed numerical reservoir model can be very complex, with millions of cells, many production zones, local grid refinements, etc. CPU time for simulating a single model may take many hours (Telishev et al., 2017; Farah et al., 2015; Klie, 2015). Evaluating the response of multiple realizations of a reservoir model is very computationally demanding.

Many companies make decisions based on a few choices (Yong et al., 2017; Baker, 2015; Sarma et al., 2013), mostly a reference model (P50), and often a low (P10) and high (P90) model. Moreover, most software is aimed at processing one model at a time. Resources are often presented as a single value instead of a distribution.

The approach of selecting a few realizations for reservoir production forecasting should be reconsidered with the recent advances in computational performance (Deutsch, 2015; de Barros and Deutsch, 2017). Uncertainty quantification helps to make more efficient decisions.

The following section presents an example of the differences between considering all realizations and the single model approach as well as the economic impact of considering all realizations in the reservoir production forecast.

3.3 - Synthetic Examples

The following two examples aim to obtain a better quantification of response uncertainty and the value of using all realizations. The proposed methodology considering all realizations is

compared with the traditional selection of a reference model (also called P50 model). The proposed workflow is shown in Figure 3.1. Realizations are generated by SGS using a single model as a "seismic" attribute (yellow boxes). The P50 approach is represented in blue. The approach using all realizations is represented in green. Realizations are ranked for selecting the P50 model. Production responses from four potential well locations are evaluated on both approaches. The well location with the maximum production is selected and evaluated on the true model. Finally, the difference between the responses from the true model based on both approaches is calculated (purple box).

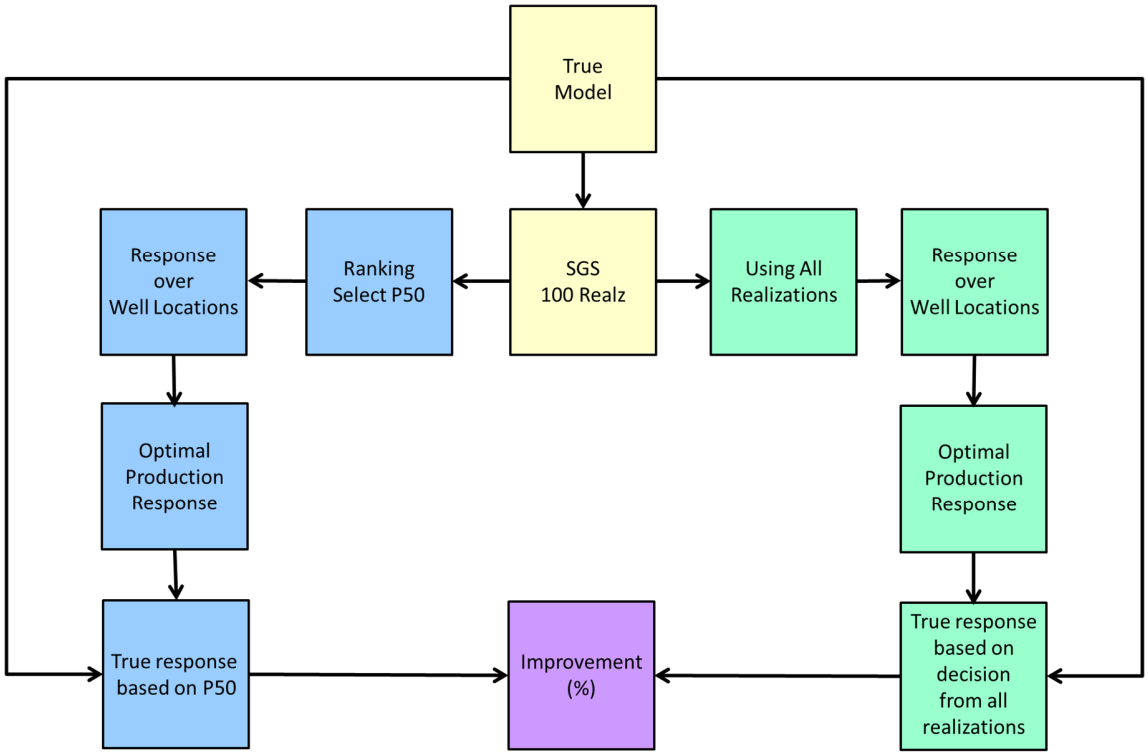

Figure 3.1: Proposed workflow for evaluating the production response based on P50 and all realizations.

3.3.1 – Synthetic Example 1 - Flow simulation approach

First, sequential Gaussian simulation (SGS) is used to generate a 2-D realization of porosity and permeability. This model represents the true reservoir and is considered unknown except at well locations. One hundred realizations are generated by SGS using the previous single model

as a "seismic" attribute, in order to ensure that all realizations are consistent with the true model. A correlation of 0.7 has been used in this example since typical correlation values between seismic and porosity range from 0.5 to 0.7 (Pyrcz and Deutsch, 2014). The closer the correlation is to 1, the stronger is the relation between the true model and the realizations.

The model contains 100 x 100 regular grid blocks with unit dimension in X and Y directions. Four conditioning data are used for simulating porosity and permeability properties (Figure 3.2). The wells are considered water injectors in the flow simulation step.

The number of wells is defined to reproduce the traditional five-spot injection/production pattern as shown on Figure 3.3. In this approach, four injection wells are located at the corners of a square and the production well sits in the center. Water is injected simultaneously through the four injection wells to displace the oil toward the central production well.

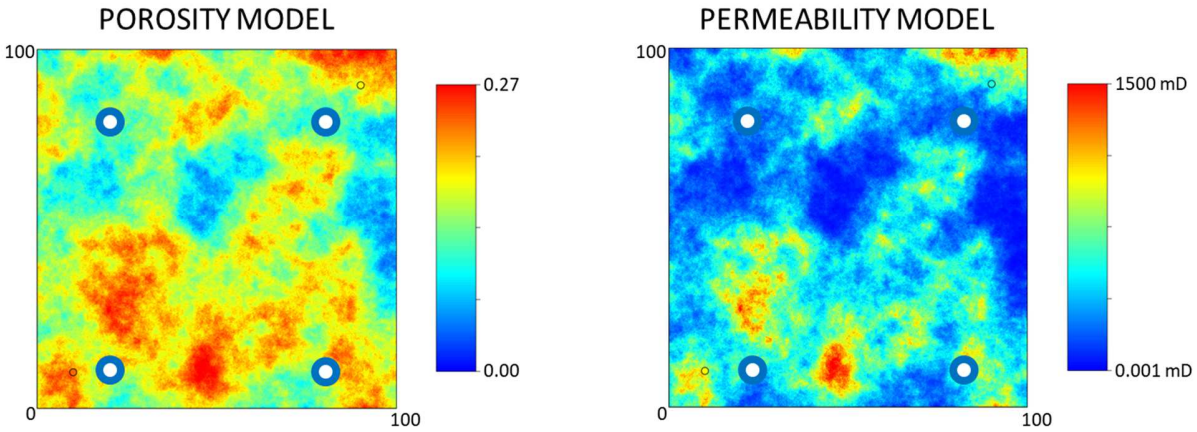

Figure 3.2: Example of a true model of porosity and permeability properties with four injector wells.

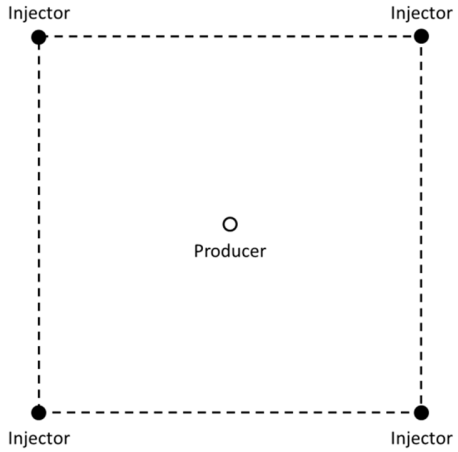

Figure 3.3: The five-spot injection/production pattern.

3.3.1.1 – Ranking and selecting P50 model

The ensemble of realizations is ranked according to the hydrocarbon pore volume (HCPV). Moreover, it is assumed that the pore space is completely filled with oil (oil saturation = 1). Thus, the HCPV from each realization is given by:

$$HCPV_l = \sum_{i=1}^{n} \emptyset_i{}^l \qquad l = 1, \dots, L \tag{3.1}$$

where n is the number of grid cells, $\emptyset_i^l$ is the cell porosity for cell i = 1,…,n for realization l = 1,…,L.

According to the ranking, the realization corresponding to the P50 quantile can be selected.

3.3.1.2 – Well location optimization

Four wells locations (A, B, C and D) are evaluated to maximize the production response (Figure 3.4). The numerical flow simulator Eclipse (Schlumberger, 2016) is used to evaluate the responses considering 15 years of production.

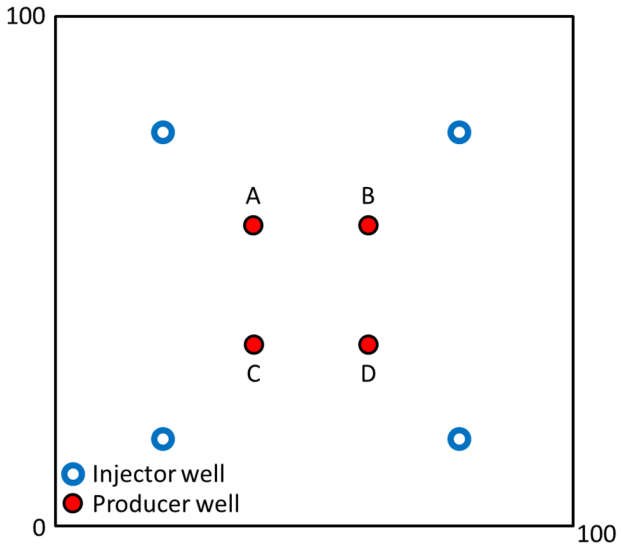

Figure 3.4: Well locations of injectors (white) and producers (red) evaluated for maximizing the production response.

The optimum well location has been defined from the P50 model and from the ensemble of realizations. The key idea is reproducing a realistic problem. The decision of drilling a new producer well is taken based on a P50 model or from the model of uncertainty assessment. The responses are obtained from the true reference reservoir, that is unavailable in practice.

Selecting the optimum well location from the P50 model is straightforward. The well location with the maximum cumulative oil production (Np) over the reservoir lifetime has been selected. For this example, 15 years of production has been considered. The selection of the optimum well location from the ensemble of realizations is shown in Figure 3.5. The expected value of Np has been computed for each well location over all realizations. The well location with the maximum expected value has been selected.

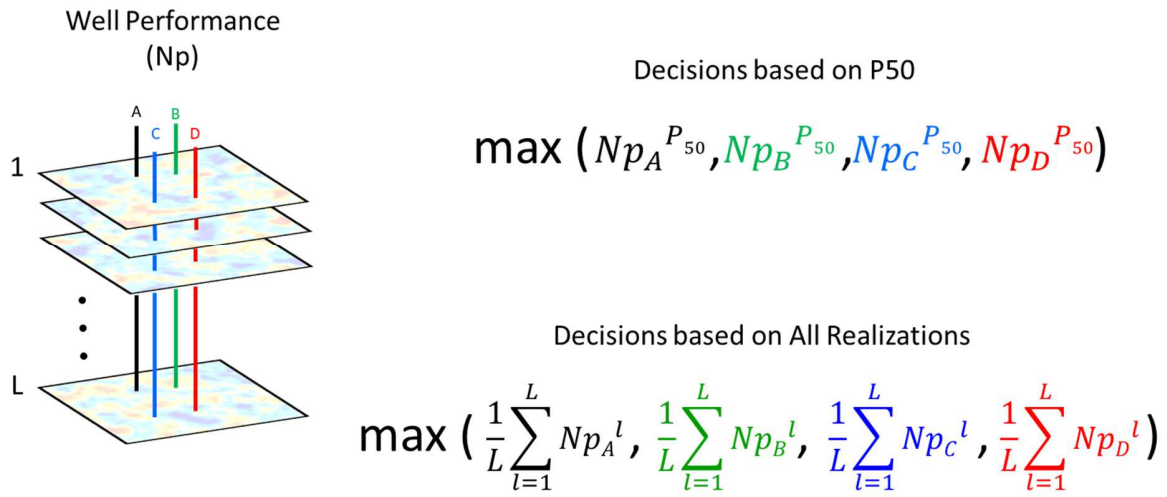

Figure 3.5: Schematic procedure used to define the optimal well location considering the P50 model and all realizations.

3.3.1.3 – Production response improvement

The well locations based on both approaches are evaluated on the true model, as shown in Figure 3.6. The optimal well location defined from P50 model may be the same location as defined from all realizations. So, the workflow has been repeated 100 times to obtain stable response variability.

The relative improvement (RI) of the production response based on all realizations over the production response based on the P50 model is calculated according to Equation 3.2:

$$RI(\%) = 100 * \frac{(E[all_{rz}] - E[P50])}{(E[all_{rz}] + E[P50])/2} \tag{3.2}$$

where $E[all_{rz}]$ is the expected value of production response over all realizations; E[P50] is the expected value of production response from the P50 realization.

Figure 3.7 shows the distribution of the reservoir production responses from the true model based on optimal well location defined by P50 and defined over all realizations. Histograms show that average of 100 cases calculated over all realizations (414 m^3) is higher than the average from cases generated by the P50 model (399 m^3).

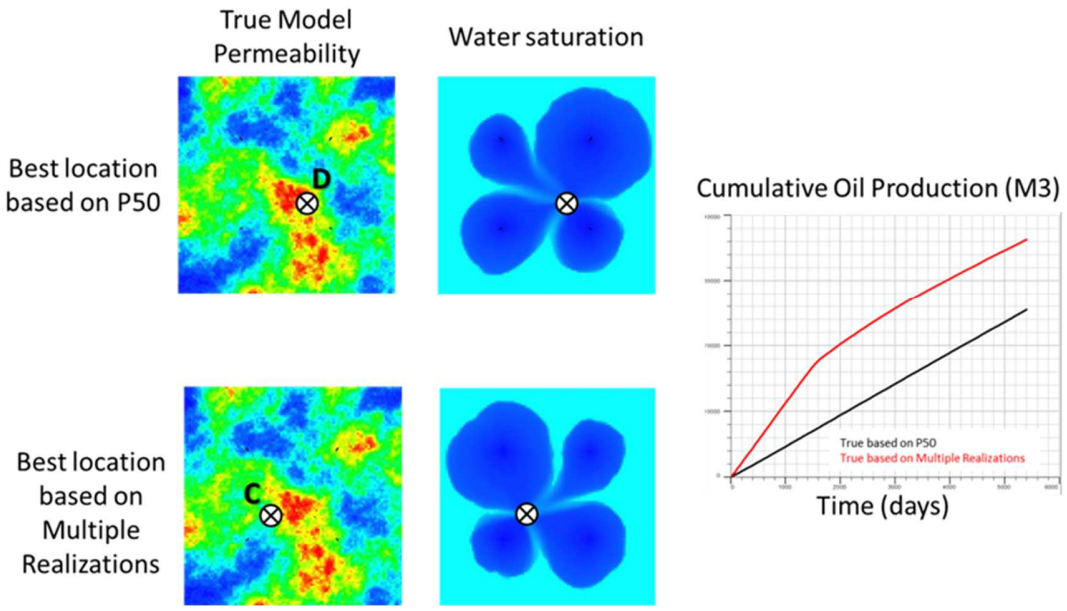

Figure 3.6: Example of one case used to compare the production response.

A cross-plot of the responses from the P50 model and all realizations shows that there are just a few cases where responses from the P50 model are higher than responses from all realizations. It does not mean that the P50 approach could be better than using the ensemble of realizations. Some realizations may present better results, by chance, than others, considering statistical fluctuations. Increasing the number of realizations would minimize these fluctuations, but there is always a probability that the P50 happens to be close to the truth. Moreover, some cases present the same responses from both approaches due to the limited size of the solution space since just four possible well locations have been tested. Once again, by chance, the optimal well location defined from P50 model may be at the same location defined over all realizations.

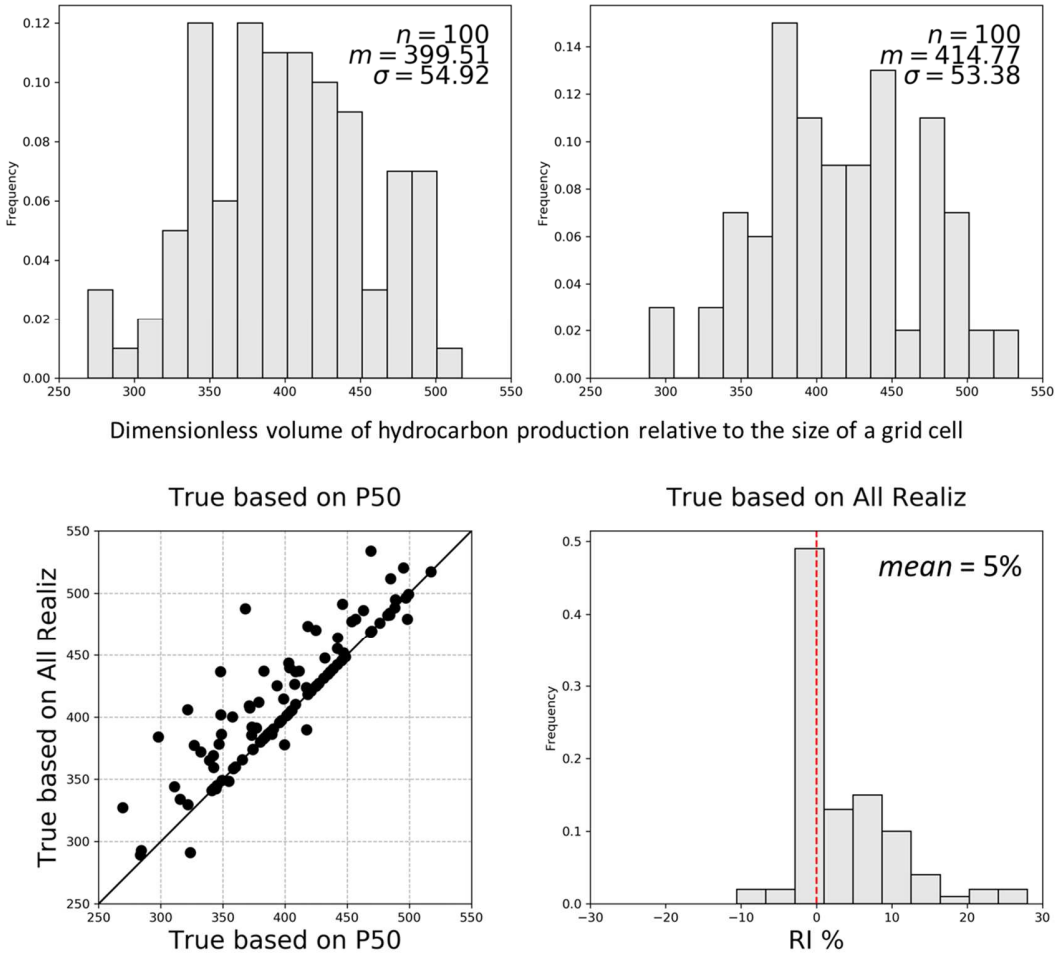

Figure 3.7: Distribution of the improvement of using multiple realizations over the P50 model considering 100 realizations.

Finally, the distribution of the RI considering all realizations over the P50 model shows a mean of 5%. According to the reservoir development plan, this number represents an increase of 5% on average on the reservoir production performance. The economic impact of this production increase will be demonstrated below.

3.3.2 – Synthetic Example 2 - Connected volume approach

Considering the workflow presented in Figure 3.1, a second synthetic example has been considered in order to evaluate the location of a producer well over all realizations. In this

example, a synthetic 2-D model is represented by a 100 x 100 uniform grid blocks with unit dimension in X and Y directions. Two conditioning data, w1 and w2, have been used for simulating a reservoir quality property (RQP) between 0 and 1. The data represent an injector/producer well pair.

Similar to the previous example, the reference model is created by SGS. This model is used as the real reservoir, unknown in practice. Then, one hundred realizations have been simulated by SGS considering the single model as a seismic attribute, applying a correlation equal to 0.7. Sixteen well locations are considered for a producer to evaluate the optimal production response, as illustrated in Figure 3.8.

Some simplifications are considered to reduce the computational time and avoid using flow simulation. Ranking realizations and selecting the P50 model have been defined based on the size of geo-objects calculated by *geo_obj.exe* (Deutsch, 1998). A threshold has been applied to the RQP for defining geo-objects. Similarly, the connected volume around the new location has been considered as the production response. This connectivity measure around the well is highly correlated to the porosity and permeability and hence to the well production response. The connectivity has been calculated by *rank_loc.exe* (Deutsch, 1998). A maximum radius for connection has been applied to the objects for measuring the connectivity.

Many parameters influence the production results. First, the reference model has been used as a seismic attribute to simulate all realizations. The influence of these secondary data on the primary property has been defined by changing the correlation coefficient in the SGS algorithm. The continuity of the simulated property also contributes to the reservoir connectivity, hence the range of the variogram is also changed.

The threshold applied to define geo-objects also influences the production response. Net is defined based on the property exceeding the specified threshold. Finally, the radius near to the well location affects the reservoir connectivity. Thus, the maximum radius for connection also has been changed.

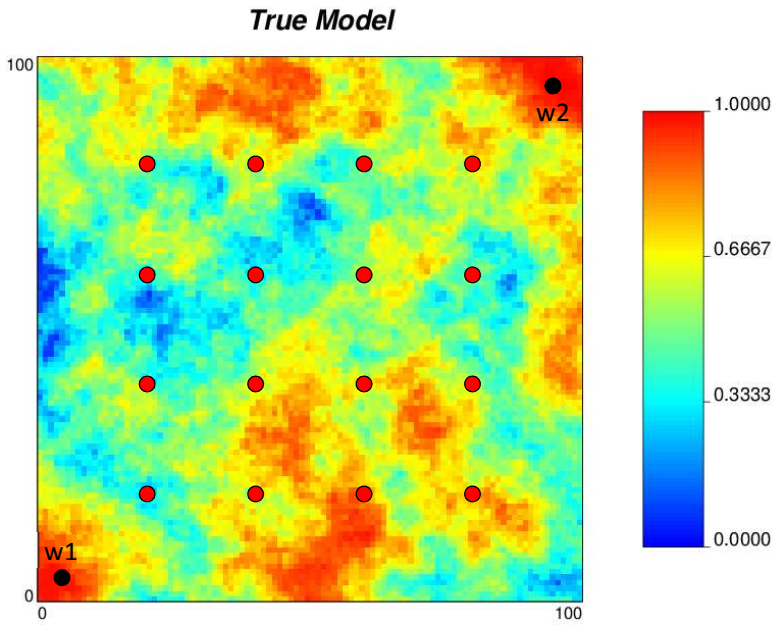

Figure 3.8: Example of a true model of RQP containing two conditioning data (black dots in corners) and 16 possible new producer well locations (red dots).

A sensitivity analysis is performed in the proposed workflow to understand the influence of these parameters on the production responses. A low, a medium and a high value have been defined for each parameter, as shown in Table 3.1, leading to 81 scenarios. Each scenario has been run 100 times, limiting stochastic fluctuations and obtaining a robust response.

Table 3.1: Parameter values for sensitivity analysis

PARAMETER	LOW	MEDIUM	HIGH
Secondary data correlation	0.3	0.5	0.7
Variogram range	10	30	70
Threshold	0.2	0.4	0.7
Maximum radius of connectivity	10	20	30

Figure 3.9 shows a cross-plot between true response based on P50 and based on all realizations for the 81 scenarios. Each scenario contains 100 realizations, and each dot

corresponds to a single realization. Points above the 45-degree line indicate better results have been obtained using all realizations instead of the P50 model.

The expected value of the production response has been calculated for each scenario, considering 100 realizations per scenario. The improvement considering all realizations over P50 has been calculated according to Equation 3.2 (Figure 3.10). Five scenarios show a negative improvement. This means the P50 responses are higher than responses from all realizations. Table 3.2 shows the corresponding parameters from each scenario and their RI values.

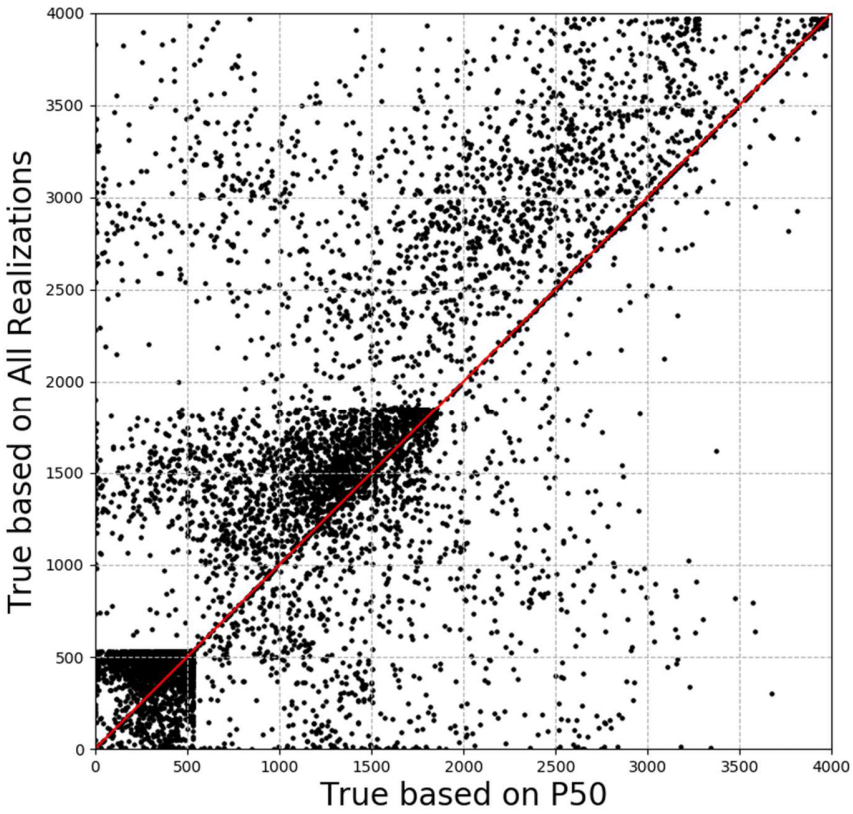

Figure 3.9: Crossplot between production responses based on P50 model and all realizations from 81 scenarios.

In general, scenarios defined with a low correlation with the secondary data, long variogram range and short radius of connection show the least improvement.

The scenario with the poorest improvement is analyzed more closely. The workflow has been run 100 more times to obtain an even more statistically robust response. Figure 3.11 shows

the distribution of the RI of these realizations. The average is close to zero (0.4%) which means the fluctuations are related to the stochastic procedure instead of a combination of parameters.

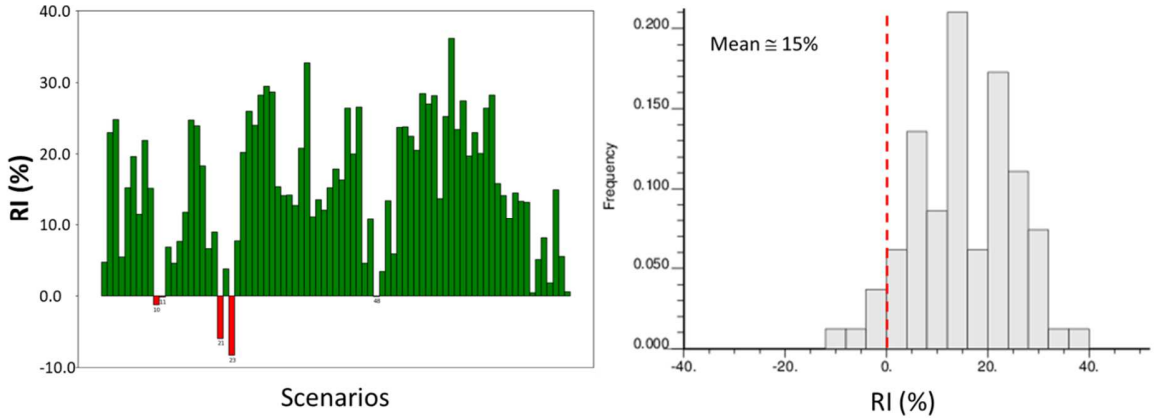

Figure 3.10: Relative improvement over 81 scenarios. Five scenarios show a negative improvement (in red).

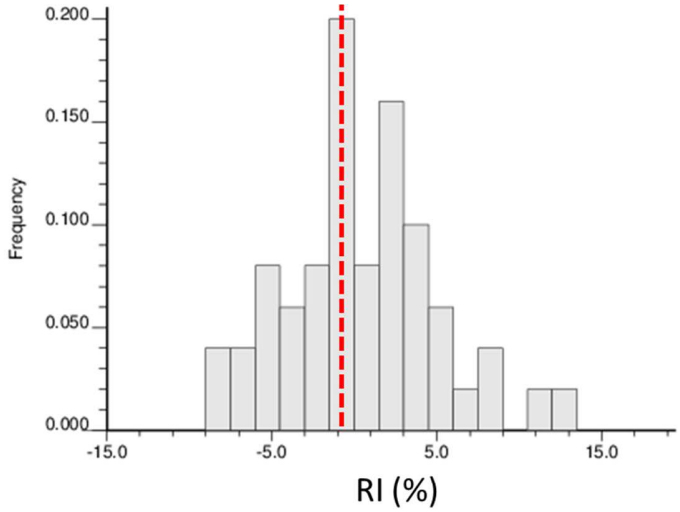

Figure 3.11: Histogram of relative improvement over 100 realizations from the scenario with the worst response.

3.4 – Value of Using All Realizations

The RI average shown in Figure 3.10 is 15%, which means the production response is increased by 15% on average considering all realizations compared with using the P50 model.

However, projects might not blindly follow the P50 model, and there is a confidence interval to select a representative model. In other words, 15% may be an optimistic production improvement, and the economic impact may be considered unrealistic in practice.

A more conservative increase in reservoir production, say 5%, is able to improve significantly the economic performance of a production project.

NPV and Internal Rate of Return (IRR) are two commonly used investment analysis methods in industry. NPV corresponds to the cumulative discounted cash flow over the production lifecycle of the reservoir. IRR is the discount rate when NPV of a particular cash flow is zero. The higher the IRR, the greater the profitability and use of capital.

In this work, the contribution to the NPV from the injection and production of fluids are considered. Other contributions, such as capital expenditures, are not considered in this formulation. In a 15-year reservoir development plan (see Figure 3.12), increasing reservoir production by 5%, due to considering all realizations, may lead to a large improvement in NPV (30%) and IRR (10%).

Reservoir uncertainty may have a significant impact on the project management, such as the selection of production development strategies. Understanding the uncertainties related to reservoir production is important for making development and management decisions through the lifetime of the reservoir. Tens of millions of dollars might be expected as a conservative increase in reservoir production of 5% due to optimization over all realizations. The magnitude of these incomes strongly supports the efforts of considering all realizations instead of just a P50 model.

Uncertainty assessment in reservoir simulation studies may be an important issue to quantify future planning risks through field development scenarios. The uncertainty comes from the sparseness of geological and reservoir data that negatively affect representing the geological environment for reservoir flow simulation. Therefore, the uncertainty should be quantified for improved future production plans.

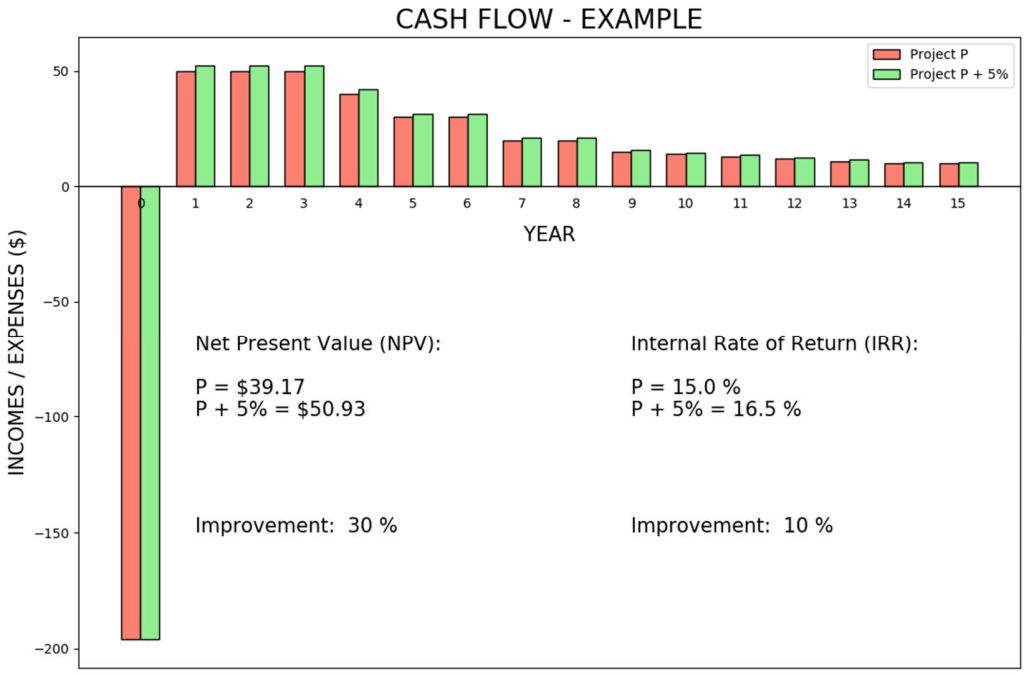

Figure 3.12: Cash flow diagrams of a hypothetical 15-year reservoir development project. Red bars represent the original cash flow project. Green bars represent the new cash flow with an increase in annual incomes.

Although additional models are selected from the ensemble of geostatistical reservoir models, such as P10 and P90, a reference case model is a conventional approach used in the hydrocarbon industry. A general concern with any realization that is claimed to be a specific P10 or P90 value is that it is not the same P value at all locations. The P value of a realization must be considered as a global parameter with little local meaning. Individual scenarios have a near-zero probability of occurrence. Any desired P model can be found or constructed. However, no single case can represent a stipulated probability of reservoir performance.

3.5 – Number of Realizations

Although all realizations might be used for a more robust uncertainty assessment, there is a concern about exactly how many realizations should be considered. Geostatistical techniques may quickly generate many realizations. However, thousands of realizations may not be a feasible number in real reservoir studies.

The number of realizations is related to the aspects of the quantified uncertainty and the precision required. The assessment of average statistics requires relatively few realizations. Uncertainty assessment with more precision requires a larger number of realizations.

Based on the synthetic Example 1 shown in Section 3.3.1, a large number of realizations (10,000) have been generated. Each realization has been evaluated using numerical flow simulation for testing four different well locations (A, B, C and D). The average response for each well location is calculated over all realizations (see Figure 3.5). This value is considered as the maximum benefit possible from a very large number of realizations.

Next, a different number of realizations are randomly selected from the total, creating subsets of realizations. The maximized production response is calculated over each subset. The procedure is repeated 1000 times to obtain the average value while minimizing statistical fluctuations. The expected production response over each subset of realizations is a fraction of the maximum value obtained over 10,000 realizations. This fraction gets closer to the original set as increasing the number of realizations in each subset (Figure 3.13). All values are normalized based on the maximized production.

Ideally, this maximized value would be obtained from an infinite number of realizations, which is infeasible. The idea here is to demonstrate the minimum number of realizations necessary for a reliable performance response. According to this example, 100-200 realizations result in 90% of the maximum benefit. There is a very slow increase in this percentage above this range. The difference around 10% of the maximum benefit (100%) considering an infinite number of realizations is due to the simplified 2-D example and the limited number of solution space. A smaller gap is expected in practical 3-D reservoir modelling decision-making processes.

3.6 – Managing All Realizations

The single-model approach for production forecasting remains popular because of simplicity and because of reduced computational effort for running a flow simulator or for history matching. Selecting a single model or few cases for evaluating the uncertainty in the reservoir production performance disregards geological uncertainty. Although significant progress has

been made in last years in the development of flow simulators and history matching, such processes still cannot deal with a large number of reservoir models.

The consolidated approach of ranking models and selecting some of them based on a simple objective function, e.g. OOIP, may result in misleading responses. This is a main paradigm that must be changed in reservoir management.

Although there are some concerns about managing all realizations, discussed in following chapters, considering all realizations can result in significant improvements in the economic performance of the projects. The following sections will address considering the ensemble of realizations in reservoir development planning.

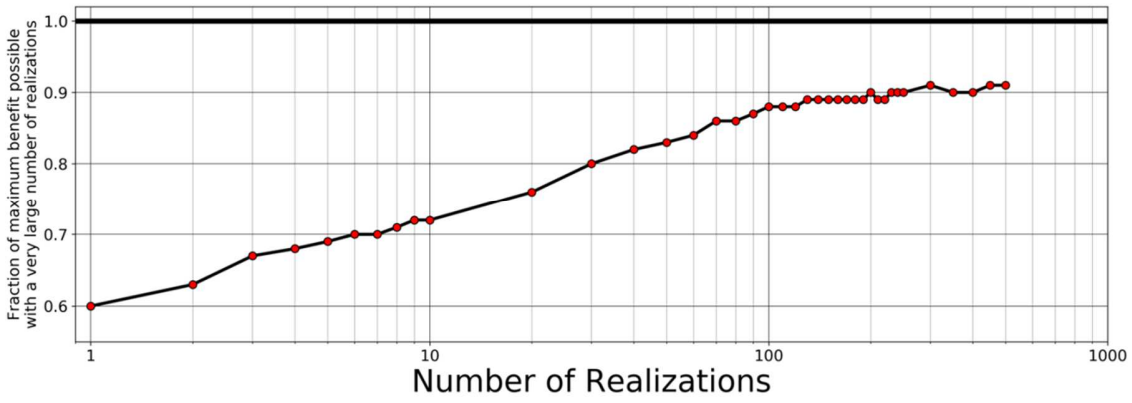

Figure 3.13: Number of realizations necessary to obtain a fraction of the maximum benefit possible from an infinite number of realizations.

3.6.1 – Making Decisions based on Multiple Realizations

Exploring hundreds of geostatistical realizations simultaneously is not well understood in reservoir management, even with recent computational advances. Realizations have been used as isolated cases, instead of considered as an ensemble with multiple realizations all used for uncertainty predictions and production optimization.

Reservoir management decisions conventionally need a single model to compute OOIP, to define the well locations, the operate facilities and to specify the reservoir development plan. However, these operations are not restricted to a single model. There are no limitations to make

a decision on all realizations; the measure of performance to make a decision is the expected value over all realizations.

Although the methodology to generate geological reservoir models is mature and well-established, the uncertainty information is often not properly used in the decision-making process. Some the reasons are the high dimensionality of the problem and the lack of a robust decision-making model that properly manages the risk associated with the geological uncertainty.

The complexity of many real response variables requires considering the ensemble of realizations for a better planning and uncertainty assessment. Managing multiple realizations must be used in measures of performance, such as OOIP and production forecasts and optimization processes, helping the reservoir team make decisions for maximizing the value of the reservoir project.

3.6.2 – Calculating Measures of Performance

In a geostatistical context, realizations of the variables of interest that characterize a reservoir model must be submitted to a transfer function. The distribution of the transfer function responses characterize the space of uncertainty and can be used in decision-making.

Any calculation performed on one reservoir model can be performed on multiple models, to generate a distribution of the response variable of interest. Realizations are equally probable, and there is no right or best realization. Individual realizations, in general, should never be used for calculations. Considering a single realization can be misleading since the realization depends on the random number generator. In most cases, the robust approach is to consider all realizations and take the expected value from the distribution of the responses as a single result.

The OOIP or net-to-gross (NTG) calculation can be considered a simple and fast transfer function using all realizations. As illustrated above, the realizations could be ranked based on OOIP, and some of the realization selected for a more complex transfer function (Figures 3.14 and 3.15).

As static properties, the ensemble of realizations can be processed in the flow simulator to obtain a distribution of reserves. Many production properties could be calculated considering all realizations, such as the outcomes at a well location, the timing for production decline and breakthrough.

Realizations must be processed one at the time, and the resultant outcomes can be represented as distributions or expected values for supporting the decision-making process in the reservoir development plan. Similarly, summarizing the ensemble of realizations can also be useful. The expected value and other statistics such as P10, P50 and P90 can be calculated from the response distributions and used as summaries of measure of performance.

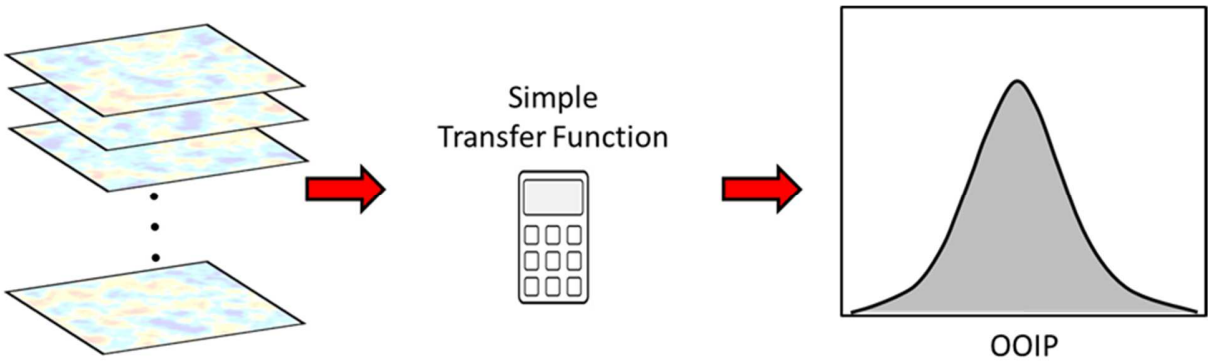

Figure 3.14: Distribution of the OOIP calculated over all realizations.

3.6.3 – Optimizing Decisions over Multiple Realizations

The primary target in many upstream studies is defining a field development plan that optimizes costs and maximizes production (maximizes NPV). In some cases, the transfer function and decision variables are well defined, for example, OOIP and reservoir production, as mentioned above. In other cases, however, practitioners should make decisions based on optimized responses.

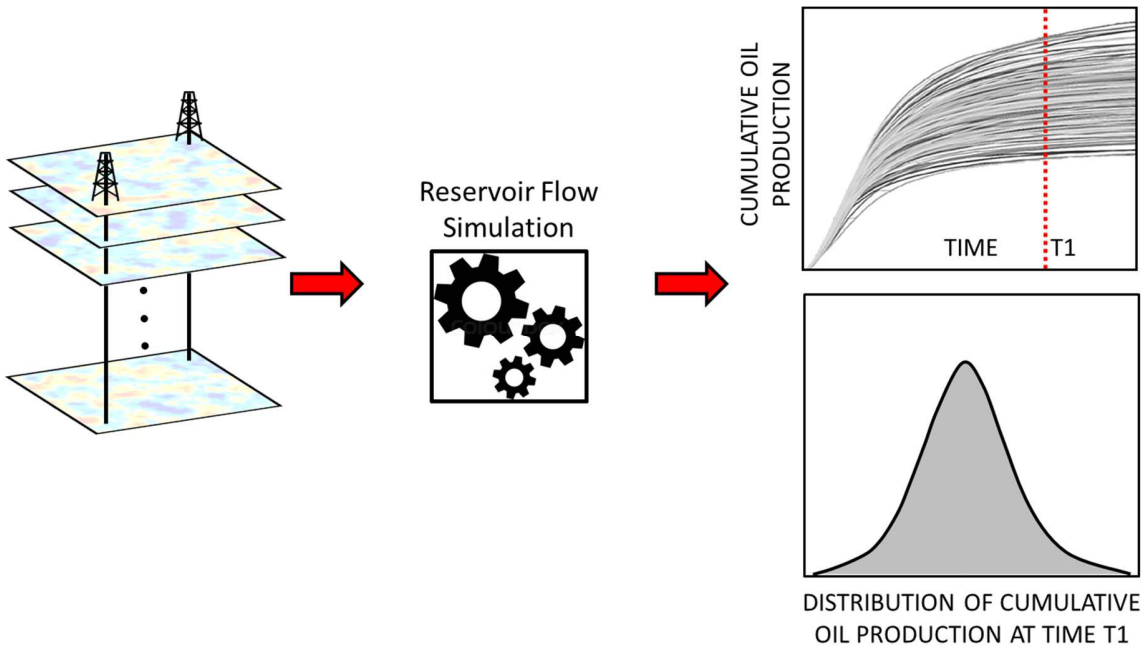

Figure 3.15: Distribution of the cumulative oil production obtained after performing all realizations in the reservoir flow simulator.

Dealing with multiple realizations should play an important role in optimization of decisions. The need to find answers for where and when to drill new wells in reservoirs with a reasonable number of calculations is a key factor in new development projects. The potential of various well types such as vertical, horizontal, and multilaterals, alternative production options (e.g. well spacing, and well scheduling) have a critical impact on hydrocarbon recovery. It is impractical to define the best number of new wells based on experience or simple tools.

The determination of optimal well location, for instance, may be important to maximize recovery from hydrocarbon reservoirs. Identification of well locations typically relies on expert subsurface knowledge and flow simulation scenarios. Such approaches, due to the complexity and uncertainty of subsurface descriptions, can easily miss profitable possibilities. The timing of well injection and production and setting surface/pipeline facilities are also reservoir issues with critical impact in the development plan that must be optimized.

In practice, such optimizations are implemented in a deterministic manner, applied to low, mid and high simulation scenarios (Ramires et al, 2017). This optimization approach may anchor

the results to particular portions of the uncertainty space, while a more robust optimization approach propagates the effect of uncertain parameters on the optimization outcomes. Due to the increase in computational power, handling multiple realizations/scenarios to investigate the uncertainty space in optimization problems is ever more feasible.

Optimization is the problem of finding the maximum or minimum of an objective function O over its domain. Considering L realizations:

$$O = \frac{1}{L}\sum_{l=1}^{L}(Goal)_l \tag{3.3}$$

The objective function is formulated according to the goal. The problem of finding the optimum number and placement wells where the maximization of a performance index, such as NPV or cumulative oil production, is sought while minimizing costs and accommodating operating limits and other constraints are recognized as a nonlinear optimization problem with integer parameters (Cullick et al, 2005).

Figure 3.16 shows a simple example of well location optimization considering multiple realizations. Four potential well locations are evaluated over multiple realizations. The distribution of objective function responses (e.g. NPV) at each well location is shown together with the expected value of each well location (red-dashed line). The optimum well location corresponds to the maximum NPV from all expected values (W4).

3.6.4 – Considering Risk in Decision-Making

Making decisions about projects in the oilfield is a routine challenge for geologists and reservoir engineers. Selections must be made from a set of feasible projects. The one implemented will add the highest possible value to the oilfield. The process is not easy since the response cannot be predicted with certainty due to the geological uncertainty (de Barros and Deutsch, 2018).

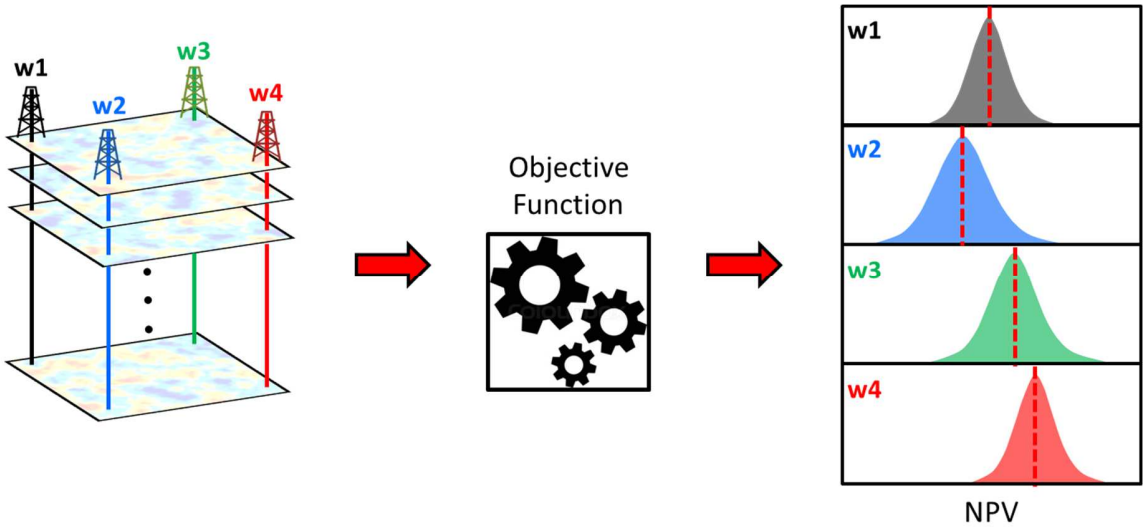

Figure 3.16: Example of optimizing well location over multiple realizations.

The geological uncertainties are coupled with economic and engineering models involve high-risk decision scenarios, with no guarantee of successfully discovering and developing hydrocarbons resources.

In the development plans, field management decisions are complex issues due to (1) the number and type of decisions; (2) the great effort required to predict production with the necessary accuracy; and (3) the dependency of production strategy definition on several types of uncertainty with significant impact on risk quantification (Suslick et al., 2009).

According to Gallardo and Deutsch (2017), the preferences and the concept of rationality are the foundations of the decision-making model. After transferring the geological uncertainty, selecting a project from the set of feasible actions is equivalent to choosing between the probability distributions of the response variable (Johnstone and Lindley, 2013). To make that choice, the preferences of the investor over the space of outcomes can be encoded in a utility function (Kochenderfer, 2015). A decision maker will make a rational decision if a project that maximizes expected utility is chosen.

The utility function can be classified into three groups according to the preferences of the decision maker: risk-averse, risk-neutral and risk-taker utility functions (Figure 3.17). A decision with risk-averse utility function will not play a fair game. According to Levy (2016), a fair game is

defined as a game in which the price of a ticket to play the game is equal to the expected prize. A decision with risk-neutral utility function is indifferent between playing the fair game or not. A decision with risk-taker utility function will play the fair game.

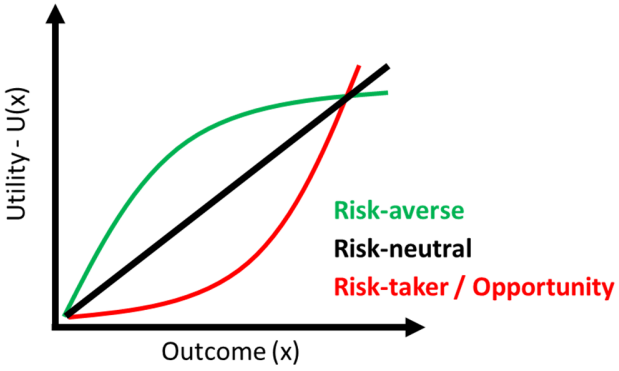

Figure 3.17: Classification of the utility functions.

Many complex exploration & production decision problems involve multiple conflicting objectives. Under these circumstances, managers have a growing need to employ improved and systematic decision processes that explicitly embody the objectives of the company, desired goals, and resource constraints. In general, the utility function of companies is unknown. Some decision criteria rank candidate projects according to partial information on the decision maker preferences (e.g. risk-averse, risk-neutral) and the response variable distribution.

Multiple methodologies provide a basis for the management of risk in a project. One of those methodologies came out of portfolio management and used risk to categorize and help choose between multiple portfolio options. This method, coined the Efficient Frontier, was proposed by Markowitz (1952) with his idea of the efficient frontier for portfolio selection.

The efficient frontier concept provides a way of ranking investments with the expected profit value on one axis and the standard deviation of the profit values, or another measure of risk, on the other axis. For any specific measure of risk, the best option is the choice with the highest expected value. This is the efficient frontier and is shown in Figure 3.18 as the red line.

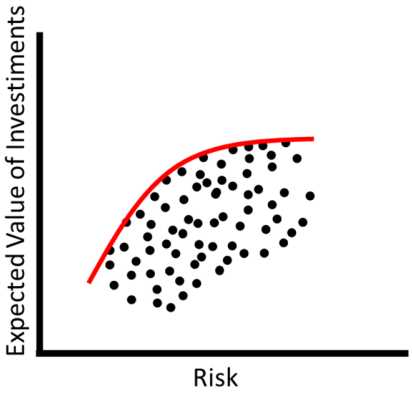

Figure 3.18: Schematic of the efficient frontier.

In risk management, finding the efficient frontier is only one step in the risk management process. Determining the optimal solution along the efficient frontier is important. This optimal solution is objective and based on the risk versus return preference of the investor (Walls, 2005a, 2005b). Some investors are more risk averse while others prefer a higher expected return regardless of the associated risk. In portfolio management, there are many different methods for finding this optimal solution (Engels, 2004).

The acceptable risk level may change throughout the reservoir lifecycle since the preferences of the decision maker may also change according to the short-to-long-term objectives. For instance, exploratory projects may consider opportunity-seeking preferences, with higher expected return regardless of the associated risk since production is not explicitly addressed. High short-term gains are often important to maximize cash flow. In medium-term, when production forecasts and surface/pipeline facilities have been already defined, a risk-averse preference is preferable. In the long-term, risk-neutral preferences may be considered.

3.7 - Discussion

The goal of this chapter is comparing the approach to decision making considering the selection of a single model and considering multiple realizations. The use of a single model

disregards geological uncertainty. Production forecasts based on a single model may not represent the response of the complete ensemble models.

Several ranking techniques are shown in Chapter 2, considering static and dynamic properties. Regardless of the ranking method, this thesis focuses on the use of multiple realizations instead of a single model. Comparing or discussing the efficacy of different ranking techniques is beyond the scope of this research. How this reference model is selected does not impact the results obtained in this research. The essential issue is the production forecasts and decision making in reservoir management are more robust and consistent when based on all realizations, rather than decisions based on a single realization.

Considering all realizations is better than choosing a single reference model. The reasons for this statement have been discussed in this chapter. Moreover, the practical benefits of making decisions based on all realizations have been illustrated with two synthetic examples. Managing and visualizing multiple realizations remains a challenge.

3.8 - Summary

- Decisions in reservoir management based on all realizations are more consistent than decisions based on a single realization;
- Considering all realizations may result in significant improvements in the economic performance of the projects;
- The ensemble of realizations must be used for calculating measures of performance and for optimization processes;
- The correct approach claimed in this thesis consists in considering all realizations and taking the expected value from the distribution of the responses.

Chapter 4

Uncertainty Visualization of All Realizations

This chapter is composed in part by de Barros and Deutsch (2017) published by Computers & Geosciences as an original work.

4.1 - Introduction

Geostatistical realizations must be treated as an ensemble. Although they may be ranked by a response variable such as in-place resources, two adjacent realizations may appear completely different due to areas of high and low values occurring in different locations. This creates a challenge for visualizing the uncertainty in an ensemble of 3-D model realizations, which is an integral part of geomodeling applications (Viard et al., 2011). Note that visualizing one realization or a single estimated model does not convey uncertainty.

In this context, advances in computational speed and storage have made it possible to study the development of complex and dynamic systems and represent results accordingly. There is an increase in productivity due to newly developed automated strategies and shared computation. Although the number of realizations of geostatistical simulation is increasing and has been automated, human inspection is still required for quality control and to analyze the results. Tools to help process and analyze an ensemble of realizations in a qualitative and productive manner are required.

The challenge is to handle the information generated by an uncertainty analysis from a geostatistical approach. Geostatistical simulation techniques are relatively well established. The application of geostatistical techniques with geospatial data and the computation of uncertainty in the resulting model are reasonably well understood. In terms of visualization, there are many programs to display and manipulate complex 3-D models and their internal properties. Representation of high dimensional uncertainty, however, is still a challenge because there are a

restricted number of available visual channels to represent it, such as data position, color, texture and opacity.

4.2 – Uncertainty Visualization

According to Potter et al. (2012), uncertainty representation must be simplified in order to display many realizations in an appropriate and effective visual manner that allows for human perception. Lamigueiro (2014) presents the uncertainty by showing realizations side by side (simultaneous) and with superimposed results (condensed). Obermaier and Joy (2014) focus on visualization methods for understanding the similarities, differences and trends among the members of the realization group. Viard et al. (2011) present three algorithms between the frames (e.g. Fisher, 1993; Srivastava, 1994; Ehlschlaeger, 1997; Davis and Keller, 1997; Dooley and Lavin, 2007).

Phadke et al. (2012) also mention an animation technique to support a set of realizations. The pairwise sequential animation method orders *n* members of an ensemble (a collection of related datasets), combines subsets of realizations, and presents them as an animated visualization using hue and texture. Höllt et al. (2014) introduce the ensemble visualization approach for spatially distributed data, defined as a collection of *n* values of a single variable in *m* dimensions. In this research, this approach is used for an ensemble of realizations generated for a geological model. The ensemble visualization approach appears in several works (e.g. Kao et al., 2001, 2005, Luo et al., 2003, Love et al., 2005, Obermaier and Joy, 2014). The procedure can be considered a specific method from the general uncertainty visualization methods, applied when uncertainties are not well represented in quantitative terms.

A novel method to sequentially display multiple geostatistical realizations is presented in this research, combining both animation methods and the ensemble visualization approach. The emphasis is on the visualization aspect of post processing and not on the details of model construction. There are many references available with model construction details. The assumption is that an ensemble of realizations is available in a common numerical format. There are likely tens to hundreds of realizations. The realizations likely contain millions of locations; however, not all locations will be visible on a particular display. Some locations will be

transparent to see deeper into the model and some locations will be blocked behind locations that are being displayed.

4.3 – Methodology

A sequence of realizations is defined by their similarities/dissimilarities. Numerical or quantitative differences between two realizations define a distance for each pair of images. Realizations that are close together are displayed one after another. The results are presented as a dynamic animation, which shows the defined sequence of realizations.

Although some results on a 2-D grid are presented, the main idea of this work is to apply the proposed approach to any visualization of 3-D geological models. A user can choose an arbitrary view plane(s) and visualize all realizations available for this plane. Figure 4.1 shows an arbitrary view with some horizontal views visible and some cross sections visible. The order of realizations would not change with zooming or panning, but would change when the position of the slices is changed. The visualization ordering would be automatically recalculated when the view plane is changed. Software would cycle the realizations in the optimized sequence at a specified speed until the view is changed. Thus, no one realization is chosen. The realizations do not change at the data locations. The greatest changes would occur away from the data.

4.3.1 – Distance between realizations for continuous variables

Even with computational advances over the years, exploring hundreds of geostatistical realizations simultaneously is not well understood. The spatial pattern of any single realization is not of particular interest. Instead, there is more information in understanding the features that can vary between realizations and the features that are consistent across realizations.

Summary models of uncertainty are useful. The local variance, probability of net reservoir or difference between realizations are useful summary statistics. Visualization of such models would quickly reveal areas that are more uncertain and areas that are less uncertain. However, these visualizations would not show the heterogeneity and joint uncertainty between multiple locations that impacts reservoir performance. Summary models inevitably change smoothly away from well control. Focusing on such models may lead the professional to believe the reservoir properties change smoothly.

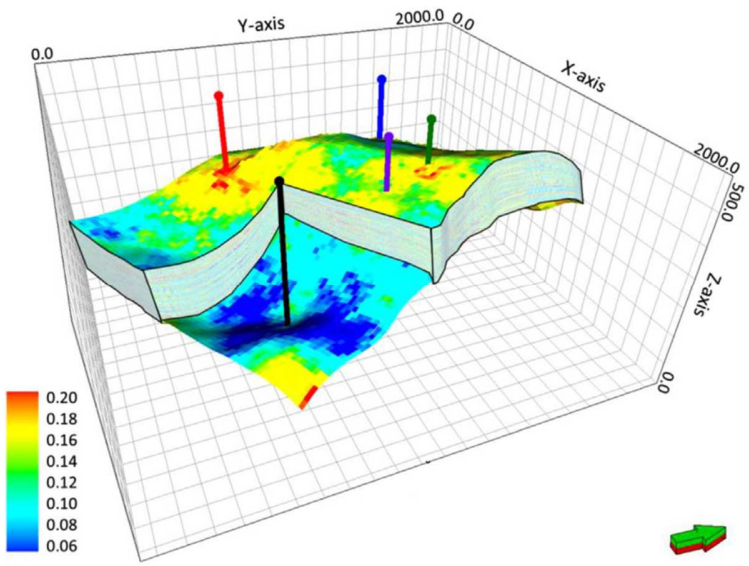

Figure 4.1: An arbitrary set of view planes from a 3-D geological model. The colormap represents the porosity of a reservoir layer.

Another approach is to define a summary response function to index the geostatistical images. This response could be used to order or classify the realizations. Several different similarity metrics are used for this purpose in the literature. In the environmental sciences, for example, similarity metrics include empirical orthogonal functions (Koch et al., 2015), connectivity analysis (Koch et al., 2016), fractions skill score (Roberts and lean, 2008), feature based analysis (Wolff et al., 2014) and spatial prediction comparison test (Gilleland, 2013).

In petroleum applications, the realizations could be ordered according to static reservoir properties such as porosity, facies proportions or hydrocarbon volume. In terms of dynamic properties, realizations could be ordered by connectivity or flow response. A scalar response would order the realizations, but the spatial similarity between adjacent realizations is not guaranteed; realizations with similar average response could be quite different. A natural ordering of the realizations requires calculating the difference between them. The greater the difference, the greater the distance between any two realizations. Formally, a distance is a function D with nonnegative real values that presents a symmetric property. Considering two

different points A and B, the distance calculated from A to B is equal to the distance calculated from B to A, i.e. $D_{A,B} = D_{B,A}$.

A spatial distance function is proposed to compare the entire set of images coming from an underlying pool of realizations. A Euclidean-based distance provides a simple formulation and a clear interpretation. Let *l* and *l'* be two realizations that are composed of *N* visible grid cells. The distance $D_{l,l'}$ is the sum of differences between realizations, which is calculated cell-by-cell as follows:

$$D_{l,l'} = \sqrt{\sum_{m=1}^{N}\{Z_{l,m} - Z_{l',m}\}^2}, \qquad l, l' = 1, \dots, L \tag{4.1}$$

where *m* denotes the grid cells that are visible, *N* is the number of visible grid cells and Z_m denotes the cell values of the two realizations.

The cells could be weighted by how much of them are visible. For example, cells on a cross section may not be as visible as those in plan view (see Figure 4.1). To avoid undue influence of extreme values, these distances could be calculated after applying a moving window filtering. This modifies a cell value by taking the average of a fixed subset of nearby cells in the image plane.

The distance matrix in Figure 4.2 shows all the spatial normalized distances calculated for *L* realizations. This matrix is symmetric, i.e., the values above the main diagonal are equal the values below the main diagonal. The values on the main diagonal are equal to zero since they correspond to the distance between a realization and itself.

Two or more properties may be combined to evaluate the distance between two images. For instance, consider combining the differences in spatial distance (previously described) with distances in the hydrocarbon resource, i.e. the amount of oil or gas contained in porous or fractured rock formation. Each property is calculated and weighted as follows:

$$D_{R\,(l,l')} = \sqrt{\sum_{m=1}^{N}\{R_{l,m} - R_{l',m}\}^2}, \qquad l, l' = 1, \dots, L \tag{4.2}$$

where D_R is the distance of the resources; R_l and $R_{l'}$ are the hydrocarbon resources of realization *l* and *l'* computed for each *m* grid cell.

$$D_{total\,(l,l')} = W_S * D_{S\,(l,l')} + W_R * D_{R\,(l,l')}, \qquad l, l' = 1, \ldots, L \tag{4.3}$$

where D_S is the spatial difference calculated according to Equation 4.1; D_R is the difference of the resource calculated according to Equation 4.2; W_S and W_R are the respective weights for spatial (D_S) and resource distance (D_R).

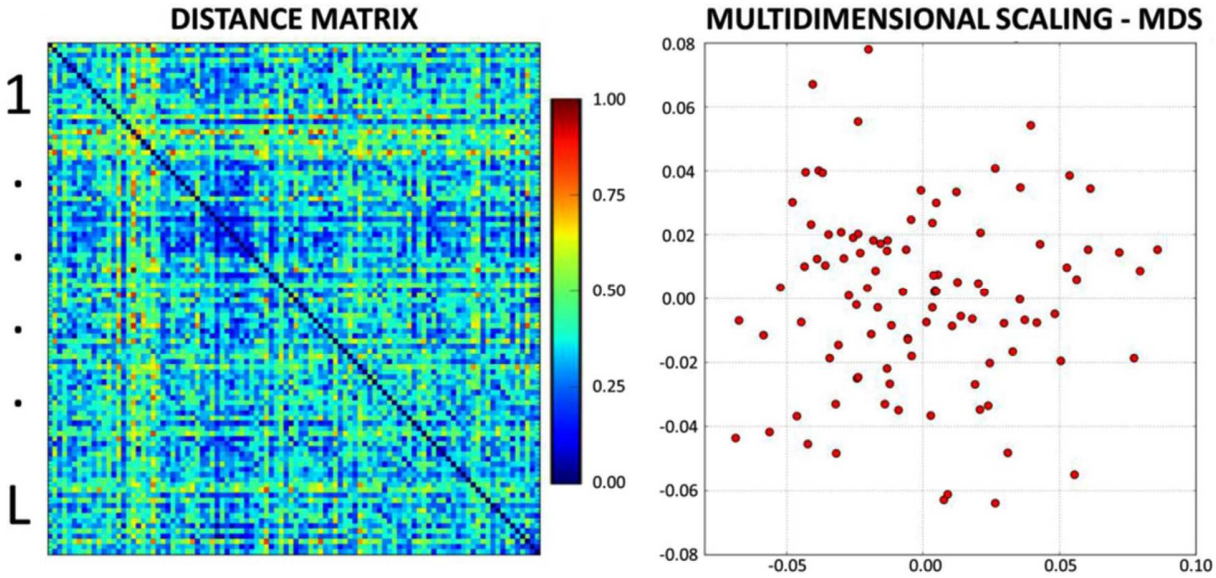

Figure 4.2: Two methods for visualizing the differences between *L* geostatistical realizations. On the left, a distance matrix shows the normalized distance between each pair of realizations. On the right, an MDS projection is shown where each point also represents a unique model.

As the number of realizations increases, the distance matrix may become difficult to understand. According to Figure 4.2 (left), there are clearly realizations different from others (hot colors) and realizations close to others (cold colors), but the relationship between all realizations simultaneously is difficult to comprehend. An alternative method for visualizing the relationship between images is shown in Figure 4.2 (right). The distances are plotted using the Multidimensional Scaling (MDS) technique (Cox and Cox, 1994). In this lower dimensional representation, the relationship between the realizations is represented by the distances on a 2-D map.

Some information about the distance matrix is represented in the MDS map. Two images that have a small distance in the matrix (blue colors) are close in the MDS representation. Images that have a large distance in the matrix (red colors) are far apart in the MDS map. Select pairs of realizations that are close and far apart in the MDS map are displayed in Figure 4.3 to illustrate this concept.

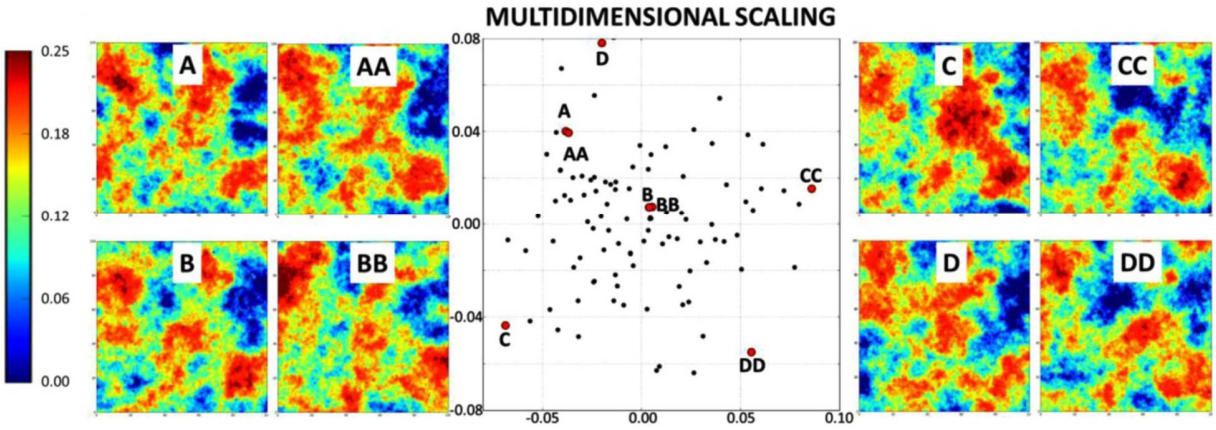

Figure 4.3: According to MDS representation, four pairs of realizations are shown. On the left, pairs A - AA and B – BB represent very close images. High and low values are well reproduced in both of the associated images. On the right, pairs C – CC and D – DD represent images with large differences, which are reflected in their position in the MDS plot.

The idea of using MDS to compare different models has been used for many years. Scheidt and Caers (2009a, 2009b) apply MDS to select a subset of reservoir models according to their uncertainty in flow response. Lajevardi and Deutsch (2014) apply dissimilarity measures that underpin MDS to compare mixtures of rock types. The main information in this research, however, comes exclusively from the distance matrix; MDS simply provides a convenient display of the realizations in low-dimensional space, which may aid in interpretation of the results.

4.3.2 – Distance between realizations for categorical variables

Categorical variables are defined for simulation considering a hierarchical sequence of facies or rock types. Facies should be ordered according to their similarities. Consider five

categories defined by grain size: 1 = coarse sandstone, 2 = medium sandstone, 3 = fine sandstone, 4 = siltstone, 5 = shale as shown in Figure 4.4. In this configuration, category 1 is more similar to category 2 than categories 4 or 5. In this example, facies 1 and 2 or 1 and 3 will present a higher correlation than facies 1 and 4 or 1 and 5.

Similarity or correlation between categories can be defined based on some properties, such as grain size, shale content or average porosity. Besides, correlation can be associated to a distance factor between categories (Figure 4.4). There is not a well-established approach on how to define those factors and this point will not be discussed in this research.

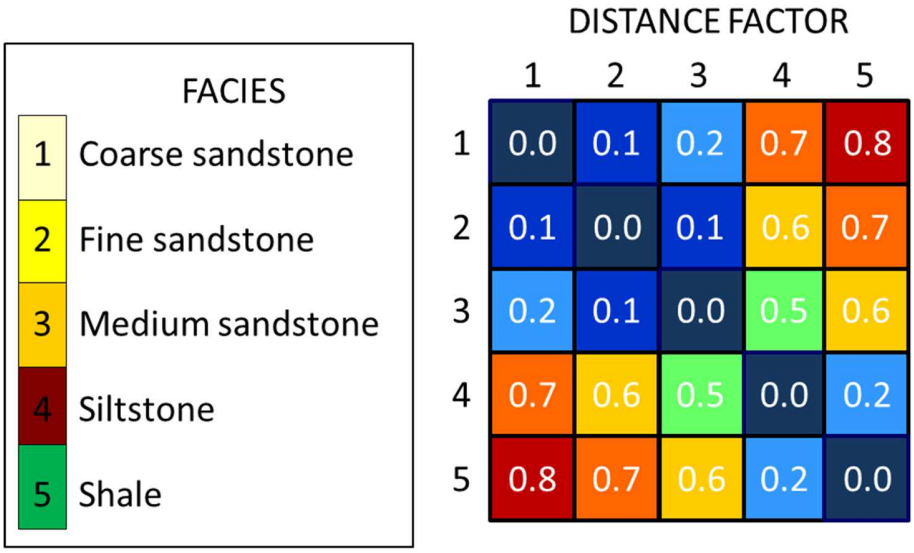

Figure 4.4: Considering five facies defined by grain size, the distance factor is shown on the right. Facies 1, 2 and 3 have high correlation as well as facies 4 and 5.

Let *I* and *I'* be two categorical realizations that are composed of *N* visible grid cells and K different facies. The distance $D_{K(l,l')}$ can be calculated as follows:

$$D_{K(l,l')} = \sum_{m=1}^{N}\{d_f[K_{l,m}; K_{l',m}]\}, \quad l, l' = 1, \dots, L \tag{4.4}$$

where D_K is the spatial distance of categories; *I*, *I'* are two realizations; *N* is the number of visible grid cells and d_f is the distance factor between facies *K* in both realizations at location *m*.

4.3.3 – Ordered Realizations

According to the distance matrix, lower distances, in general, represent similar images while higher distances represent visually different images. Next, a procedure to order the images according to their distances is required. The order or sequence of images should follow a cyclical path going through all realizations to permit continuous visualization of all realizations without any abrupt changes. This is an optimization problem very similar to the famous Traveling Salesman Problem (Flood, 1956). The problem consists in finding the shortest cyclical itinerary for a traveling salesman who must visit each of N cities in turn in a sequential path (Figure 4.5). Simulated annealing (SA) can solve this typical problem.

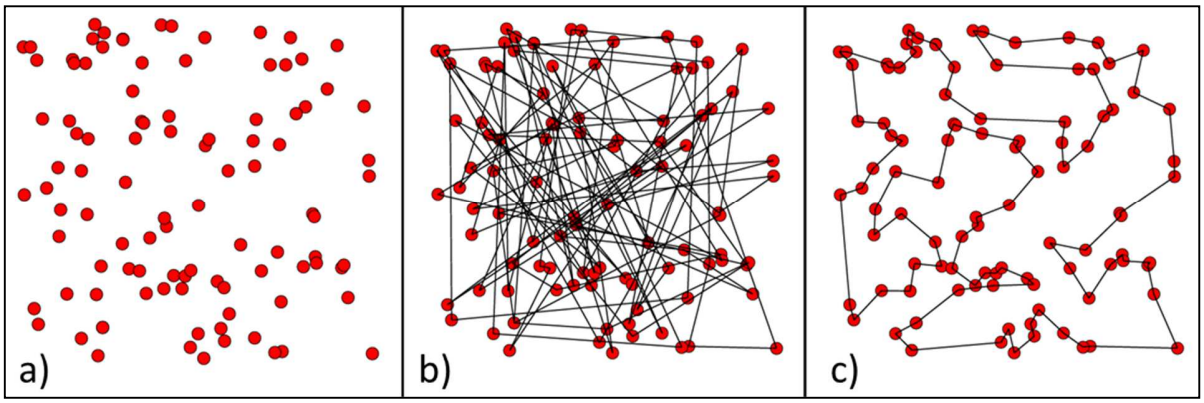

Figure 4.5: Example of a Traveling Salesman Problem - a) consider N = 100 cities; b) a random path configuration; c) a near-optimal solution using simulated annealing procedure (modified from Rossi and Deutsch, 2014).

4.3.4 – Simulated Annealing

Simulated annealing is a classical optimization technique. The central idea is based on an analogy with thermodynamics, specifically with the way liquids freeze and crystallize, or metals cool and anneal. The essence of the process is slow cooling to allow time for redistribution of atoms and avoiding local optima (Kirkpatrick et al., 1983; Deutsch, 1992).

Pyrcz and Deutsch (2014) and Deutsch (1992) explain implementation details of this technique. The SA algorithm changes the system from an initial solution *E1* to a solution *E2* by a given perturbation parameter *t*. The acceptance probability of this new solution is given by:

$$P(E_1, E_2) = \begin{cases} 1, & if\ E_2 \leq E_1 \\ \exp\left(\frac{E_1 - E_2}{t}\right), & otherwise \end{cases} \quad (4.5)$$

where $P(E_1,E_2)$ is the acceptance probability, E_1 is the old solution, E_2 is the new solution and t is the perturbation parameter.

Each iteration forms a random nearby solution. If this solution *E2* is better than the current solution *E1*, it will replace it. If *E2* is a worse solution, it may be chosen to replace the current solution with a probability that depends on the parameter t (Figure 4.6). As the algorithm progresses, the perturbation parameter decreases, giving worse solutions a lower probability of replacing the current solution. According to the physical process of annealing, the perturbation parameter is related to the temperature, which must not be lowered too fast because the system never will achieve the optimum solution.

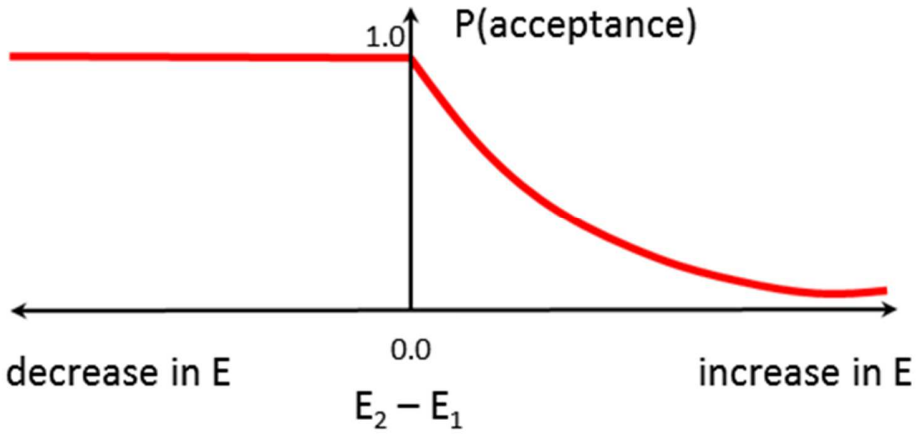

Figure 4.6: Probability of accepting a change to the system in Simulated Annealing. The probability is 1.0 when the objective function decreases and the probability follow an exponential distribution when the objective function increases (Pyrcz and Deutsch, 2014).

The approach shown in Figure 4.5 can be applied to ordering realizations, defining a near-optimum sequence of images based on the distances between all realizations. The path should be reasonable, but need not be strictly optimal. The computational speed of calculating the new

path should be reasonable because it must be recomputed when the visible portion of the model is changed.

4.3.5 – Image Morphing

The images ordered according to the preceding algorithm could be cycled at a specified speed, i.e., setting a transition time between realizations. However, there may be some visually jarring or abrupt changes. The concept of image morphing (Ehlschlaeger et al., 1997) is used to ensure that the transition between images is smooth and cohesive.

Morphing is a special effect in motion pictures and animations that changes (or morphs) one image or shape into another through a seamless transition. Most often, it is used to depict one person turning into another through technological means or as part of a fantasy or surreal sequence. Traditionally such a depiction would be achieved through cross-fading techniques on film. Since the early 1990s, this has been replaced by computer software to create more realistic transitions (Shamsuddin et al., 2012).

The traditional morphing process involves two steps: warping, to align features that appear in both images; changing their shapes; and cross-dissolve their colors, using intermediate images between each two original images (Figure 4.7). The warping step is not necessary for ordering realizations. Possible geological features, such as faults, will be present at the same location on the grid in all realizations. Intermediate images are created using a linear interpolation as shown:

$$\Delta_{ll',m} = \frac{Z_{l,m} - Z_{l',m}}{P+1} \tag{4.6}$$

where *l* and *l'* are two realizations; *P* is the number of intermediate planes to morphing; *Zm* corresponds to the cell value on both realizations at m location.

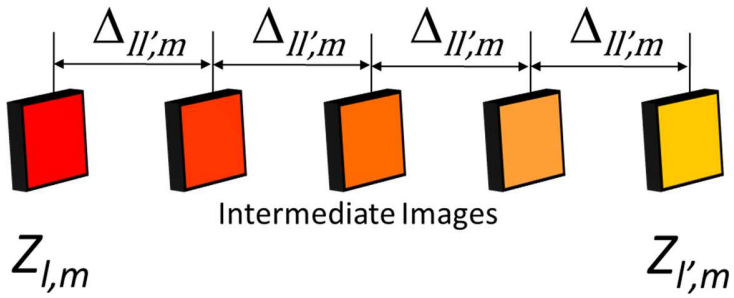

Figure 4.7: Cross-dissolve using linear interpolation to create 3 intermediate images between two original images.

Although the intermediate images are somewhat smooth due to morphing, the realizations are unchanged. In the end, only the realizations are used for calculations and the morphed images are not kept.

4.4 – Synthetic examples

The proposed algorithm is straightforward to code. Two examples considering continuous and discrete realizations are presented below with some results, as well as the CPU time for each step of the methodology. All tests are performed using a CPU Intel Core i7 @ 2.80 GHz and 24 GB of RAM memory.

4.4.1 – Synthetic Example 1 - Continuous property

SGS is used to generate 100 realizations of a continuous variable across a 250 x 250 grid. A limited number of conditioning data are available for this simulation, as displayed in Figure 4.8. Unlike estimation methods, SGS correctly reproduces the statistical characteristics of the conditioning data as well as the spatial continuity of the variable.

A moving window filter is applied before calculating the Euclidean-based distances. The Euclidean-based distance metric is a robust approach for quantifying the similarity between realizations. A relatively simple metric, such as the correlation coefficient between realizations,

is shown in Figure 4.9 for comparison. On average, the correlations are very similar and the comparison between the images is not clear.

CPU time is dependent on the number of realizations and grid cells. A computer time analysis is shown in Figure 4.10. No filtering means that all cells from the grid are used to compute the distance between images. Increasing the window size decreases the distance calculation time while increasing the time to perform the filtering. In this example, considering 100 realizations and a 250 x 250 grid, a window size of 15 minimizes the total runtime to around 60 sec.

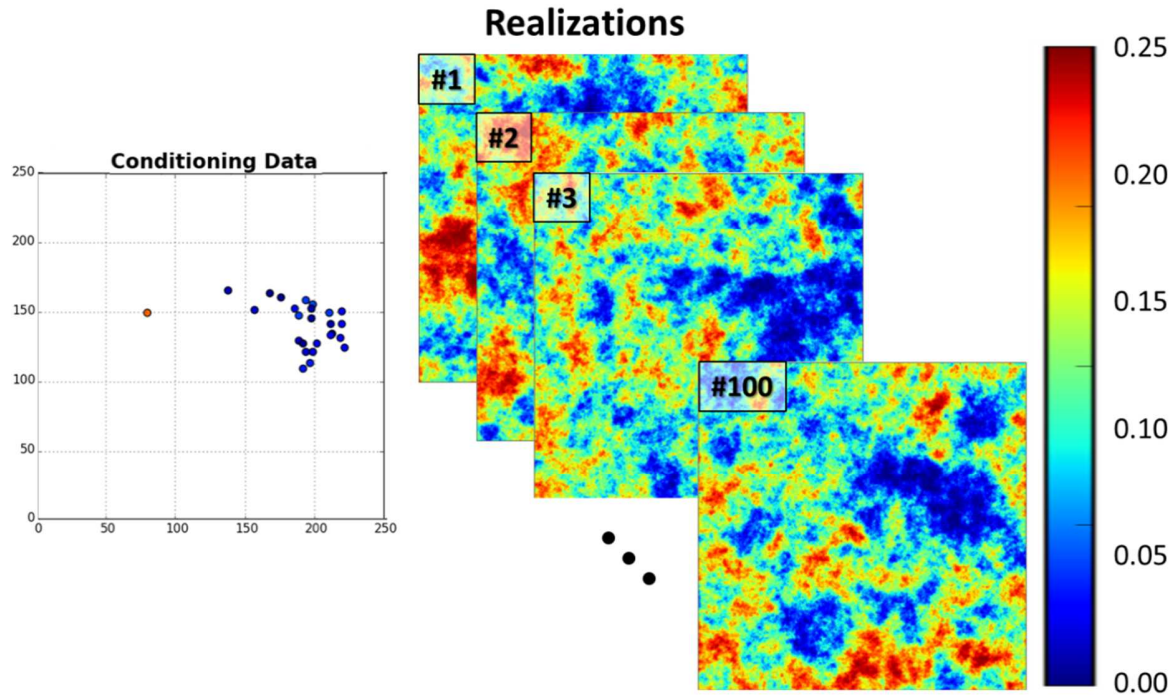

Figure 4.8: Conditioning data used for generating 100 geostatistical realizations in Example 1.

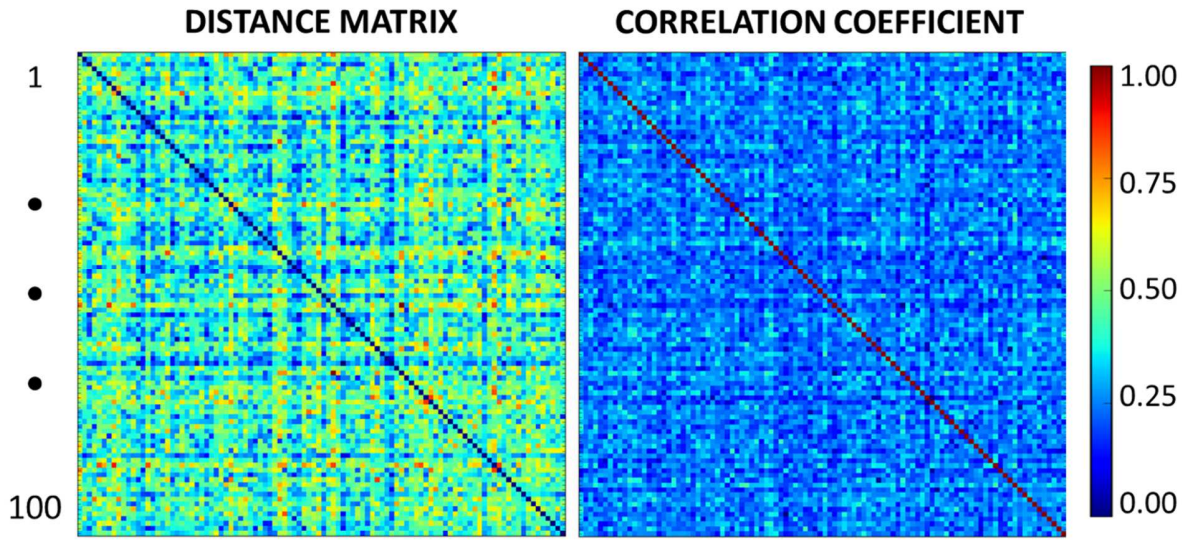

Figure 4.9: Comparison between distance matrix and a simple correlation between realizations. While the distance-based approach presented in this work show a wide range of high and low values, correlation coefficients present a low variation, making it hard ordering the realizations.

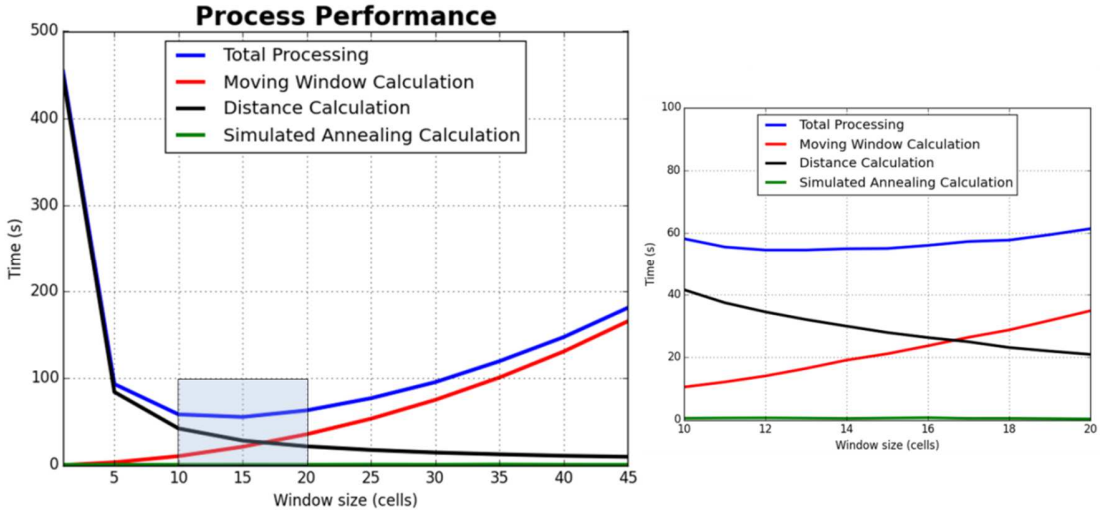

Figure 4.10: Algorithm performance according to time-consuming processes. The window size varies from 1 (no filtering) to 45 cells in the x and y directions. The blue line represents the total time. The red line represents the filtering time. The black line represents the distance calculation time. The green line represents the simulated annealing time. On the right: a detailed view of window size from 10 to 20.

After the simulated annealing algorithm gives the sequence of realizations, image morphing is applied to ensure a smooth transition between the realizations. Tests using 2 to 4 intermediate planes are enough to ensure a pleasant sequence of images (Figure 4.11). Finally, the ordered sequence of realizations creates a dynamic animation that shows all realizations.

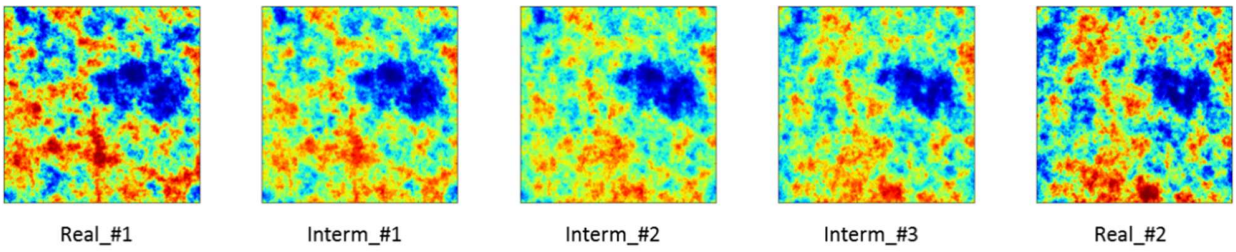

Figure 4.11: Image Morphing Process: Cross-Dissolve between two images. Between two realizations (Real_#1 and Real_#2), morphing process creates some intermediate images. In this case, morphing created three images, preserving the realizations characteristics present in the original images.

4.4.2 – Synthetic Example 2 - Categorical property

This example considers 100 discrete geostatistical realizations of 55 x 100 grid cells with four categories. Figure 4.12 illustrates the distance matrix and a near-optimal solution using the simulated annealing procedure. Three intermediate planes are defined for the image morphing, as shown in Figure 4.13. The moving window-filtering step was not considered in the discrete realizations. In this example, the total CPU time was 35 sec considering a 55 x 100 grid with 100 realizations and 4 categories.

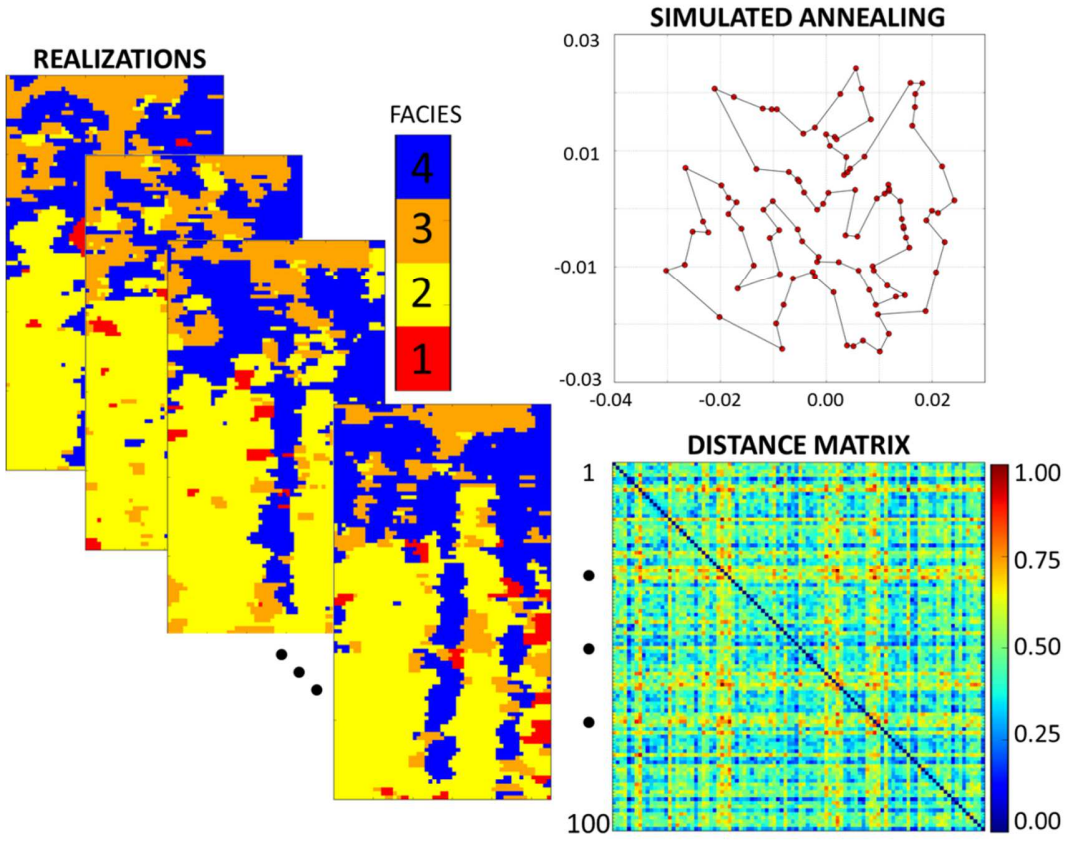

Figure 4.12: Realizations from the set of 100 simulations in a 55 x 100 grid (left) and their locations using MDS (upper right), based on Distance Matrix (lower right). Vertical scale is magnified x20.

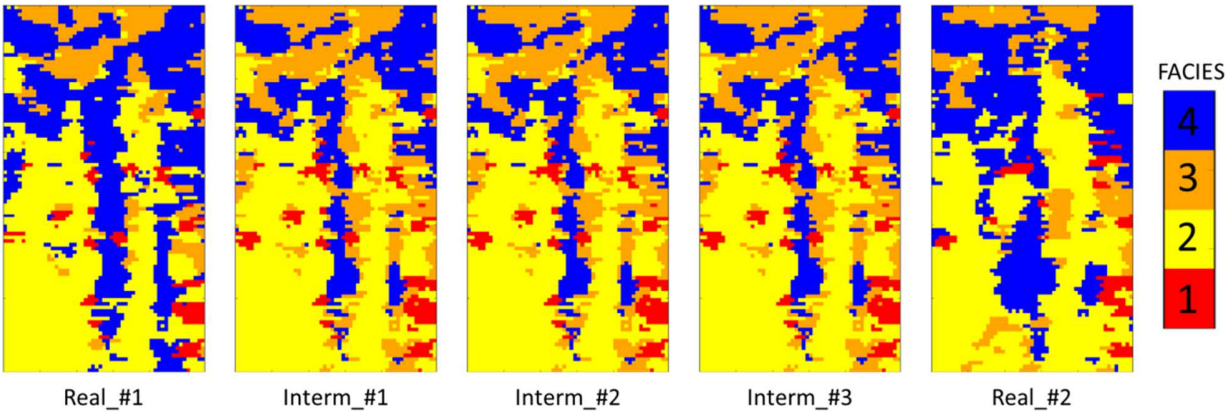

Figure 4.13: Image morphing between two realizations (#1 and #2), using three intermediate images. Vertical scale is magnified x20.

The Euclidean-based distance between the realizations appears reasonable to capture the similarities and differences between the realizations. Other distance measures could be considered including the use of connectivity and other flow-related properties.

Computing the distance between continuous variable realizations is straightforward. On the other hand, a hierarchical ordering of categories should be defined. A geologically reasonable ordering is possible in many cases. However, this may be a limitation when categories do not have an intrinsic ordering. To improve the visualization and consequently the understanding of uncertainty, the color scale must be chosen considering the similarities of the categories.

The animations for each test, showing the proposed ordering, may found on YouTube: https://www.youtube.com/channel/UCi5BiKxmcVlN0dbr5voOEiQ.

4.5 - Discussion

Uncertainty visualization is an emergent subject with several applications in technological areas, mostly in weather forecast and financial analysis. Some of these concepts have been brought to the hydrocarbon industry, adapting them to be suitable for geostatistical realizations.

A novel method to sequentially visualize multiple geostatistical realizations has been presented. The implementation makes it easier to visualize and understand the uncertainty.

According to the proposed methodology, the computational requirements for visualizing and understanding the geological uncertainty over multiple realizations are technically feasible. However, handling all realizations is still complex due to the demands for performing the numerical flow simulations, considering the current computational architecture. The novel architectures in the last few years present an opportunity for increasing the processing speed, which allows handling multiple models.

4.6 - Summary

- Visualizing the uncertainty in an ensemble realizations is a challenge;
- A new method to sequentially visualize multiple geostatistical realizations is presented;
- In the future, the proposed approach should be implemented for any visualization of 3-D geological models into the commercial modeling software.

Chapter 5

Computational Resources for Multiple Realizations

Three-dimensional reservoir models require significant computational resources. Nowadays it is essential to provide a realistic description of the reservoirs, characterizing in detail their petrophysical and dynamic properties, for a good evaluation of the production forecast and its uncertainties.

It is generally believed that models with higher resolution are more accurate regarding reservoir behavior prediction (Avansi et al, 2016; Vakili-Ghahani and Jansen, 2012). Improvements in reservoir data acquisition have increased the complexity of the reservoir model and thus the time required to execute it. Reservoir models must be high resolution and must be fast enough to process for common reservoir management tasks. The computational requirements for history matching and flow simulation are a main reason to avoid dealing with all the realizations all the time.

The purpose of this chapter is to explore some aspects of the reservoir characterization, mainly reservoir simulation, which could offer the computational speedup necessary to enable the hydrocarbon industry to better consider geological uncertainty. The following sections show that the technological challenges are being overcome with the exponential growth of computational performance over last decades. Managing multiple geostatistical models for improving production reservoir forecasts are possible with such advances.

5.1 – Historical Perspective

Since the availability of digital computers to the petroleum industry in the 1950s, hydrocarbon reservoirs have been increasingly studied with the aid of computer programs to simulate the fluid flow through porous media.

The evolution in reservoir simulation over the last 70 years has been due to two major factors: the rise in computational power and the development of new and advanced simulation techniques and software.

Reservoir simulation involves the use of mathematical equations or a computable procedure to obtain some insights into the behavior of a reservoir. Simulation helps to solve complex reservoir problems that cannot be analyzed by other means (Aronofsky, 1988). The flow equations governing reservoir behavior are highly nonlinear and time consuming to solve for real reservoirs. The nonlinear differential equations describing fluid flow are transformed into a set of finite-difference equations that, in turn, are more amenable to numerical solutions. The reservoir is divided into blocks. The division of reservoirs into many blocks provides the opportunity to vary the rock and fluid properties for each block better describing geological heterogeneity. However, for a larger reservoir with millions of blocks, more computer power is needed to formulate a solution strategy and to interpret results (Aronofsky, 1988).

5.1.1 - Evolution of Computer Performance

The earliest computers were little more than adding machines by today's standards (Watts, 1997). The fastest computers available in the 1970s and early 1980s were slower and had less memory than current electronic devices.

Statistics on high-performance computers are of major interest to manufacturers and users. It is important to know not only the number of cores but also the location of the various supercomputers within the high-performance computing community and the applications for which a computer system is being used. Such statistics facilitate the establishment of collaborations, the exchange of data and software, and provide a better understanding of the high-performance computer market.

An early list of supercomputers was published in 1986 (Meuer and Gietl, 2013) and, annually, it has been updated with counts of the major vector computer manufacturers, based principally on those at the Mannheim Supercomputer Seminar. Statistics based merely on the name of the manufacturer are no longer useful, however. New statistics are required that reflect the diversification of supercomputers, the enormous performance difference between low-end and high-end models, the increasing availability of massively parallel processing systems, and the strong increase in computing power of the high-end models of workstation suppliers.

Since 1993, the TOP500 project (http://www.top500.org) has ranked and detailed the 500 most powerful computer systems in the world. The project publishes an updated list of the supercomputers twice a year. The first of these updates coincides with the International Supercomputing Conference in June, and the second is presented in November at the ACM/IEEE Supercomputing Conference. The project aims to provide a reliable basis for tracking and detecting trends in high-performance. The University of Tennessee and the NERSC/Lawrence Berkeley National compile the TOP500 list.

Figure 5.1 shows the growth of the performance of the top supercomputer since 1993. On that year, the 500th fastest supercomputer processed around 800 MegaFlops (Floating-Point Operations per Second) and the fastest supercomputer processed around 100 GigaFlops. In 2018, the computational performance has increased six orders of magnitude. The fastest supercomputer processes 100 PetaFlops (10^{15} Flops) and the 500th supercomputer processes around 1 Petaflop (10^{15} Flops). Generally, it takes six to eight years for a supercomputer to move from position 1 to position 500.

Such growth in computational capacities makes it possible to generate and to deal with multiple reservoir models with hundreds of parameters.

5.1.2 – Computer Memory

The computational capability of a system is dependent not just on the number of calculations that it can perform in a second. It is also important the capability and efficiency of the system for staging data to these calculations. These data include auxiliary tables that need to

be referenced, as well as data produced in the course of calculations that need to be available by the computational units. All this information needed by computation is brought into the memory of the computer. Access to instructions and data must be fast so that the expensive calculating units are well utilized during the program.

Memories have played an important role in computers since the early days of computing. Throughout, the principal use of memories has been to help complete a calculation, whether by storing the input needed for simulation or for transaction processing, holding the intermediate results produced during the course of the calculation, or saving the results of a calculation before they are archived or presented to a consumer (Singh et al., 2018).

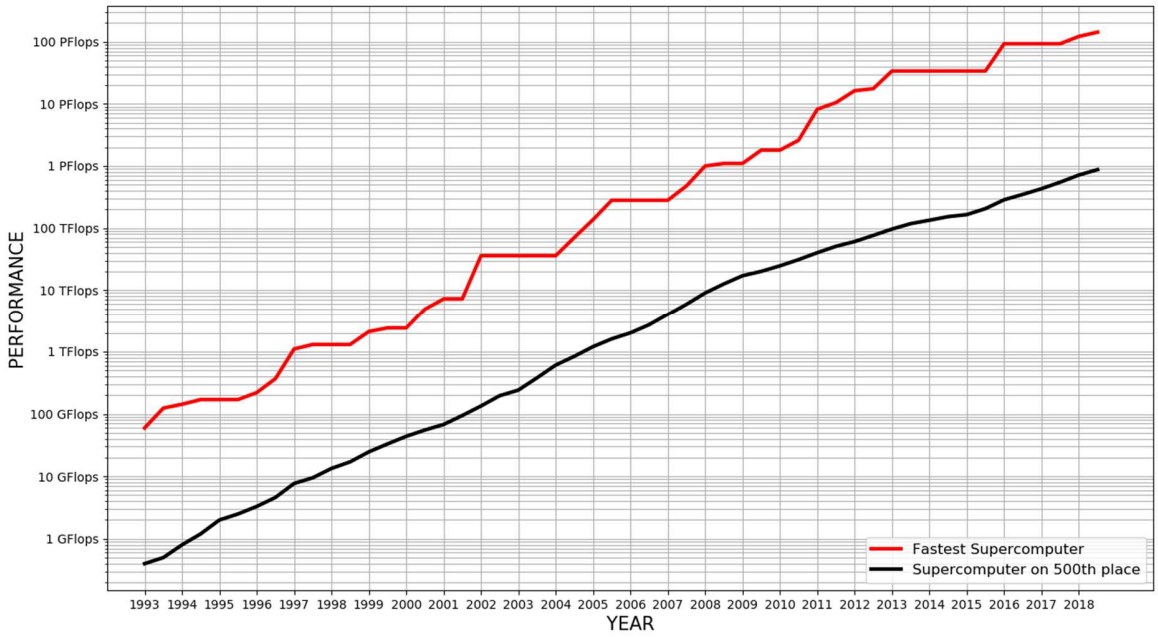

Figure 5.1: Evolution of supercomputer performance according to TOP500 project from 1993 to 2017. The fastest supercomputer performance is in the red line. The 500th supercomputer performance is in the black line. Y-axis is based on Floating-Point Operations per Second (FLOPS).

A steady increase in available memory allows larger and more complex programs to be executed. In the 1970s, the best computers available had only several Megabytes of memory. Today, a regular personal computer could have 4-8 Gigabytes of memory, and parallel supercomputer could have over 50 Gigabytes of memory (Khait and Voskov, 2017).

The needs of computing can no longer be assessed by the requirements of a single computer. Computing today involves processing of data in a large connected world. Paradigms for using and programming computers have changed to keep up with these new requirements, and so has the role of memory.

The role of memory is changing from being a place to store information for a transient calculation to a place where rapidly retrievable information is stored over long periods. There is a perception that moving data across the memory hierarchy is not efficient enough across nodes in large distributed systems. Memories will be called upon to serve data not only from computing elements local to their node but from computing elements located anywhere on a large distributed system (Ahn et al., 2016).

The capacity of a memory chip has steadily increased from 1 kb in the 1970s to 8 Gb nowadays, an eight million-fold increase in nearly 50 years. Such a density allows the total main memory of a system to be as large as 16 Tb in a system (Nair, 2015). Increased memory helps significantly in improving the performance of queries on the databases.

5.1.3 – Computational Reservoir Applications

Over the last 50 years, high-performance computing has had a significant impact on the evolution of numerical predictive methods throughout science and engineering. In particular, petroleum-engineering applications have seen a significant enhancement in capabilities for reservoir simulation engineering. The complexity of geological and reservoir simulation models has led to computational requirements that have consistently challenged the fastest hardware platforms. The increase in grid resolution (Figure 5.2) is linked to the advance in computer hardware technology and the price/performance of the overall hardware platforms (Fjerstad et al., 2005; Cao, 2002, and Watts, 1997).

Early hardware platforms were largely based on mainframes that provided efficient processing but considering coarse models. In the 1960s, the maximum model size was approximately 200 grid blocks. By 1970s, it had grown to approximately 2000 grid blocks (Watts, 1997). The emergence of workstations in the late 80s not only made computing hardware more

accessible to the engineer but also enabled more refined models that more closely resembled geological models. According to Watts (1997) and Cao (2002), the model size in the 1990s was roughly 500,000 grid blocks increasing up to 16 million grid blocks in the 2000s.

The evolution of workstations towards cluster computing emerged as reservoir characterization, and upscaling tools become more advanced and more easily accessible to the engineer. This enabled a step change in grid resolution as existing simulator technologies were migrated towards taking advantage of parallel processing.

According to an important event in the Reservoir Simulation Community, the SPE Reservoir Simulation Symposium – RSS, approximately 20% of papers have mentioned the simulation CPU time since 1995 (Table 5.1).

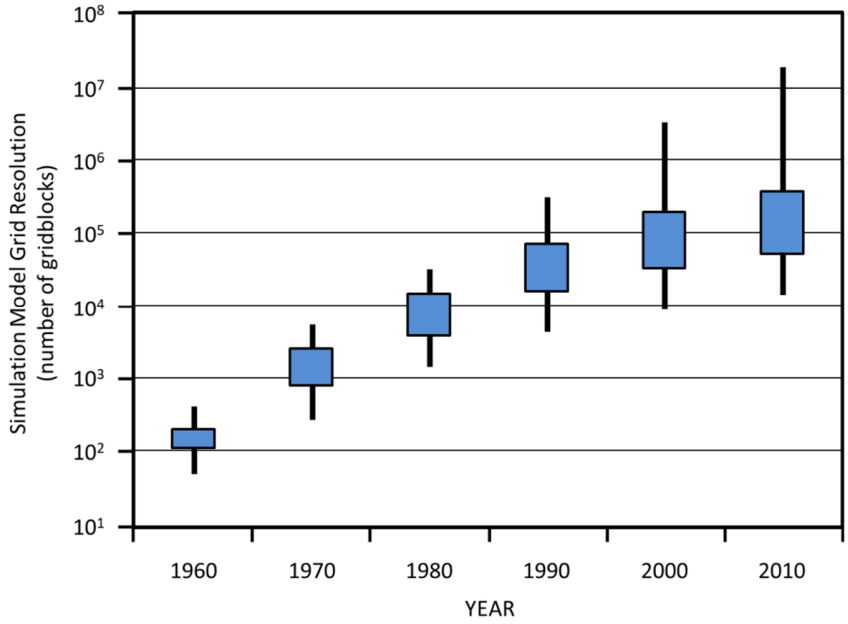

Figure 5.2: Industry trend of model grid resolution (modified from Fjerstad et al., 2005).

Although the computational performance has increased exponentially over the last 20 years, reservoir flow simulation has kept the same runtime as shown in Table 5.1 and Figure 5.3. In this period, runtime flow simulation is nearly 8 hours in average with a standard deviation of around 7 hours. Reservoir models are presenting higher resolution over the time, and flow

modelling is focusing on improving the understanding of the physics of the fluid flow in a porous media.

These numbers show that the computational challenges mentioned have been overcome. Despite the increase in computer performance over time, the simulation runtime is at the same level. The focus has been on making the models more complex and not on transferring geological uncertainty through the decision-making process.

Table 5.1: According to SPE-RSS, the proportion of papers mentioning runtime simulation is approximately 20%. Average runtime is nearly 8 hours with a standard deviation of around 7 hours since 1995.

SPE RESERVOIR SIMULATION SYMPOSIUM

YEAR	PAPERS	REPORTING RUNTIME		RUNTIME(hr)	
				Average	Std. Dev.
1995	37	6	16%	6	6
2005	48	10	21%	7	6
2015	115	23	20%	10	13

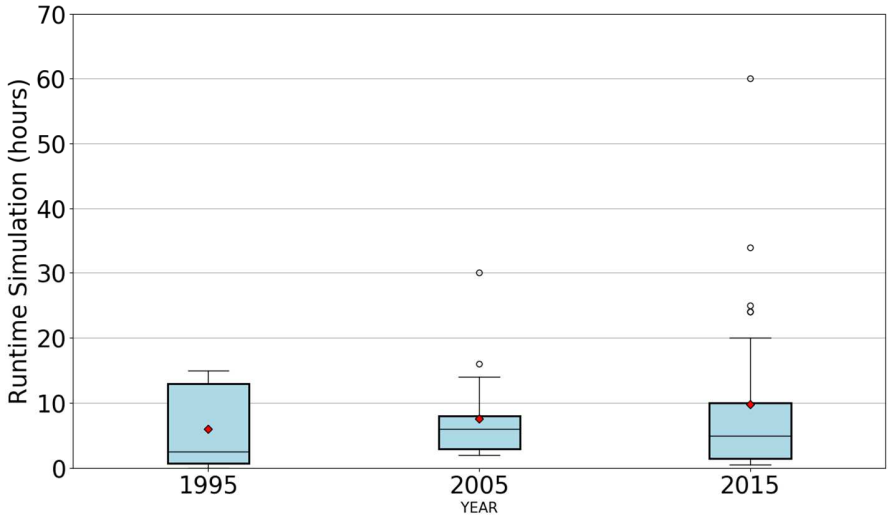

Figure 5.3: Variation of runtime simulation according to the SPE Reservoir Simulation Symposium in three different years – 1995, 2005 and 2015.

5.2 – Computer Demands for Multiple Realizations

The computational time for running a flow simulation is strongly related to the complexity and size of the reservoir model. Even though the computational performance has increased exponentially over the last 20 years, reservoir flow simulation has kept the same runtime on average, as discussed above.

Regarding complexity, the understanding of the subsurface system and the hydrocarbon field is becoming increasingly more sophisticated over the years. Since 1990s, unstructured grids have been used in reservoir modeling, forcing gridblocks to conform to major geological features. Modern reservoir models may have millions of cells with highly complex structures and property distributions. Moreover, the physical models used to represent the dynamic recovery processes have grown in complexity. Physical and chemical processes involved in the understanding the fluid behavior throughout reservoir production are increasingly being incorporated in reservoir characterization. Reservoir simulators should simultaneously handle multiple reservoir production zones, surface facilities and rock mechanics. Examples include compositional representations with large numbers of components, coupled thermal-compositional processes and geomechanical properties. The importance of geomechanical events, such as wellbore stability, hydraulic fracturing, fault-reactivation, early water-cut, top surface subsidence, reservoir compaction and water/gas flooding, has increasingly high impact in the reservoir management.

Up to this point, this research has dealt with black-oil simulation, which corresponds to more than three-quarters of all simulator applications. Black-oil means immiscible flow under conditions either such that fluid properties can be treated as functions of pressure only or as functions of pressure and solution gas/oil ratio (Mattax and Dalton, 1990). Black-oil simulators are inadequate for studies that must account for mixing of fluids having significantly different properties, displacement of oil by miscible or conditionally miscible fluids, displacements involving chemicals that can affect fluid properties, non-isothermal flow or special reactions (Mattax and Dalton, 1990).

Concerning model size, grid resolution has increased over the years (Figure 5.2). Fine-scale geological models often contain tens of millions of cells.

However, such high resolution may not be always required. The common approach before running flow simulator is to upscale a high-resolution geological model to the flow simulation blocks. Such process is not trivial and depends on how complex the models need to be for a given decision process. Caers (2011) discusses how increasing complexity of the models requires more parameters and hence increasing uncertainty since such parameters cannot be deterministically defined from data.

The complexity of reservoir models are increasing over last decades and there are some approaches to evaluate and scoring the level of complexity. However, there is no one unified methodology for evaluating the reservoir model complexity. Several approaches in literature have been created according to different field development conditions. Evaluation of reservoir complexity has previously been used by Dromgoole and Speers (1997) to assess recovery factors in North Sea fields. Their scoring approach is based on nine geological parameters. Nishikiori et al. (2008) uses six scoring parameters, combining both geological and fluid attributes to evaluate reservoir complexity. Wickens and Kelly (2010) correlate recovery factor and reservoir complexity index based on four key parameters. Jia et al. (2016) define a reservoir complexity index applied to heavy oil reservoirs.

5.2.1 – Grid-based Upscaling

The uncertainty in the geological parameters is increasingly taken into account by simulating an ensemble of geological realizations, which significantly increases the computational demands. Despite the rapid increase of massively parallel computing, reducing the number of grid blocks, through upscaling remains a computational necessity.

Grid-based upscaling techniques vary from simple averaging methods on uniform Cartesian cells to sophisticated flow-based techniques on adaptive and unstructured grids. An extensive review of different upscaling methods can be found in Vakili-Ghahani and Jansen (2012), Durlofsky et al. (1997) and Durlofsky (2005).

To illustrate the difference in forecast production response with different model resolution, an example is shown in Figure 5.4. A reservoir model is presented with three grid resolutions and

100 permeability realizations each. The production has been simulated for a period of 4 years. Cumulative production data and production rates are nearly similar for this period (Figures 5.5 to 5.7). More details about the reservoir model can be found in Jansen et al. (2014).

Figure 5.8 shows the correlation of cumulative oil production after four years between the finest grid (120x120x14 cells) and the other ones. Since a high correlation is observed at different grid scales, production data are considered consistent. High values in one scale are also observed at another scale. However, more detailed studies could be done concerning the limitation of upscaling. The response of the finest and the coarsest grids is shifted from the 45-degree line. Such behavior may be an indication that upscaling and numerical dispersion are having an influence.

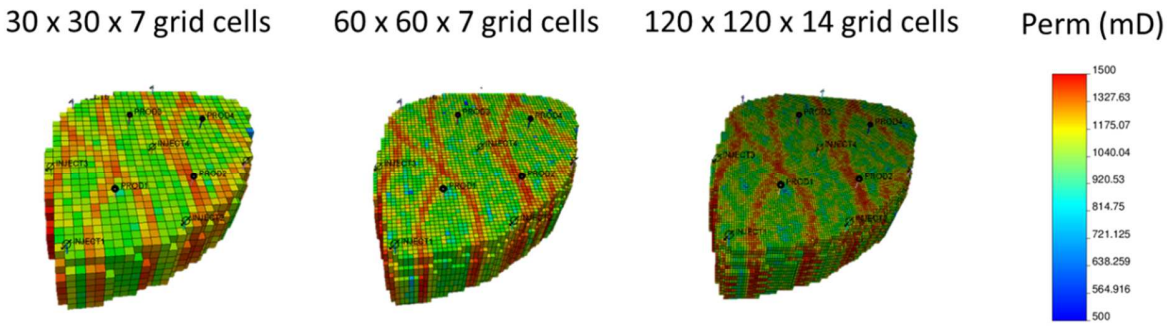

Figure 5.4: Same reservoir model with different grid resolutions have been used to compare the production results after four years. Each model presents 100 permeability realizations.

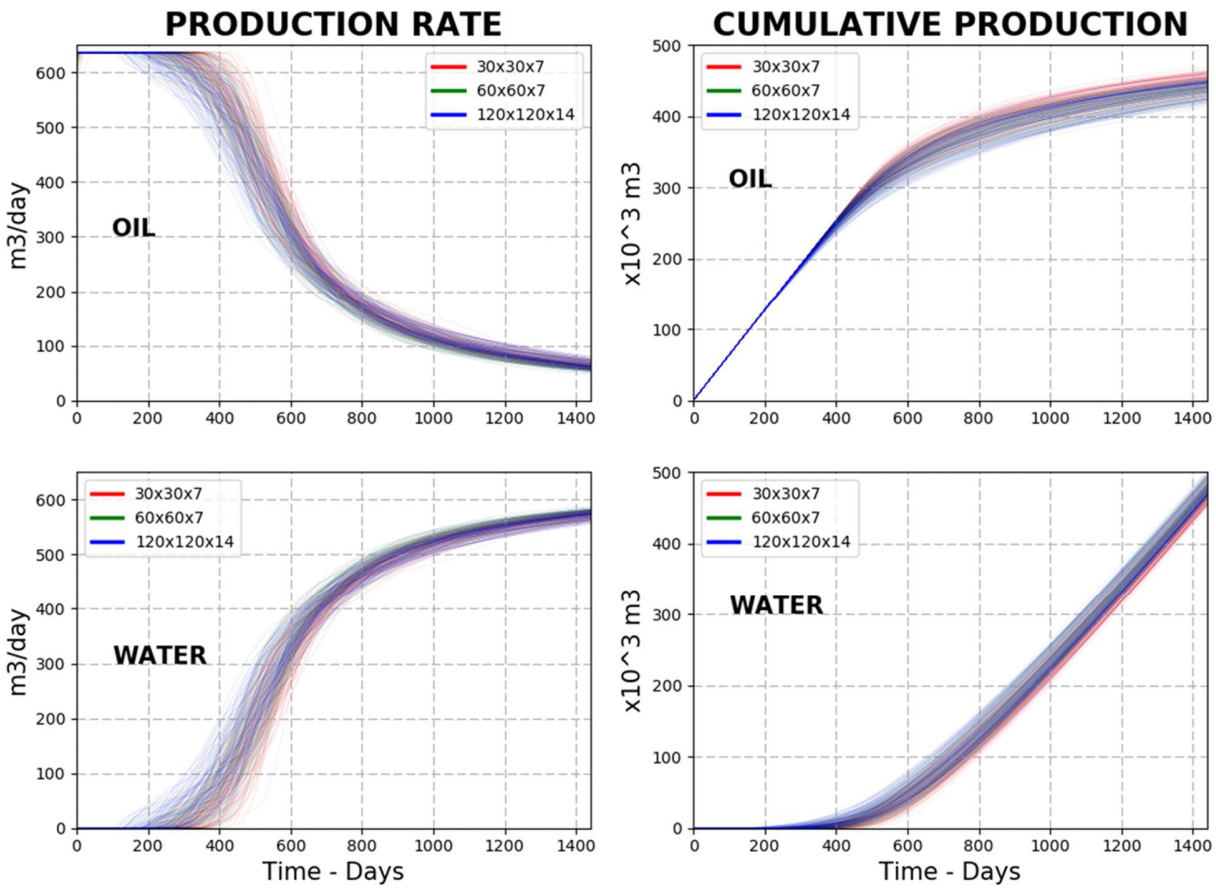

Figure 5.5: Production rate and cumulative production (oil and water) from the three grid resolutions. The simulation period is equal to 4 years.

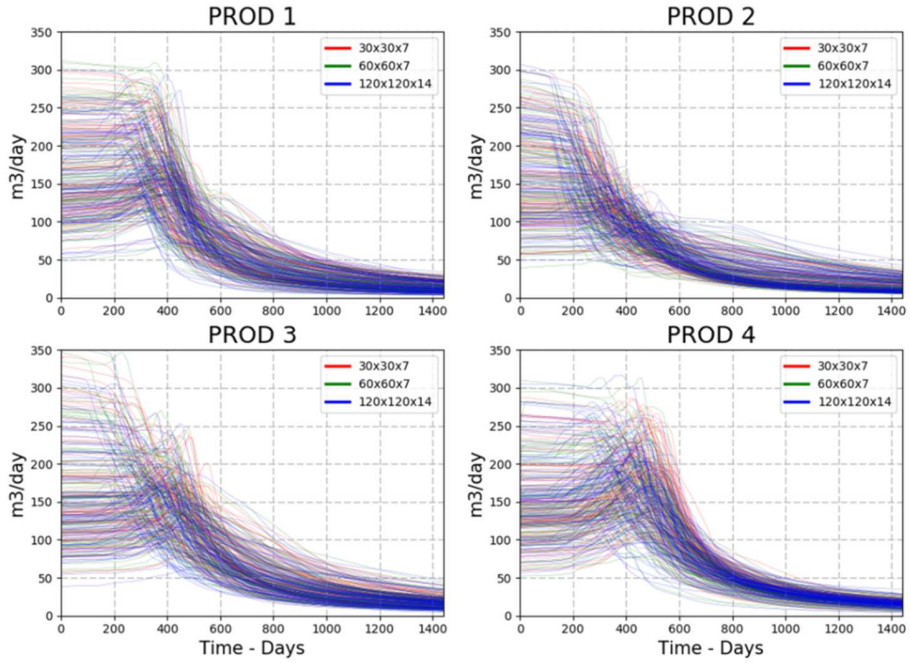

Figure 5.6: Oil production rate by well from the three grid resolutions. The simulation period is equal to 4 years.

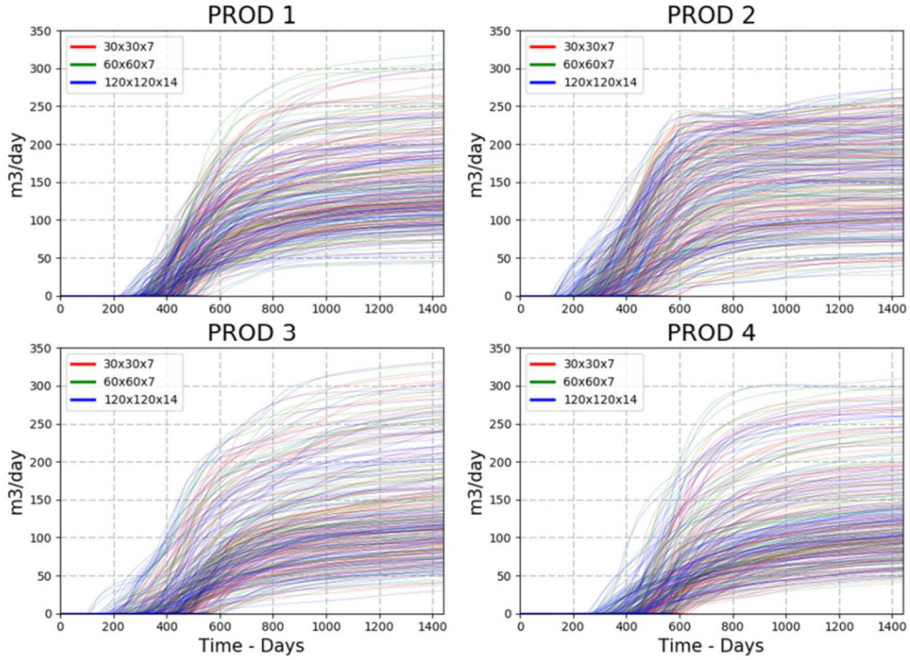

Figure 5.7: Water production rate by well from the three grid resolutions. The simulation period is equal to 4 years.

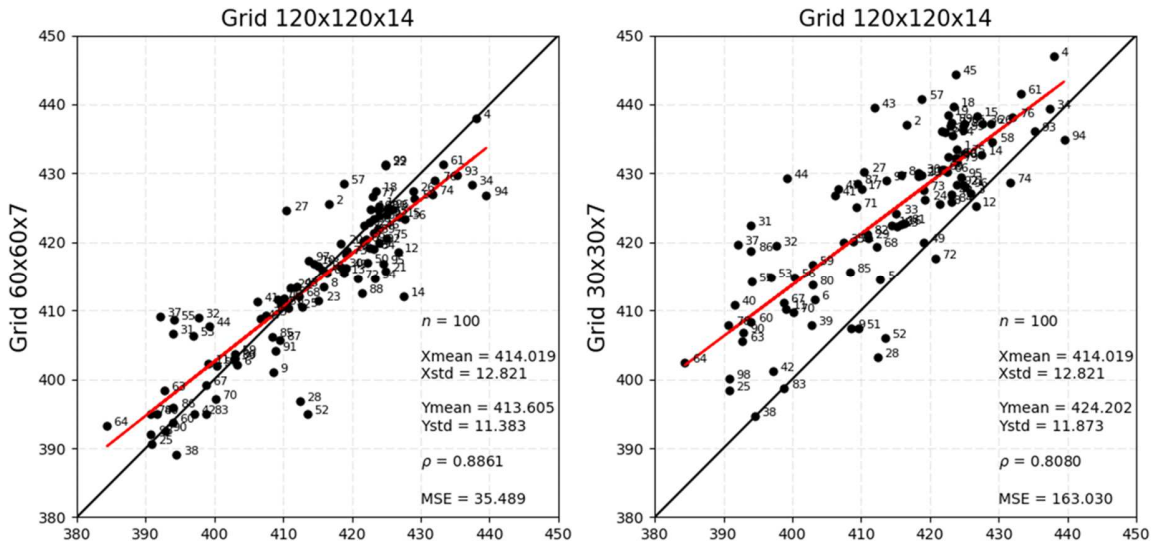

Figure 5.8: Correlation of the cumulative oil production after four years among the three grid resolutions. Black dots correspond to the realizations at different grid resolutions.

Considering 100 realizations for each grid resolution, the reduction of flow simulation runtime is roughly two orders of magnitude, as shown in Figure 5.9. Simulation responses show consistent results at all grid resolutions, dealing with multiple realizations in shorter simulation time.

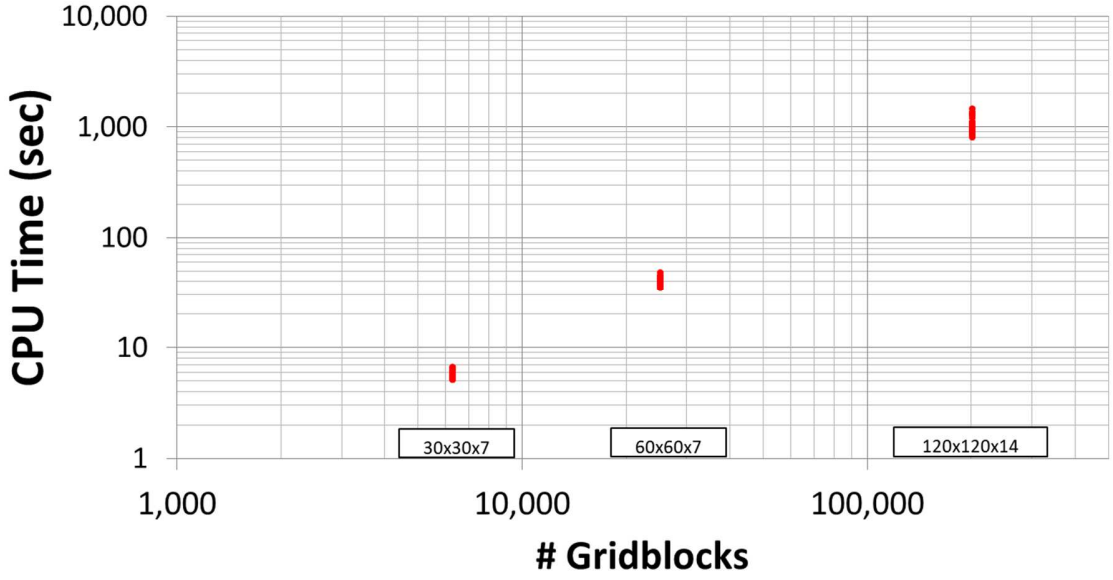

Figure 5.9: Simulation time for 100 realizations considering different grid resolutions.

This section illustrates one simple alternative to making fast decisions over multiples realizations. Changing the reservoir grid resolution by upscaling techniques is a current approach for performing flow simulation in many companies. The precision and robustness of the upscaling techniques is quite dependent of the complexity of the reservoir. The upscaled properties should be checked in order to keep the consistency and quality of the results in different grid resolutions. This enables the efficient simulation of multiple realizations, as is required for uncertainty quantification.

5.3 – Discussion

The problem of efficient utilization of computational resources according to the growing demands in the quality and details of 3D reservoir models. The efficiency of modern computer systems exhibit continuous growth due to increasing numbers of computational cores. High-performance hardware costs are decreasing every day, and hardware-software systems that were extremely expensive just a couple of years ago can be purchased for a reasonable price. Taking into account the availability of multi-CPU computers, we should pay more attention to the software side in order to utilize all computational resources in parallel simulations. Due to outdated software architecture, most common reservoir simulators skip most of the available computation power.

This chapter have discussed that the reservoir simulation time can be efficiently scaled on the modern CPU-based computers and clusters. Simulation time can be reduced considering extra computational power. The combination of CPU and GPU architectures present the most impact in the computational simulation performance. In addition to the number of cores (CPUs), GPUs present a significantly greater memory bandwidth, which is equally important for efficient parallel simulations as it is effectively the speed of communication between the cores. According to Telishev et al. (2017), the mostly of the total time spent on the linear solver iterations is due to limited memory capabilities to provide the cores with data to handle. The authors mention the bandwidth of the GPU models has grown to 700 GB/s since 2015, while the CPU bandwidth values remain one order of magnitude lower.

The choice of hardware options for handling multiple realizations should be made carefully with account for specific model features, especially the grid size, computational power, amount of memory, and number of realizations. The variety of options has become wider as the costs of GPUs become cheaper and equally more efficient and powerful.

The current level of detail and complexity of reservoir models requires a high computational cost. Such large computer demand is one of the main reasons to avoid correct management of the ensemble of geological realizations.

Some alternatives are discussed in this chapter to overcome such limitations, furthering the transfer of geological uncertainty throughout reservoir management. Recent advances on the computational performance support the premise to managing multiple realizations. Parallel architecture with multiple cores and GPUs has been recently applied in reservoir simulation.

To improve the reliability of reservoir predictions, historical pressure data and production rates should be incorporated into the reservoir models. This history matching process is another challenge for handling multiple geological realizations.

5.4 – Summary

- The computational requirements for HM and flow simulation are a main reason to avoid dealing with all the realizations;
- Although the complexity of reservoir models are increasing over last decades, the exponential growth of computational performance allows considering multiple models;
- Parallel architecture with multiple cores and GPUs are already been applied in reservoir simulation, allowing the industry to consider whole geological uncertainty in reservoir decisions.

Chapter 6

Flow Simulation Considering Multiple Realizations

Although many realizations can be generated by geostatistical simulation, reservoir simulation commonly considers just a few models. The main reason to avoid managing multiple realizations in flow simulation is the excessive computational requirements to perform the history matching for each reservoir model. Since HM is an optimization problem, hundreds or possibly thousands of flow simulations may be required to find a match (Thiele et al., 2010). Regardless of computer demands, history matching is conventionally done on a single model. Changes to one model may not be the same as another. However, the recent advances in computational performance described in Chapter 5, and the developments in the ensemble-based HM techniques, encourage the use of a large number of reservoir models to improve the production forecasts.

6.1 – Current Practice in Flow Simulation

In general, the underlying geostatistical model is assumed to be fixed (Gautier and Noetinger, 2004). In practice, the geostatistical parameters are estimated using geological information and statistical analysis of the available static petrophysical data. Global and local adjustments are done to the model properties so that the production response of the reservoir model matches field observations (Abdollanzadeh et al., 2013). These properties are mostly derived from static data since information from dynamic data may be lacking and indirect measurements of rock properties.

There are many initiatives trying to integrate dynamic data into geological modeling (Deutsch, 1993; Yadavalli et al., 1994; Holden et al., 1995; Gautier and Noetinger, 2004; Zheng et al., 2007; Hamdi et al., 2011; Hamdi, 2014). Data from well-test analysis (WTA) may be available at the time of geological modeling. However, there is no established methodology to incorporate such data into the reservoir modelling workflow. Other initiatives include identifying flow paths and barriers and interwell communications on the basis of fluctuations in production and injection rates (Mirzayev and Jensen, 2016; Bouffin and Jensen, 2010; Yousef et al., 2006).

One of the main reasons to avoid managing multiple realizations in flow simulation is the excessive computational requirements for performing HM for each reservoir model. The following sections will discuss some recent advances in reservoir engineering In order to facilitate considering the ensemble of geological models in HM, resulting in a more robust uncertainty assessment for reservoir management and decision-making.

6.2 – History Matching

The process of conditioning the geological model to production data is typically known as HM. The economic viability of a hydrocarbon project is greatly influenced by the reservoir production performance under current and future operating conditions (Satter and Iqbal, 2015). One goal of HM is to assign values to the parameters such that the mathematical model of the reservoir reproduces the observed behavior during the prediction period. The true usefulness of the model, however, is a result of its ability to predict future behavior with increased confidence.

HM is a type of inverse problem. Instead of using a set of variables to predict the reservoir performance (forward problem), HM uses observed reservoir behavior to estimate the variables that caused the behavior (Oliver and Chen, 2011). Many reservoir parameter combinations may result in equally good matches to the historical observations. Although a single HM model may be useful, the better solution to a HM problem would include an assessment of uncertainty in reservoir properties and in reservoir predictions.

With the development and popularization of geostatistics in the petroleum industry in the mid-1980s and early 1990s, a large number of realizations could be easily generated instead of a single estimate.

These advances have increased the research effort on HM. The large number of model parameters significantly increases the dimensionality of the inverse problem, but is often necessary for characterization of the reservoir and for matching well production history. The ultimate goal of HM has changed from finding a single correct set of model variables to finding multiple HM models that can be used for uncertainty quantification of future reservoir performance (Oliver et al., 2008).

HM can be framed as finding an ensemble of reservoir model variables that is the solution to the forward model that predicts reservoir behavior, according to the observed data and their uncertainties. The choice of model parameters for HM involves judgment and an understanding of reservoir processes. Common parameters involved in HM are pressure, water oil ratio, water gas ratio, water and gas arrival times, etc.

The production data used in HM corresponds to a series of measurements of flow rate or pressure data, made in producing and injecting wells. Since the production observations are made at well locations, such data are usually quite limited in number. Although the measurements are repeated frequently and the amount of production data for a field can be quite large, the information content is often relatively low. These factors imply that some discrepancies may occur between the forward model parameters and the observed data.

HM usually requires numerous iteration runs that make this procedure computationally costly. According to Carlson (2006), HM is the phase that takes up the largest portion of study time. It is not only difficult to solve but it is also a challenging inverse problem leading to non-unique predictions.

6.2.1 - Manual History Matching

Manual HM is the process based exclusively on manual perturbations to preselected HM parameters. There is no standardized method of how to conduct a manual HM (Gilman and

Ozgen, 2013). Manual HM requires that the reservoir model run the entire historical period to establish a comparison of the model to the known performance of the field. Once differences are established, some adjustments are performed in the simulation model in order to improve the match (Ertekin et al., 2001). For every adjustment, the simulation model is rerun and the resulting model performance assessed. Experience is valuable since it increases the understanding of reservoir mechanics and allows one to identify possible changes that might improve the match (Mattax and Dalton, 1990; Gilman and Ozgen, 2013).

According to Oliver and Chen (2011), manual HM methods can often result in an acceptable match to field performance, and even to the production of key wells. However, it is very difficult to obtain acceptable matches for the entire field. Moreover, regional multipliers are often used in manual HM, and the attempt at a detailed HM typically results in a loss of geological realism and thus very limited prediction power.

6.2.2 – Assisted History Matching

Manual HM can be a time-consuming process and may take significant time to yield even one acceptably matched model for large fields (Thiele et al., 2010; Oliver and Chen, 2011),

Assisted history matching (AHM) relies on non-linear optimization techniques in order to achieve a best fit between observed and calculated data (Mattax and Dalton, 1990). Generally, AHM methods can be categorized into gradient methods, stochastic methods, and data assimilation methods.

In gradient methods, use is made of local gradients to drive the parameter choice toward values that minimizes some measure of the difference between observed and calculated data. Gradient methods are usually fast, but have the disadvantage that they are easily trapped in local minima and thus may not give the best HM (Oliver and Chen, 2011; Cancelliere et al., 2011).

Stochastic algorithms incorporate a random component and, by allowing the search to move toward worse solutions occasionally, gain the ability to seek out the global optimum. Genetic algorithms (Romero et al., 2000; Erbas and Christie, 2007), gradual deformation (Hu,

2000; Le Ravalec and Noetinger, 2002), and neighborhood algorithm (Subbey et al., 2003), are some examples of stochastic algorithms that have been deployed in AHM.

In data assimilation algorithms, the model parameters are calibrated in a sequential process, with new observations updating the best estimate of the model state, including the unknown model parameters (Abdollahzadeh et al., 2013). Markov chain Monte Carlo (MCMC), randomized maximum likelihood (RML), and ensemble Kalman filter (EnKF) are some examples of data assimilation algorithms. Liu and Oliver (2003); Cancelliere et al. (2011); and Gao et al. (2016) have presented some comparisons of these algorithms.

Data assimilation methods are especially important for uncertainty assessment since they provide multiple solutions and will be discussed in the following section.

6.2.3 – Ensemble-based Techniques

Ensemble-based HM techniques employ an ensemble of initial realizations of the reservoir properties that consistently honor the static and dynamic data, while capturing the model uncertainty (Saetron et al., 2015). A set of initial model realizations honoring static data is generated using standard geostatistical techniques. The dynamic data conditioning is conducted using the correlations provided by the ensemble. Although these methods present robust and efficient solutions to the shortcomings of the traditional approach to HM, the ensemble-based techniques could be numerically unstable (Perrone et al., 2017). A proper parameterization and regularization constraint is proposed to mitigate these numerical issues (Oliver and Chen, 2011; Saetron et al., 2015).

The number of applications of ensemble-based HM techniques is quite large with successful results (e.g., Evensen et al., 2007; Haugen et al., 2008; Cominelli et al., 2009; Zhang and Oliver, 2011; Emerick and Reynolds, 2013; Chen and Oliver, 2014; Emerick, 2016). The advantages attributed to these methods include the computational efficiency, the ability to work with large dimensions and the ease of implementation (Canchumuni et al., 2017).

Many recent developments in HM are associated with the application of the EnKF whose development is previously reviewed by Aanonsen et al. (2009). EnKF provides a way to generate

simultaneously multiple history matched models that approximately characterize the uncertainty.

EnKF is a Monte Carlo based technique for data assimilation (Aanonsen et al., 2009). This technique implements an ensemble of model states and approximates the covariance matrices sequentially in time as new observations become available. Diverse applications of EnKF have been successfully used for HM of some real petroleum reservoir models (Vallhs and Naevdal, 2009; Zhang and Oliver, 2011; Gao et al., 2016; Abadpour et al., 2018).

Some spurious and erroneous correlations may be introduced by EnKF, leading to ensemble spread underestimation and eventually ensemble collapse (Emerick and Reynolds, 2010; Bocquet and Sakov, 2014). Alternative implementations have been proposed to address some of these deficiencies, such as covariance localization (Emerick and Reynolds, 2011; Chen and Oliver, 2010), iterative EnKF (Li and Reynolds, 2009, Sakov et al., 2012), and ensemble smoother (Chen and Oliver, 2012; Emerick and Reynolds, 2013; Bocquet and Sakov, 2014). Although each of these approaches has been applied in the industry, none has emerged as the dominant method of choice.

The ensemble-based HM techniques allow overcoming the challenge of considering all geological realizations in the decision-making process since this approach generate and ensemble of multiple matched models.

6.3 – Sequential Gaussian Simulation with Rejection Sampling

As discussed above, ensemble-based techniques, such as EnKF, provide an ensemble of matched models. This creates the opportunity of considering all reservoir geostatistical realizations for forecasting and decision-making processes.

Dynamic data such as WTA and production history are valuable information that could be used to improve the geological models. Appendix A provides a detailed description about WTA and the equations to calculate the average permeability (K_{avg}) and the radius of influence (r_i). This research presents an alternative to the ensemble-based techniques in order to incorporate

dynamic data into the geological modeling workflow. The information from WTA, K_{avg} and r_i, are applied to the SGS algorithm using rejection sampling.

The idea behind the proposed methodology is running SGS just inside a region of interest around the input data location. The area is equivalent to r_i defined by WTA. For each realization performed around the data location, an average simulated value (Sim_{avg}) is calculated and compared with K_{avg} from the input data. If the difference between both values is greater than a previously defined tolerance error, the realization is rejected, otherwise the realization is kept. It has been assumed that the inner radius of the wellbore is very small compared to the radius of investigation and can be neglected for the proposed methodology.

According to the SGS algorithm, the previous simulated values are used to perform the next data location. Since the regions around all input data location have been simulated, the rest of the grid is filled. Figure 6.1 shows the proposed simulation workflow.

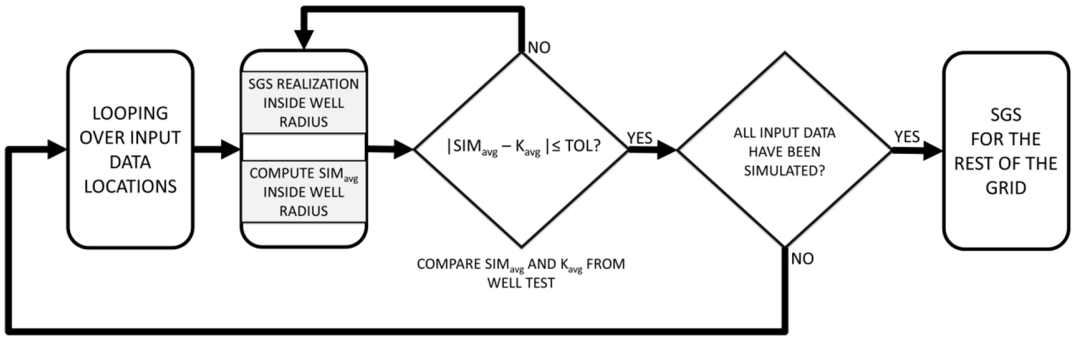

Figure 6.1: Proposed simulation workflow considering average permeability from well test data.

Although the rejection sampling technique presents some similarities with screening approach, both methods are quite distinct. Realization screening approach usually applies some measure of performance over the ensemble of realizations. The goal is to group the realizations into categories or sets with similar responses. Only a few realizations from each set must be select for a detailed study.

In this research, a single realization is simulated at a time. So, the average of this realization is compared with the average property from WTA. Another realization is simulated just if the previous one is rejected, i.e. the difference is greater than the tolerance error.

6.3.1 - Implementation

The proposed algorithm is implemented in the ***sgsim_rej*** software, based on the traditional ***sgsim*** (Deutsch and Journel, 1992). An example of the parameter file with parameter is detailed in Figure 6.2.

There are two differences in the parameter files between the traditional ***sgsim*** and the ***sgsim_rej*** program. Line 6 corresponds to the columns in the data file, including parameters from WTA: K_{avg}, inner and outer radius (see Figure 6.3 and Figure 6.4). Line 37 is the tolerance error, i.e., the acceptable difference between Sim_{avg} and K_{avg} computed within the r_i from the input data.

```
1                  Parameters for SGSIM_REJ
2                  ************************
3
4   START OF PARAMETERS:
5   welldata.dat       -file with data
6   1 2 0 3 0 0 4 5 6  -X,Y,Z,vr,wt,sec.var,well.avg,inrad,outrad
7   -4.0  4.0          -trimming limits
8   1              -transform the data (0=no, 1=yes)
9   sgsim.trn          -file for output trans table
10  1                  -consider ref. dist (0=no, 1=yes)
11  nscore.out         -file with ref. dist distribution
12  2  0               -columns for vr and wt
13  0.000   0.350          -zmin,zmax (for tail extrapolation)
14  1   0.000          -lower tail option (1=linear), parameter
15  1   0.350          -upper tail option (1=linear), parameter
16  0                  -debugging level: 0,1,2,3
17  sgsim.dbg          -file for debugging output
18  sgsim.out          -file for simulation output
19  100                -number of realizations to generate
20  256 0.5 1.0     -nx,xmn,xsiz
21  256 0.5 1.0     -ny,ymn,ysiz
22  1   0.5 1.0     -nz,zmn,zsiz
23  6069               -random number seed
24  0.000   0.350          -min and max original data for sim
25  24                 -number of simulated nodes to use
26  1                  -assign data to nodes (0=no, 1=yes)
27  1     3            -multiple grid search (0=no, 1=yes),num
28  0                  -maximum data per octant (0=not used)
29  120.0   120.0   30.0       -maximum search radii (hmax,hmin,vert)
30  0.0 0.0 0.0     -angles for search ellipsoid
31  0   0.60    1.0     -ktype:0=SK,1=OK,2=LVM,3=EXDR,4=COLC,corr&VRF
32  lvmfl.dat          -file with LVM, EXDR, or COLC variable
33  1                  -column for secondary variable
34  1   0.00           -nst, nugget effect
35  1 1.00 0.0  0.0 0.0   -it,cc,ang1,ang2,ang3
36    50.0 50.0 1.0       -a_hmax, a_hmin, a_vert
37  0.05               -tolerance error
```

Figure 6.2: Example of parameter file to run ***sgsim_rej*** program.

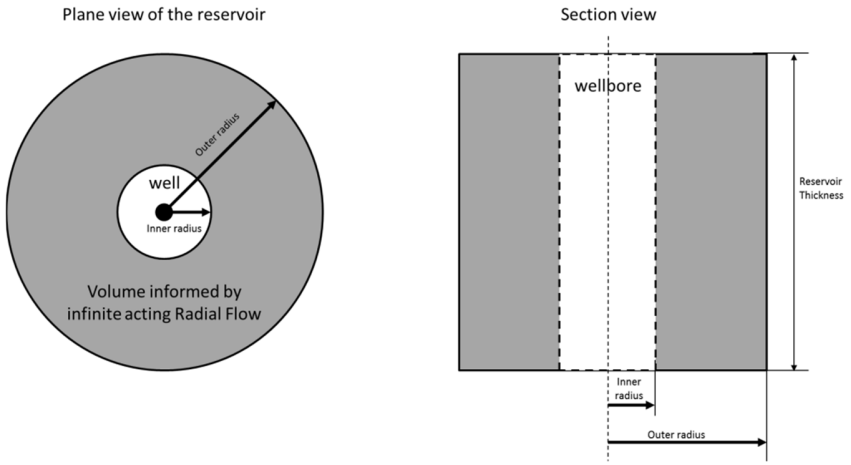

Figure 6.3: Reservoir plane view showing inner and outer radius from well test and the area of influence (on left). Section view shows the reservoir thickness considered to calculate the average permeability (on right).

```
1   Input data
2   6
3   Coord X
4   Coord Y
5   Property at Data Location
6   Avg Property
7   InnerRadius
8   OuterRadius
9    50.0   56.0  0.24   0.125  3.030.0
10 200.0  156.0  0.27   0.135  3.035.0
11 220.0   56.0  0.20   0.165  3.040.0
12 100.0  125.0  0.19   0.150  3.020.0
13  30.0  206.0  0.31   0.280  3.015.0
```

Figure 6.4: Data file for ***sgsim_rej*** program. Each row corresponds to a well and contains the coordinates, the property value, the K_{avg} from WTA as well as the inner and outer radius (r_i).

6.3.2 – Synthetic Example

A synthetic 2-D model is represented by 256 x 256 x 1 regular grid blocks with 10m dimension in X and Y directions and 5m dimension in Z direction. Five wells are randomly located in the grid, as shown in Figure 6.5. Table 6.1 presents the well parameters.

Table 6.1: Well parameters for the synthetic example. The two last columns are related to the WTA.

Input data	Perm at data location (mD)	Kavg (mD)	r_i (m)
1	1000	955	30.0
2	1125	1063	35.0
3	833	688	40.0
4	792	625	20.0
5	1292	1167	15.0

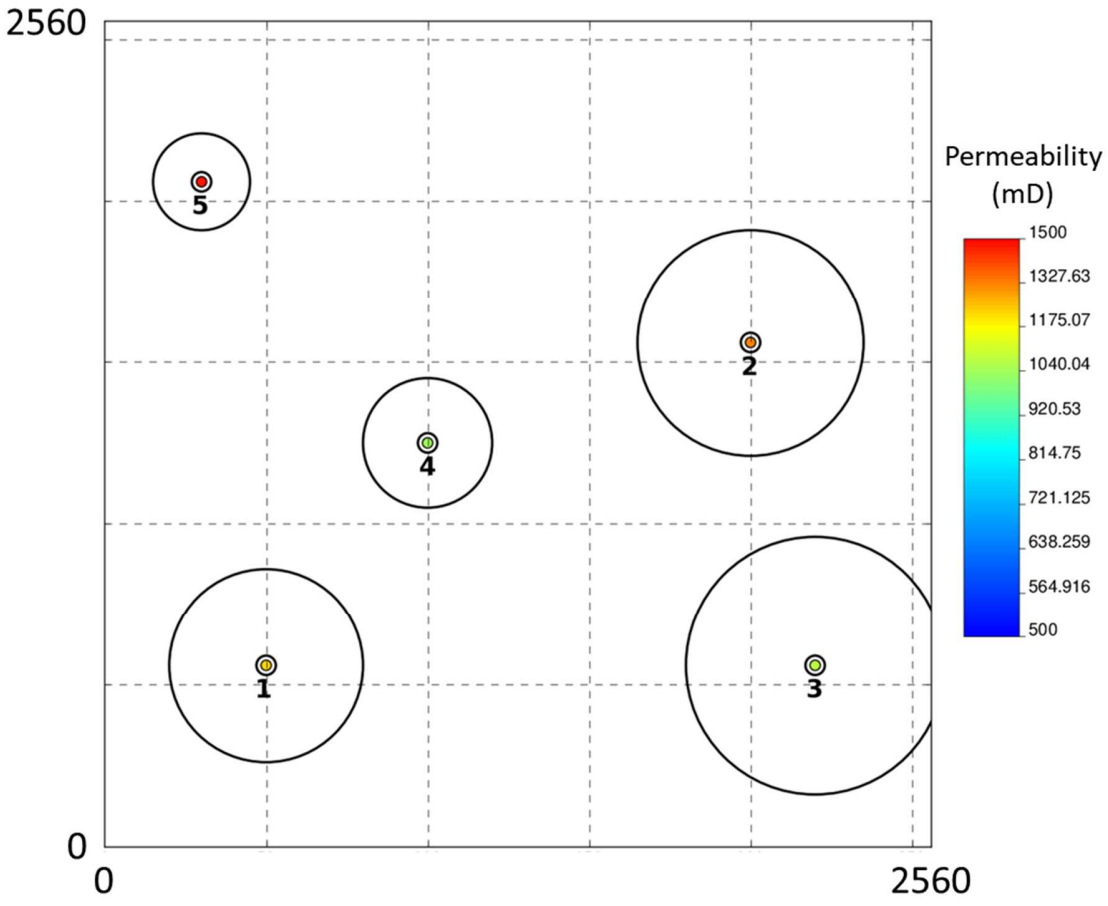

Figure 6.5: Example of 256 x 256 grid with five input data with different r_i.

SGS is performed just inside the area on the input data (Figure 6.6). In this approach, the average inside this area (Sim_{avg}) for each realization is compared with the K_{avg} according to the tolerance error defined in the parameter file. A realization is rejected if the difference is higher than the tolerance error, otherwise, the realization is kept and the simulation is performed in the next input region.

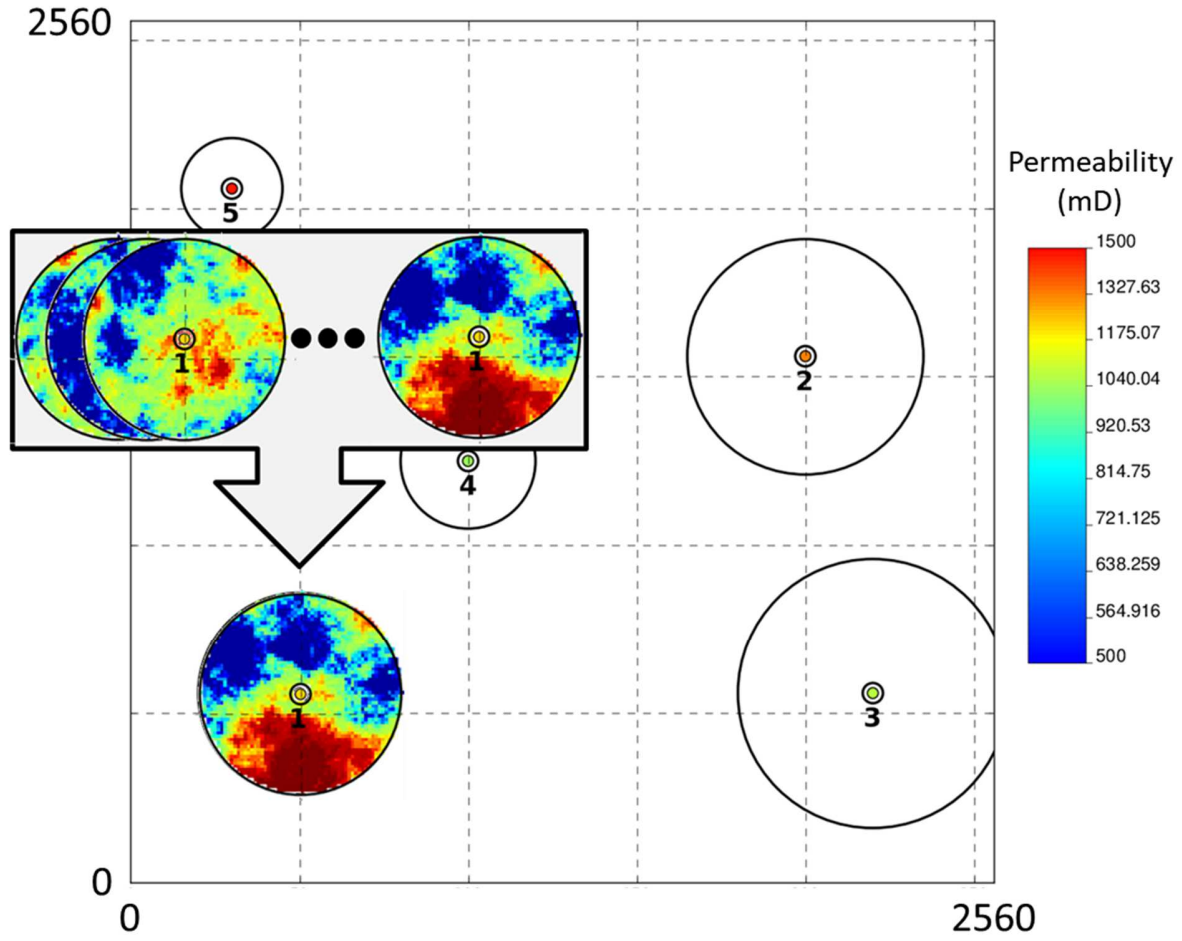

Figure 6.6: Set of realizations around the data location 1 and comparison with K_{avg}. Information of K_{avg} and r_i are obtained from WTA. If the average of the realization inside the radius of investigation matches with K_{avg}, the realization is kept.

The algorithm simulates all areas around the input data. Next, SGS is performed in the rest of the grid (Figure 6.7). One hundred realizations have been generated considering this workflow. At the end of the process, all realizations are compatible with the WTA.

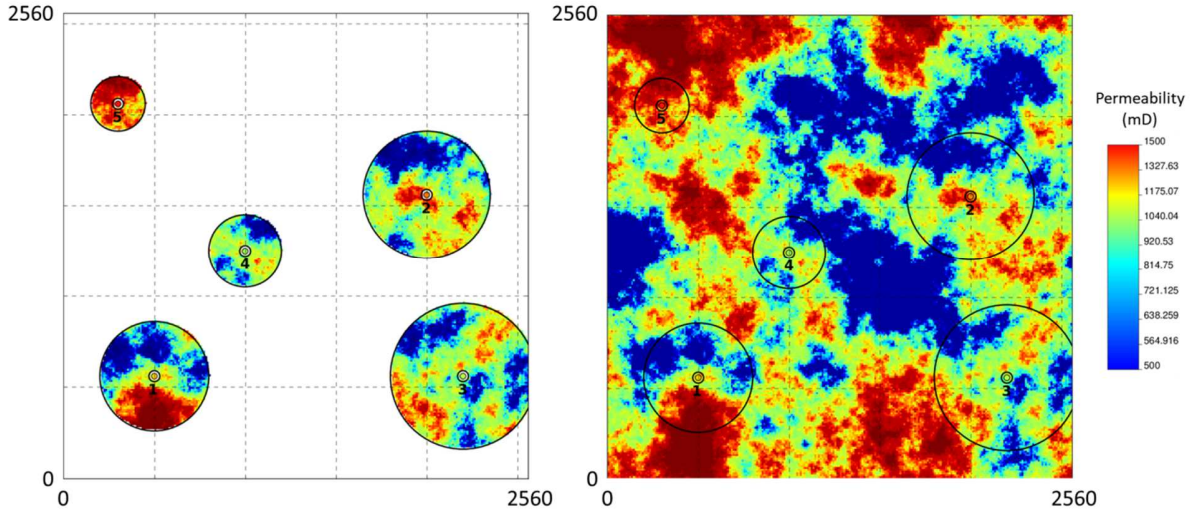

Figure 6.7: Simulated values around input location (on the left) and the complete simulated grid.

A 24 hours drawdown test on each well location has performed in the ensemble of realizations to simulate a WTA. The goal is validating the proposed algorithm. Table 6.2 summarizes the results of the average permeability and the radius of influence of the test. The simulated values show a good match with the information from WTA.

Table 6.2: Average permeability and radius of influence over 100 realizations for each input data, comparing with data from WTA.

Input data	SGS_{avg} (mD)	K_{avg} (mD)	r_i avg **(m)**	r_i (m)
Well 1	969	955	30.3	30.0
Well 2	1087.45	1063	35.3	35.0
Well 3	681.64	688	39.72	40.0
Well 4	627.77	625	20.17	20.0
Well 5	1166.14	1167	15.07	15.0

Figures 6.8 to 6.12 show the variation of the BHP from each well, as well as the derivative plot of the drawdown tests.

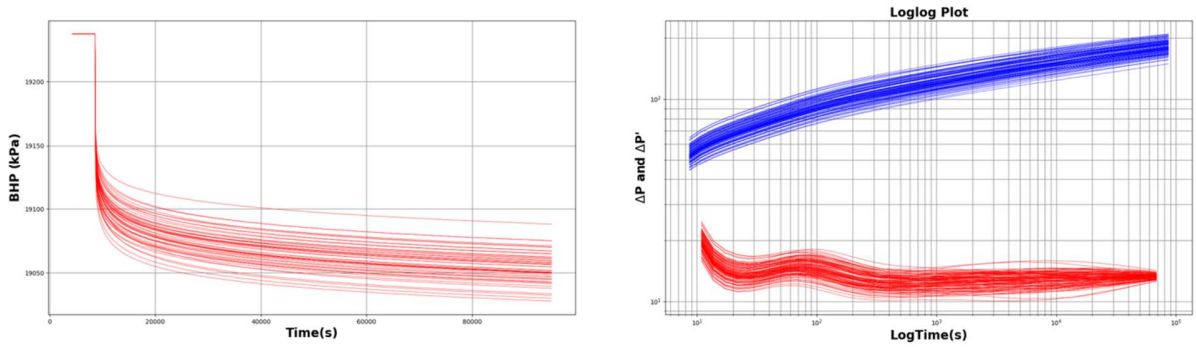

Figure 6.8: Bottom-hole pressure and derivative plot of the drawdown test from Well 1.

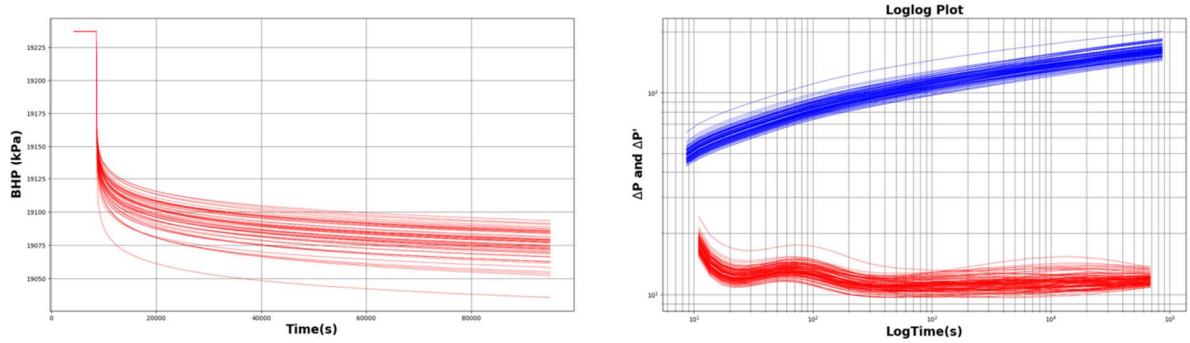

Figure 6.9: BHP and derivative plot of the drawdown test from Well 2.

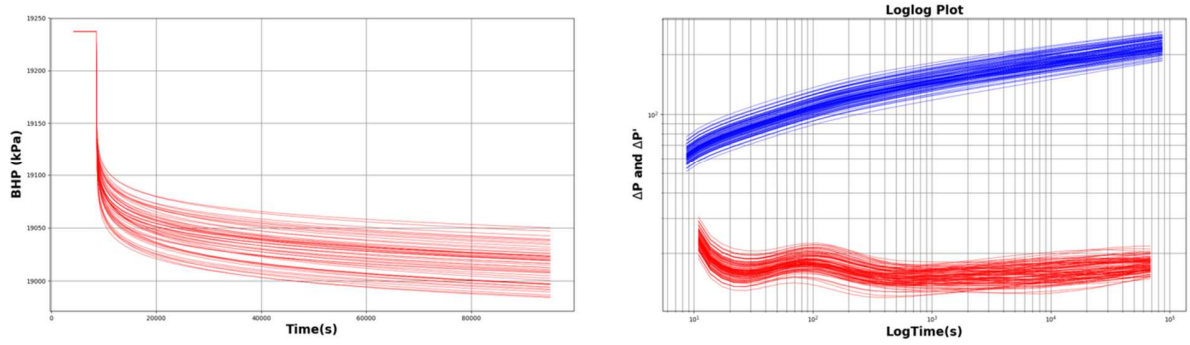

Figure 6.10: BHP and derivative plot of the drawdown test from Well 3.

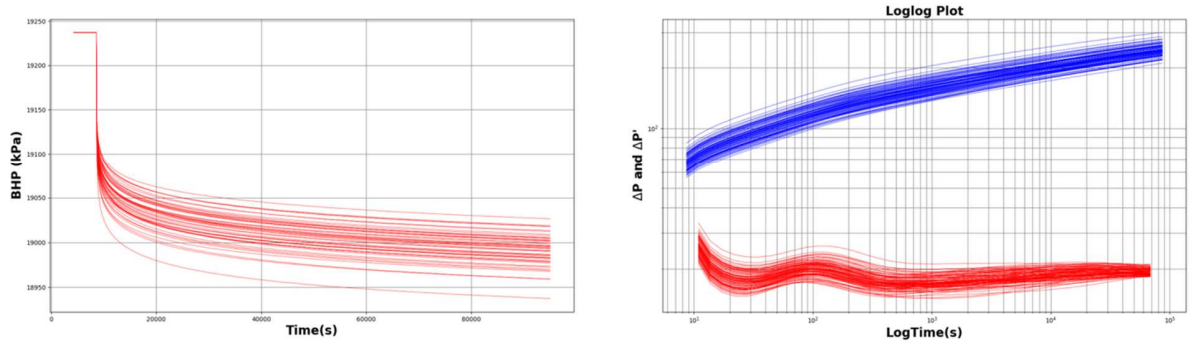

Figure 6.11: BHP and derivative plot of the drawdown test from Well 4.

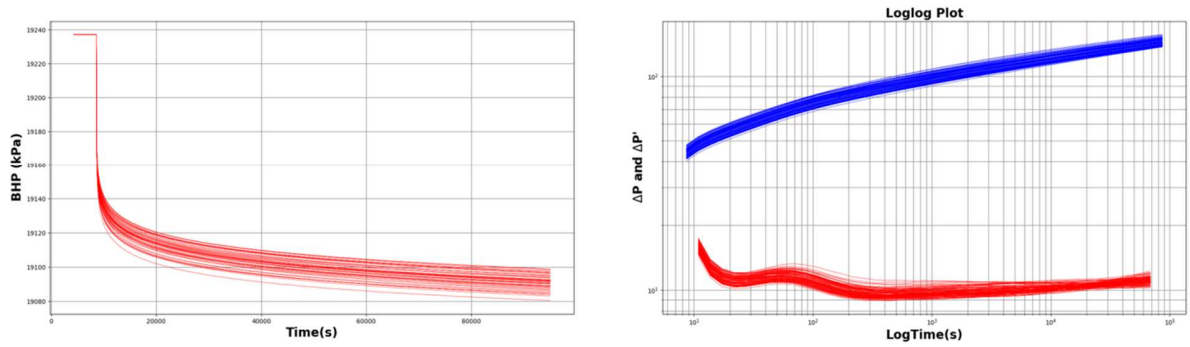

Figure 6.12: BHP and derivative plot of the drawdown test from Well 5.

Figures 6.13 to 6.17 show the distribution of the average permeability and the radius of influence calculated for each well location over all realization. The red dashed line in the histograms represents the value from WTA.

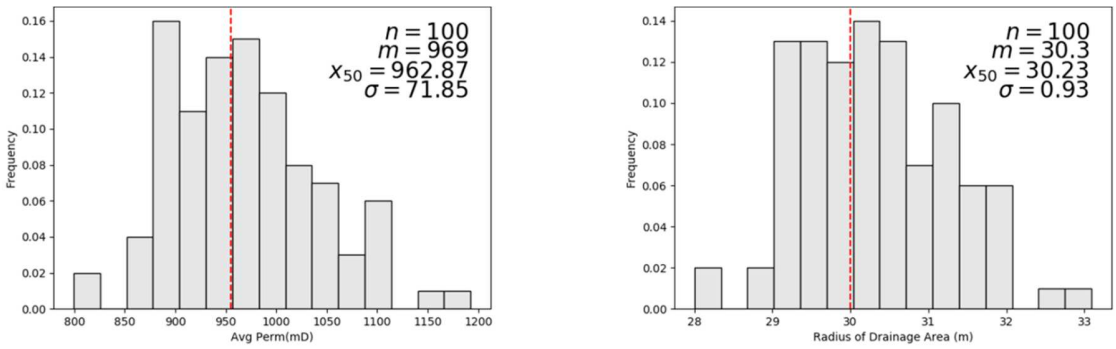

Figure 6.13: Distribution of the average permeability and radius of influence calculated over all realizations in Well 1.

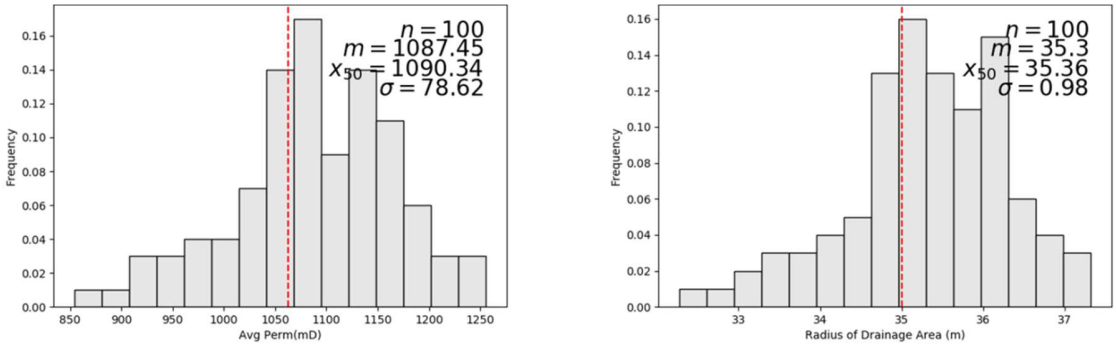

Figure 6.14: Distribution of the average permeability and radius of influence calculated over all realizations in Well 2.

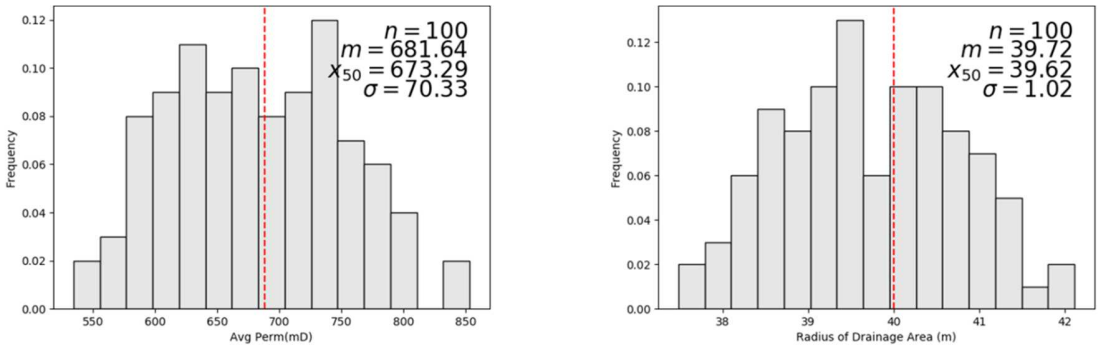

Figure 6.15: Distribution of the average permeability and radius of influence calculated over all realizations in Well 3.

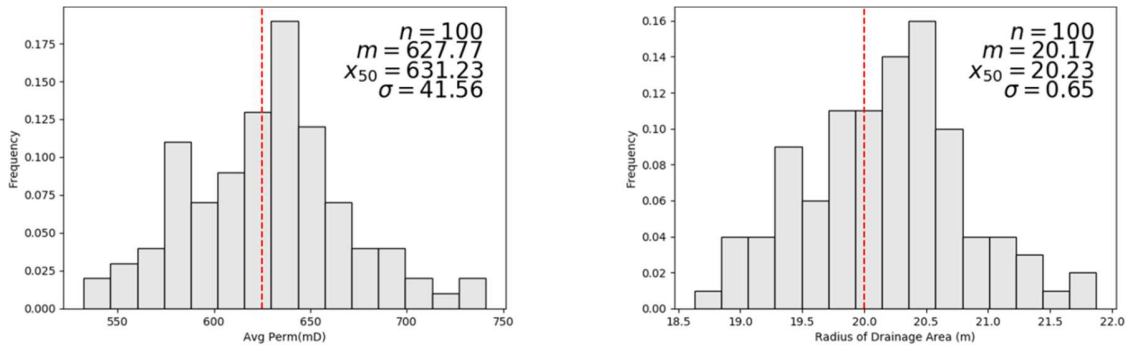

Figure 6.16: Distribution of the average permeability and radius of influence calculated over all realizations in Well 4.

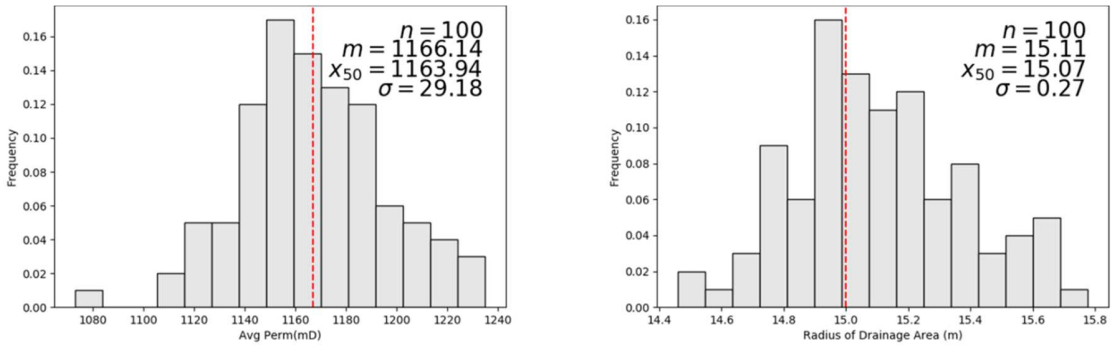

Figure 6.17: Distribution of the average permeability and radius of influence calculated over all realizations in Well 5.

Data should be consistent at all scales. High continuity properties must be reflected in the large-scale data. In this case, the definition of cell size has a significant impact in the proposed methodology. Geostatistical simulation considers the value of input data valid for the whole cell location. Large-scale data should represent an area larger than cell size to maintain the data consistency. The reservoir management team must reconsider the model parametrization for any discrepancy of different data scales.

6.4 - Discussion

HM is an inverse problem, with many possible results for a single reservoir model. It is a very time consuming process and that is the main reason that prediction over multiple models is

still a challenge in reservoir management. Deterministic solutions have been preferred and the reservoir uncertainty has been neglected by older techniques.

However, a variety of ensemble-based methods is presented in this chapter. This demonstrates that it is possible to generate multiple consistent and reservoir models, honoring both geological and production data, and capturing the reservoir uncertainty.

An alternative approach to integrate WTA data into the geological modeling workflow is developed in this chapter. The proposed methodology is able to condition an ensemble of reservoir models to the available static and dynamic data, while preserving the geological consistency.

Consistent integration of geological and dynamic data by ensemble-based techniques or the proposed methodology allows more accurate uncertainty quantification, which helps reservoir management decisions.

6.5 - Summary

- HM is conventionally done on a single model since numerous iteration runs are usually required to perform this procedure;
- The ensemble-based HM techniques encourage the use of all realizations since an ensemble of multiple matched models are generated;
- An alternative technique to incorporate dynamic data into the geological modeling workflow is presented;
- The information from WTA are considered in the SGS algorithm for estimating the reservoir properties;
- The ensemble of realizations is generate conditioned to the static and dynamic data, keeping the geological consistency.

Chapter 7

Case Study

The consideration of all realizations in reservoir management is presented in previous chapters. Some synthetic examples have been presented to compare the approach to the P50 model paradigm. Computational and practical limitations have been discussed in order to overcome the challenges.

This chapter presents the application of the proposed methodology, considering all realizations, in a reservoir case study. The P50 model and all realizations approaches are applied in the Brugge benchmark (Peters et al., 2010). The impact of considering all realizations in the decision-making process is discussed, as well as the visualization of multiple realizations.

7.1 – Background

A 3-D dataset for the Brugge field is available with properties of North Sea Brent type reservoirs (Zhang et al., 2018). According to Peters et al. (2010), the field dimensions are approximately 10 km x 3 km x 60 m. The structure consists of an east/west elongated half-dome with a large boundary fault at its northern edge (Figure 7.1). The Brugge field consists of four main reservoir zones, from bottom to top: Schie, Waal, Maas, and Schelde (Chen and Oliver, 2010). There is no continuous shale barrier between the reservoir zones. The field has been developed by 20 vertical producer wells and 10 vertical injector wells.

According to Chen and Oliver (2010), every well has multiple completions that correspond to the different reservoir zones. The field was produced without individually controlling different completions in the first 10 years. The injectors are constrained by water-injection rate, and the

producers are constrained by fluid-production rate. BHP at the 30 wells and oil- and water-production rates at 20 producers are provided monthly.

Originally, the high-resolution model consists of 20 million grid cells, with average cell dimensions of 50 m x 50 m x 0.25 m. The grid was populated with the essential properties for reservoir simulation: facies, porosity, permeability, net-to-gross ratio and water saturation. The geological model is upscaled to a 450,000-grid-cell model. The simulation model shared in the literature is a further upscaled model to 139 x 48 x 9 gridblocks. The total number of active cells is 44,550. Table 7.1 shows the average reservoir properties and the depositional environment of the four reservoir zones. The Schelde Formation corresponds to the top two layers (layers 1 and 2) of the simulation model; the Maas Formation corresponds to layers 3, 4 and 5; the Waal Formation corresponds to layers 6, 7 and 8; and Schie Formation corresponds to layer 9. The Waal Formation is the major producing reservoir zone.

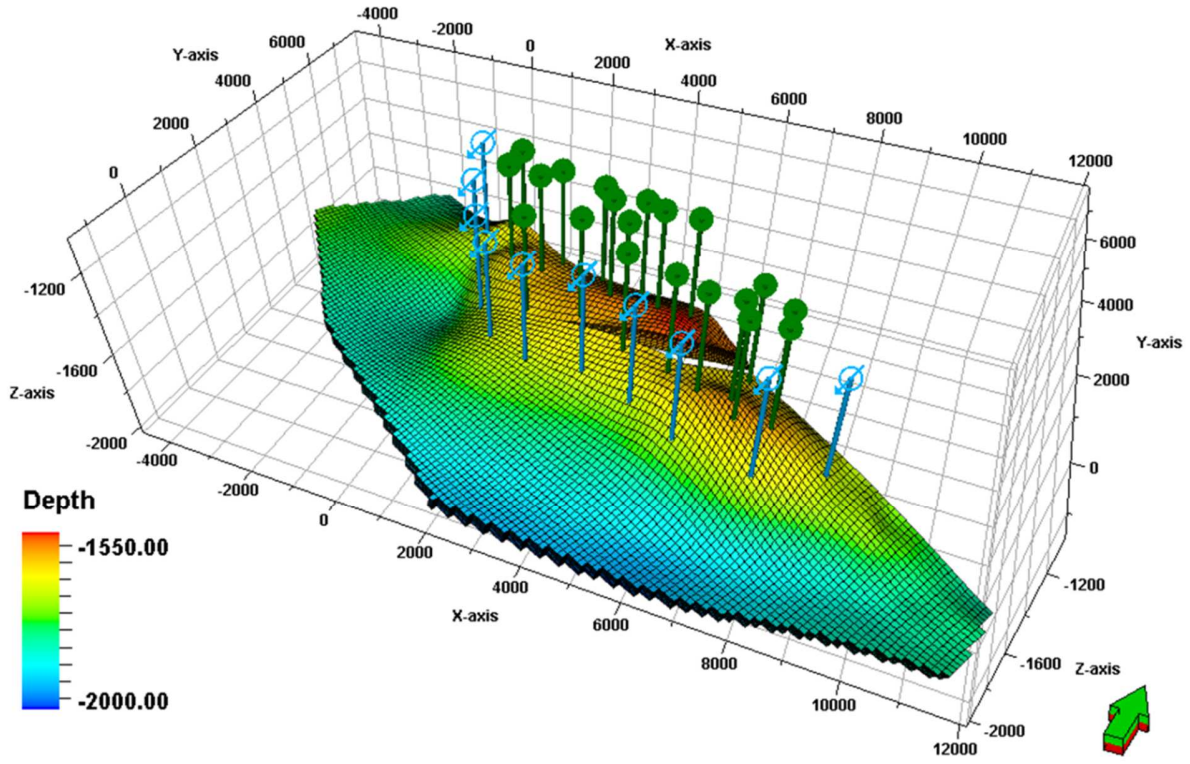

Figure 7.1: Top depth of the Brugge field and the location of the wells. Injector wells in blue and producer wells in green.

Table 7.1: Properties of the reservoir zones of the Brugge field (modified from Chen and Oliver, 2010).

	Schelde	Maas	Waal	Schie
Layers	1 – 2	3 – 4 – 5	6 – 7 – 8	9
Average thickness (m)	10	20	26	5
Average porosity (%)	20.7	19.0	24.1	19.4
Average permeability (mD)	1105	90	814	36
Average NTG	0.60	0.88	0.97	0.77
Depositional environment	Fluvial	Lower shoreface	Upper shoreface	Sandy shelf

7.2 – Available Data

A total of 104 upscaled realizations of reservoir properties have been created by the Dutch Organization for Applied Scientific Research (TNO) as a benchmark study (Peters et al., 2010).

According to the authors, the initial properties have been based only on the well data and some regional knowledge. The fluvial Schelde Formation has been modeled either as channel objects in a shale background or as a sequential indicator simulation (SIS). Porosity has been generated by SGS. Permeability has been generated according to three criteria: (1) deterministically, based on a single porosity-permeability regression; (2) deterministically, based on a porosity-permeability regression per facies; and (3) stochastically, with a cokriging simulation on porosity. Figure 7.2 shows the relations between porosity and permeability derived from original data and used in reservoir modeling (according to Peters et al., 2010).

The 104 realizations have been simulated by combining the different options. Each of the realizations contains the following properties: facies, porosity, NTG ratio, water saturation and permeability in x-, y-, and z-direction (Figure 7.3).

The initial reservoir pressure is 170 bar at reference depth of 1700m. Initial oil-water contact is at 1678m. Residual oil saturation is constant at a value of 0.15. The maximum rate for the wells is 318 m^3/day for the first 10 years of production.

Figure 7.3 shows porosity, permeability in x-direction and water saturation for all nine layers from realization 1.

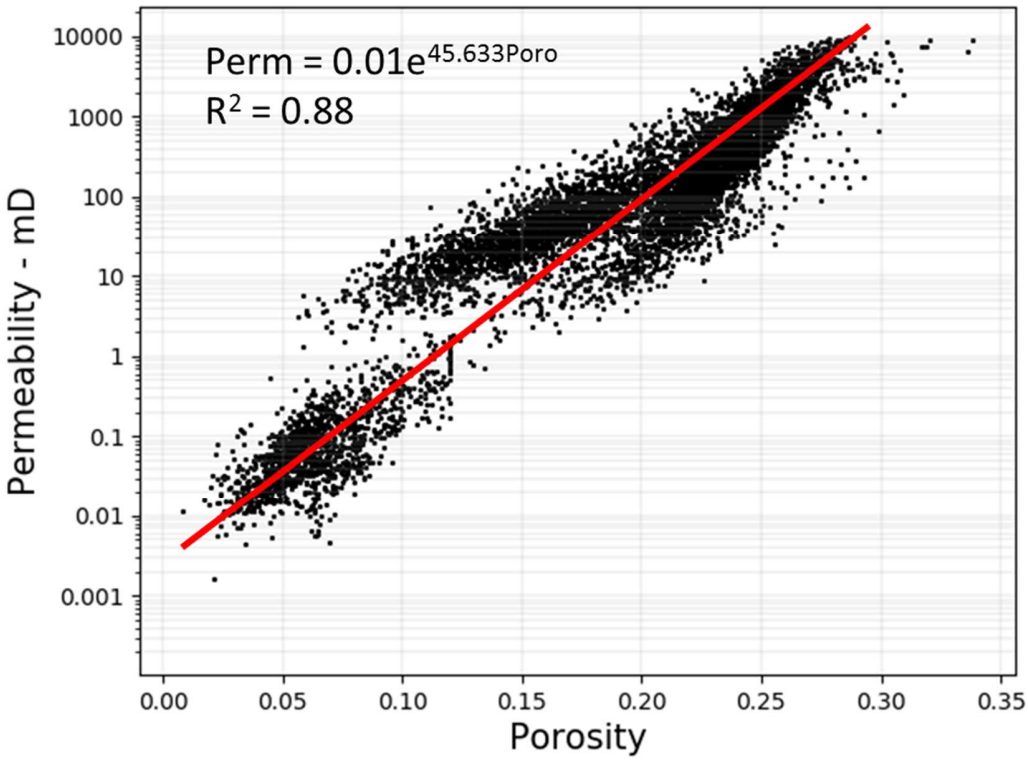

Figure 7.2: Crossplot between porosity and permeability in Brugge Field (Peters et al., 2010).

7.3 – Results

In the following sections, the proposed methodology for considering all realizations is applied to the Brugge Field. First, the visualization of all realizations is presented for selected cross-sections. Next, production performance based on the P50 model is compared with the production performance based on all realizations. Computational performance and decision-making based on both approaches are discussed.

7.3.1 - Uncertainty Visualization

Based on the 104 realizations from Brugge Field, some view planes have been defined, according to Figure 7.4. One view plane has been defined in principal x-, y- and z-orientation.

The proposed methodology described in Chapter 4 was applied to visualize all realizations available for these planes. Figures 7.5 to 7.7 show a sequence of two realizations as well as the intermediate planes calculated to smooth the visualization. The sequence of animations may found on YouTube:
https://www.youtube.com/playlist?list=PL9xpYwHhASq85W4mSnuHOWkrl3rlv0-ph.

The XY plane view presents a smooth transition through the realizations. The XZ and YZ cross-sections, however, present some noise and sharp transition among the realizations. This may occur due to the different characteristics of the reservoir zones. Layers 6-8 (Waal) present higher porosity and permeability values, differently from the adjacent layers.

Ordering the realizations according to the reservoir zones instead of considering the entire cross-sections may present an improved approach to visualize the sequence of realizations.

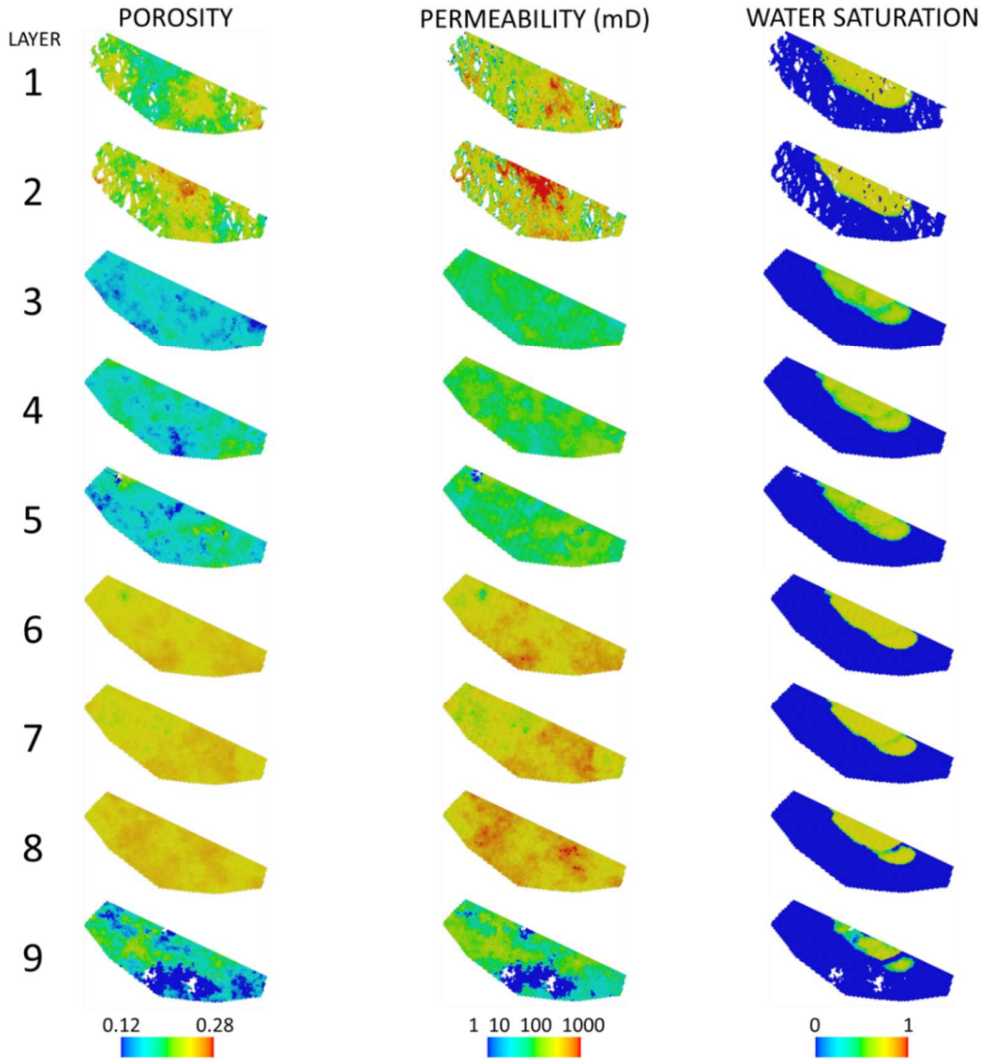

Figure 7.3: Porosity, permeability in the x-direction and water saturation for all nine layers from realization 1.

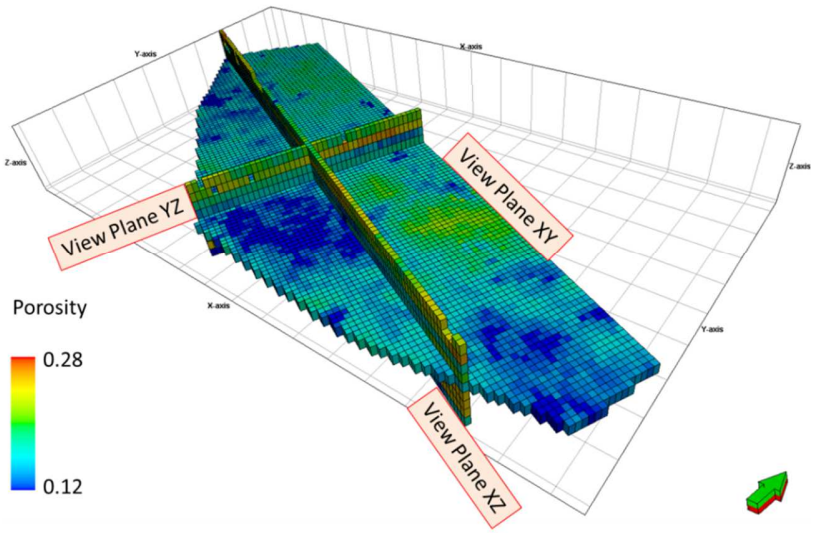

Figure 7.4: View planes defined from the 3-D geological model in x-, y- and z-direction. The reservoir property represented in this visualization is porosity.

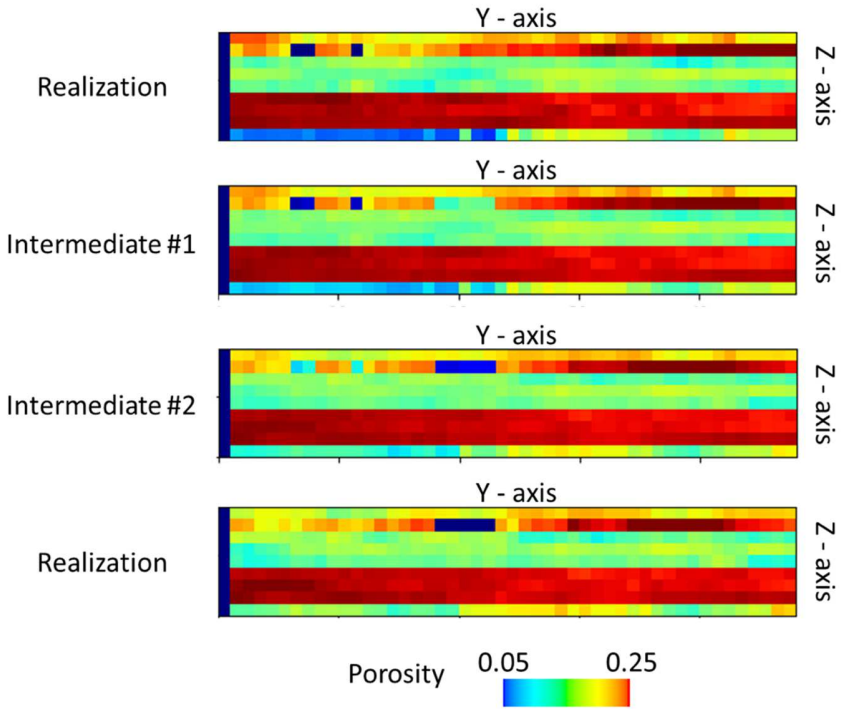

Figure 7.5: View plane YZ showing sequence of realizations and the intermediate planes.

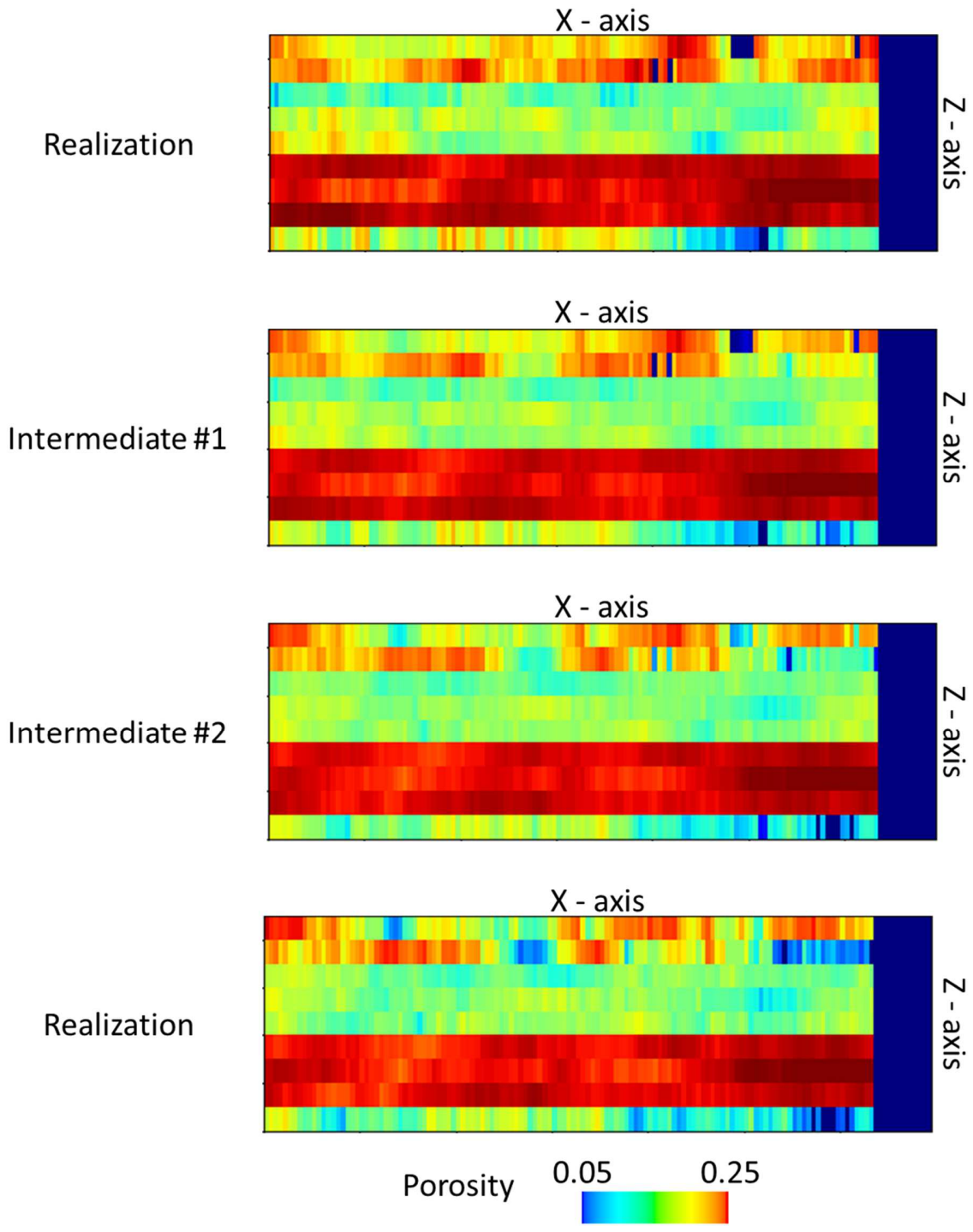

Figure 7.6: View plane XZ showing sequence of realizations and the intermediate planes.

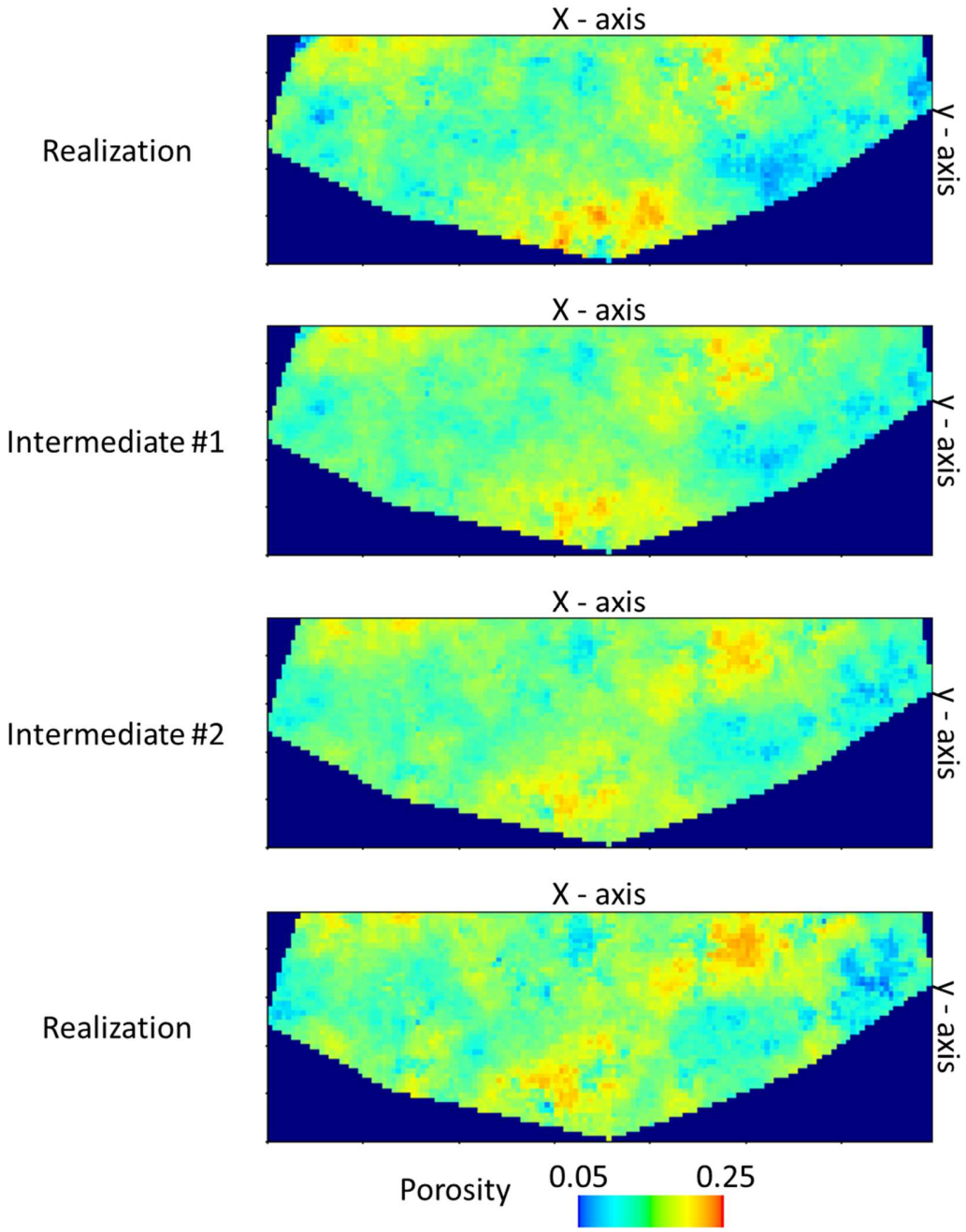

Figure 7.7: View plane XY showing sequence of realizations and the intermediate planes.

7.3.2 - P50 Approach

The ensemble of realizations is ranked according to the Hydrocarbon Pore Volume for oil (HCPVo). The HCPVo from each realization is given by:

$$HCPVo_l = \sum_{i=1}^{n} Bulk_i^l * \phi_i^l * NTG_i^l * (1 - Sw_i^l) \qquad l = 1, \dots, L \qquad (7.1)$$

where ***n*** is the number of grid cells, ***Bulk*** is the cell volume, ϕ is the cell porosity, ***NTG*** is the net-to-gross ratio and ***Sw*** is the water saturation for cell i = 1,…,n for realization l = 1,…,L.

According to the ranking, the realization corresponding to the P50 quantile can be selected (Figure 7.8).

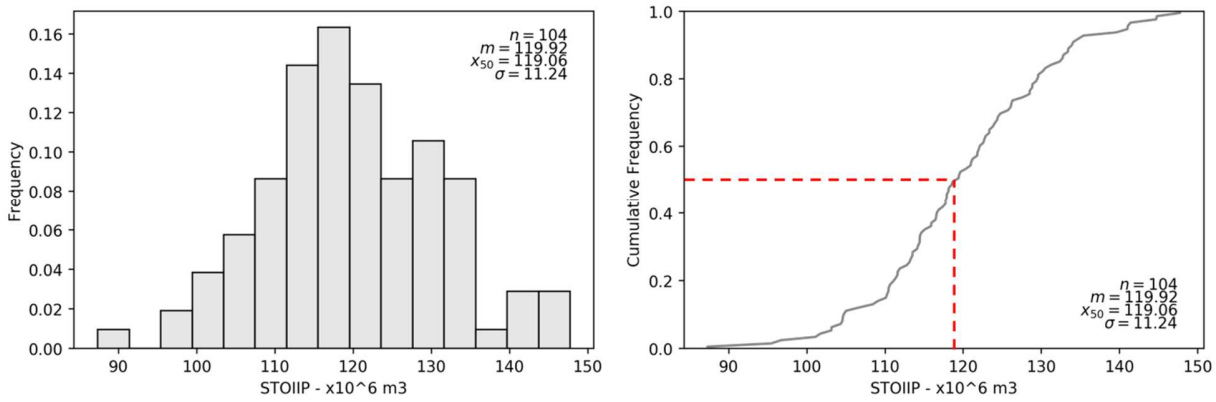

Figure 7.8: Traditional approach to reservoir management: The 104 geostatistical realizations are ranked according to the HCPVo. Realization related to the P50 quantile is selected for further studies, through the flow simulator.

7.3.3 – Using All Realizations

The ensemble of 104 realizations of the Brugge Field has been passed through the flow simulator. The results of the flow simulation for all realizations are shown in Figure 7.9. The cumulative fluid production curves and the fluid rates curves correspond to 10 years of production. The production curves representing the P50 model are highlighted.

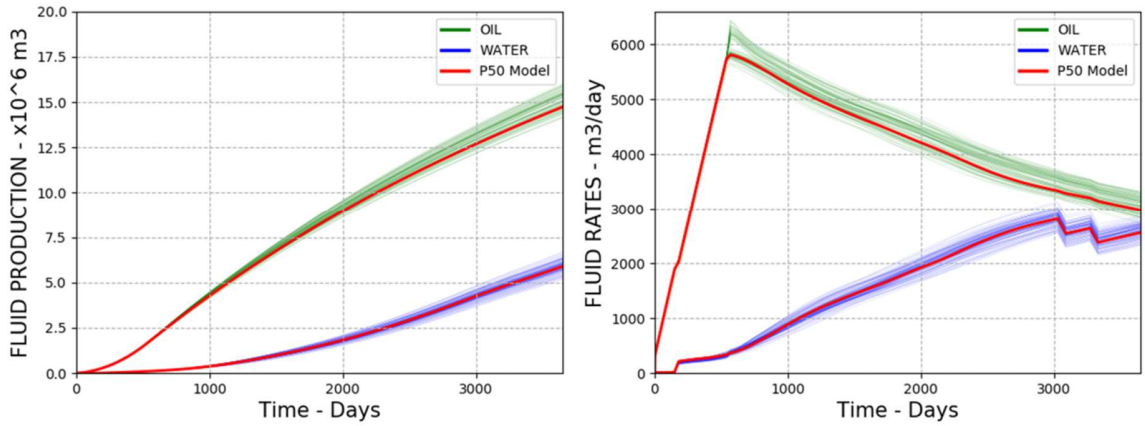

Figure 7.9: Left: Cumulative oil (green curves) and water (blue curves) of 10 years of production from 104 realizations in Brugge field. Right: Field oil (green curves) and water (blue curves) rates of 10 years of production from 104 realizations in Brugge field. Red curves represent the production related to the P50 model.

The production curves from P50 model do not always represent the average production of the 104 realizations. At the end of a 10-year production, there is an underestimation of the oil produced by the P50 model, according to the curves from Figure 7.9. The figure also shows an underestimation of oil production rates. Although the selected P50 realization represents the average model in terms of resources, the production responses do not represent the responses from the full set of models.

Figures 7.10 to 7.12 show the BHP, oil and water rates forecast from some wells, comparing the curves from all realizations and from the selected P50 realization. The P50 curves in Figure 7.10 show an overestimation of the BHP in the producer wells. The oil rate curves in Figure 7.11 also present an overestimation of oil rates from the P50 model in producer wells P10, P12, P13, P14, P18 and P19. Finally, Figure 7.12 shows that water rates from P50 model are underestimated in producer wells P13, P14, P15, P16 and P19.

According to these figures, the decisions based on P50 model may be in error for the reservoir development plan, since oil production is overestimated and water production is underestimated.

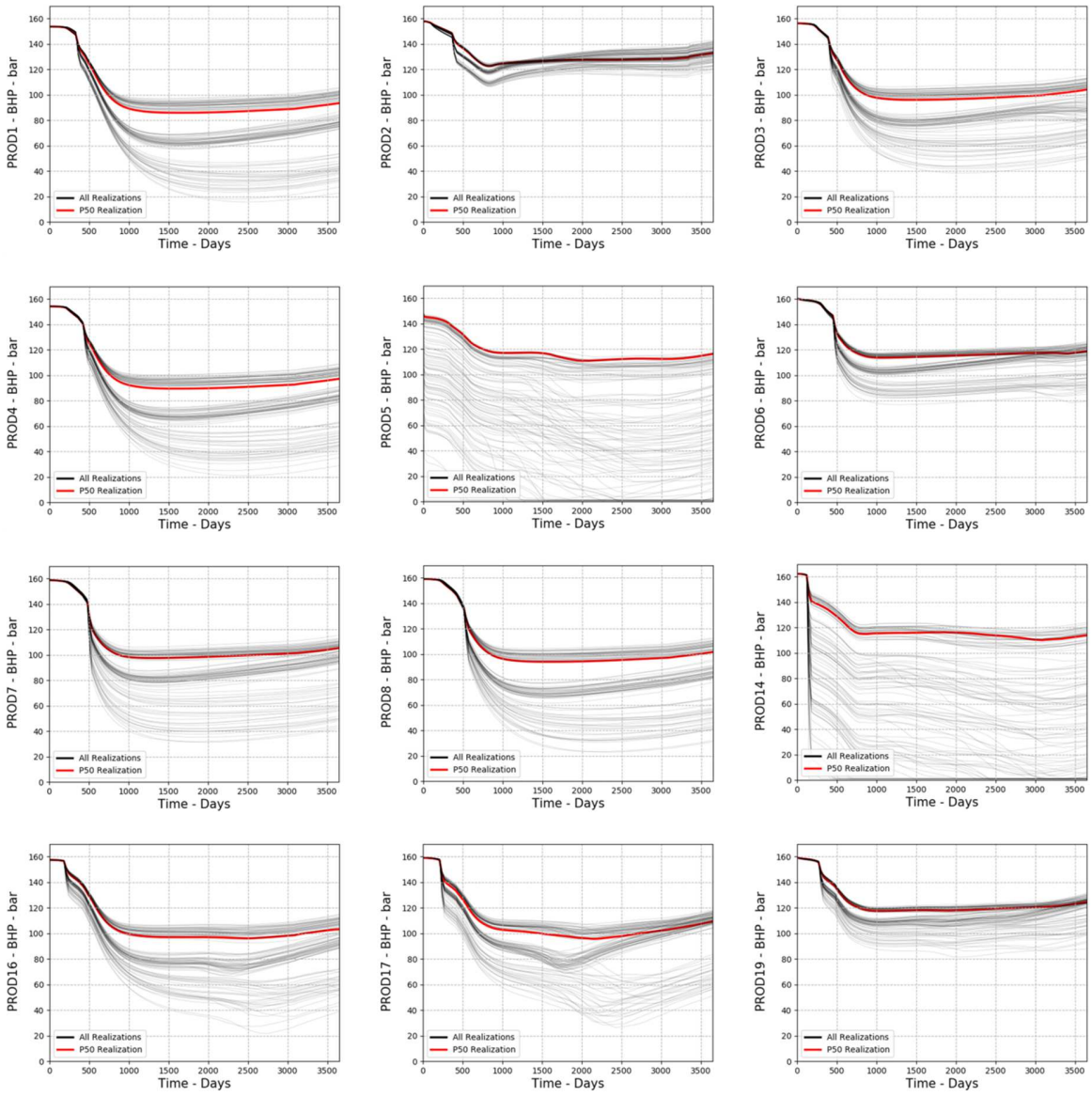

Figure 7.10: BHP curves from some wells, highlighting curves from P50 realization (in red) over all realizations.

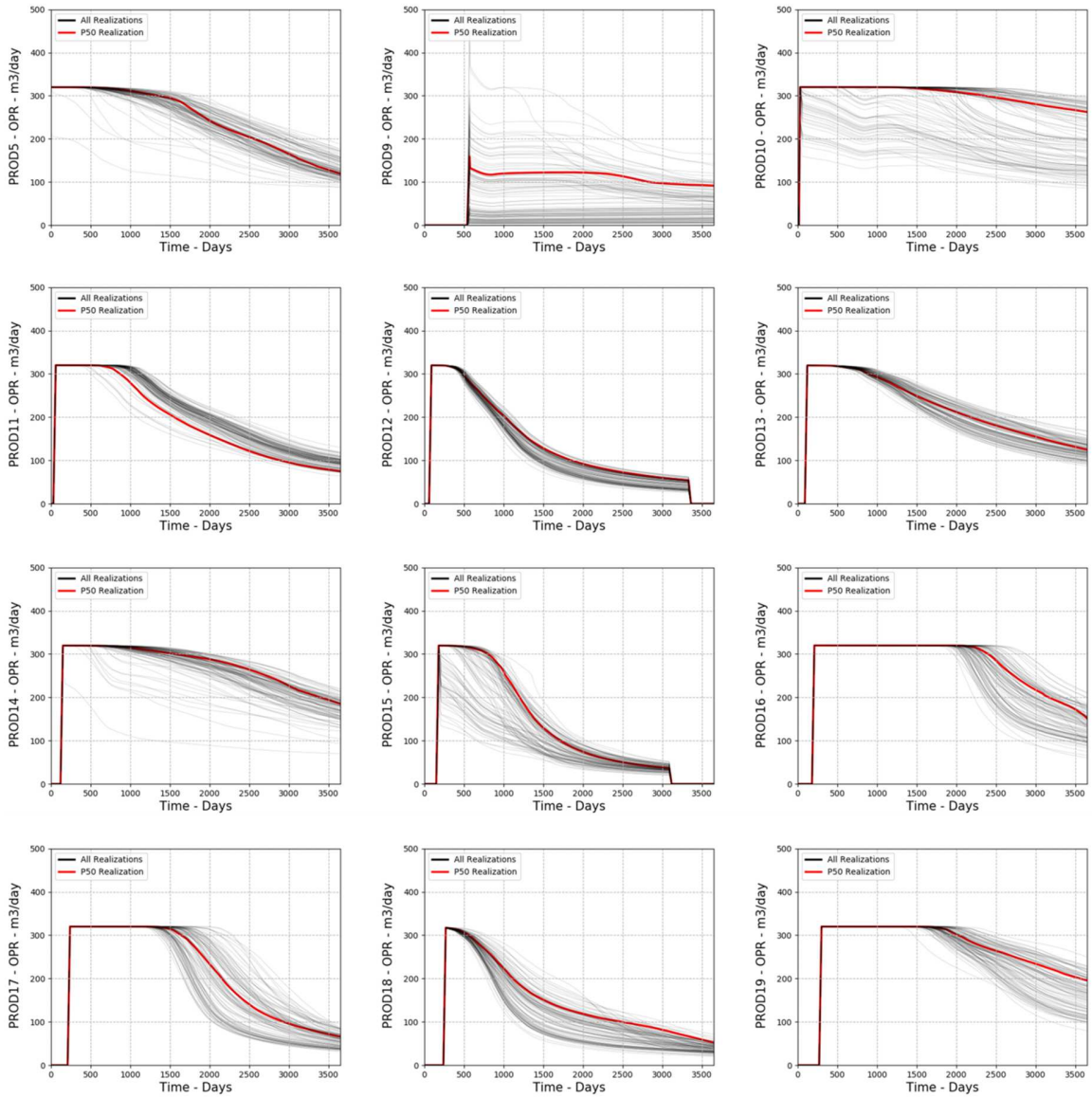

Figure 7.11: Oil production rates from some wells, highlighting curves from P50 realization (in red) over all realizations.

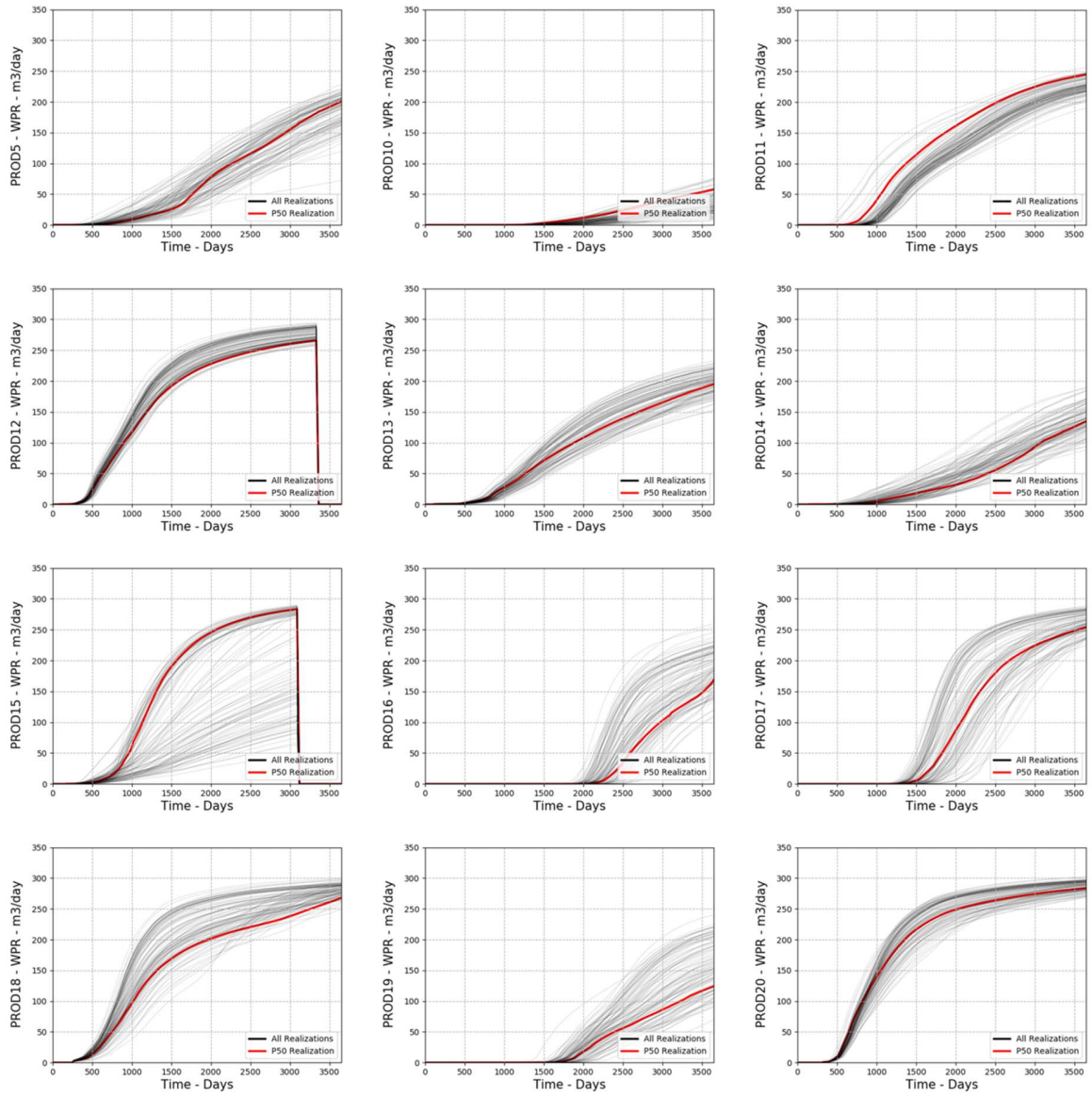

Figure 7.12: Water production rates from some wells, highlighting curves from P50 realization (in red) over all realizations.

7.3.4 – Computational Performance and History Matching

According to Peters et al., (2013), the computational resources required to simulate the Brugge model are moderate. Although 10 years of production data have been provided by TNO, the ensemble of 104 geological models has been passed through the flow simulator to reproduce

the original production responses from Peters et al., (2010). Figure 7.13 shows the distribution of the computational time required to simulate 10 years of production. All runs have been performed sequentially, using a CPU Intel Core i7 @ 2.80 GHz and 24 GB of RAM memory.

Considering the advances in the computational performance mentioned in Chapter 5, the spread of massively parallel computing platforms supports the proposed premise of managing multiple realizations. The flow simulation for each realization may be distributed through multiple cores, maintaining the consistency of the results and reducing the reservoir simulation times.

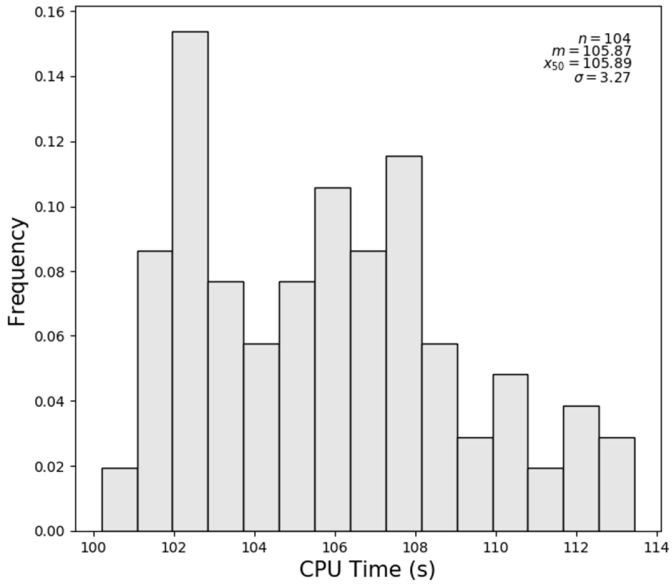

Figure 7.13: Distribution of CPU time for running the flow simulation for each of the 104 realizations from Brugge Field.

Historical production data should be incorporated into the reservoir models to improve the reliability of reservoir predictions. The Brugge Field has been broadly used in HM literature (Lorentzen et al., 2009; Schulze-Riegert et al., 2009; Chen and Oliver, 2010; Peters et al., 2013; Emerick and Reynolds, 2013; Zhang et al., 2018). The feasibility of using all realizations in HM may be demonstrated, in practice, based on the results of such papers.

The results of this section are based on the HM performed by Emerick and Reynolds (2013). The authors have compared some ensemble-based HM methods (EnkF, ensemble smoother – ES; and ES with multiple data assimilation – ES-MDA). History production data in this study correspond to measurements of the oil and water rates at the producing wells and BHP at the producing and water injection wells.

The computational cost to perform HM in all realizations is shown in Table 7.2. The results have been computed by measuring the CPU time required during HM divided by the average CPU time required for one reservoir simulation run. Considering the average CPU time required for one reservoir simulation run is 105s, the absolute CPU time required for HM is also shown in Table 7.2.

According to Emerick and Reynolds (2013), the normalized data mismatch objective function for each method is computing using:

$$O_{N,d}(m) = \frac{1}{2N_d}(d - d_{obs})^T C_D^{-1}(d - d_{obs}) \tag{7.2}$$

where $\boldsymbol{N_d}$ is the number of ensemble models; $\boldsymbol{m}$ is the vector of model parameters; $\boldsymbol{d}$ is the vector of predicted data; $\boldsymbol{d_{obs}}$ is the vector of observed / history data; and $\boldsymbol{C_D}$ is the covariance matrix of observed data measurement errors.

Results on Table 7.2 show that ES-MDA improves significantly the final data matches and the mismatch of predicted and observed data area about three times lower than EnKF and about twelve times lower than ES, in average. There is no indication in the original paper which of the production data is more sensitive to HM (BHP, oil rate or water rate).

Table 7.2: Computational cost for HM and average mismatch over 104 realizations in the Brugge field (according to Emerick and Reynolds, 2013). The total CPU time is based on the average CPU time required for one reservoir simulation run, using a CPU Intel Core i7 @ 2.80 GHz and 24 GB of RAM memory.

Method	Number of equivalent simulation runs	Total CPU time (hours)	Average mismatch of the objective function
EnKF	367	10.70	16.5
ES	106	3.09	60.3
ES-MDA	430	12.54	5.6

Figures 7.14 to 7.16 show the original BHP, oil and water rates curves from the 104 realizations and the matched curves after HM, according to results from Emerick and Reynolds (2013). The matched curves have been obtained according to ES-MDA method.

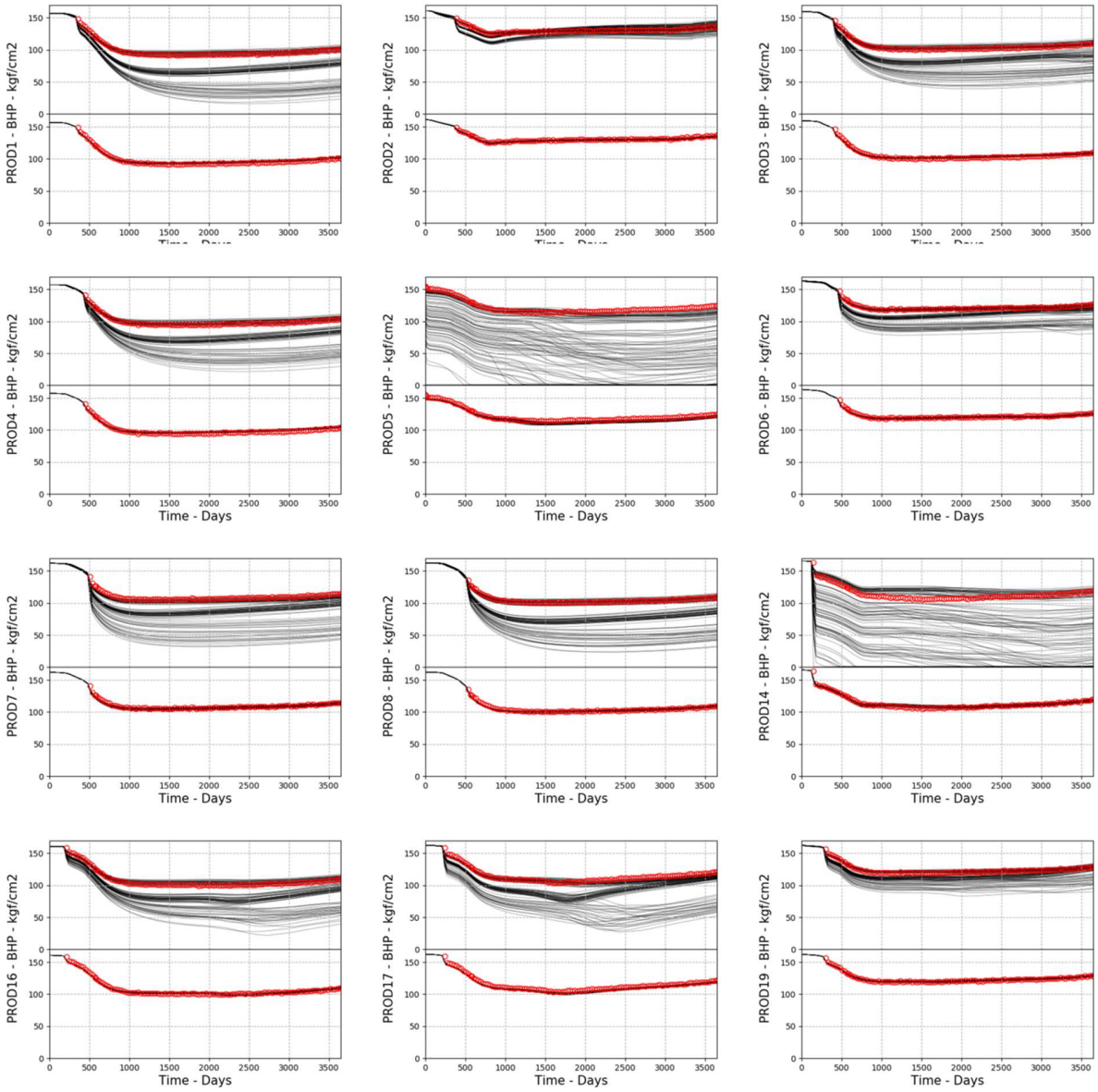

Figure 7.14: The original BHP curves from some wells, and the matched curves, after ES-MDA method. The historical production data are shown in red.

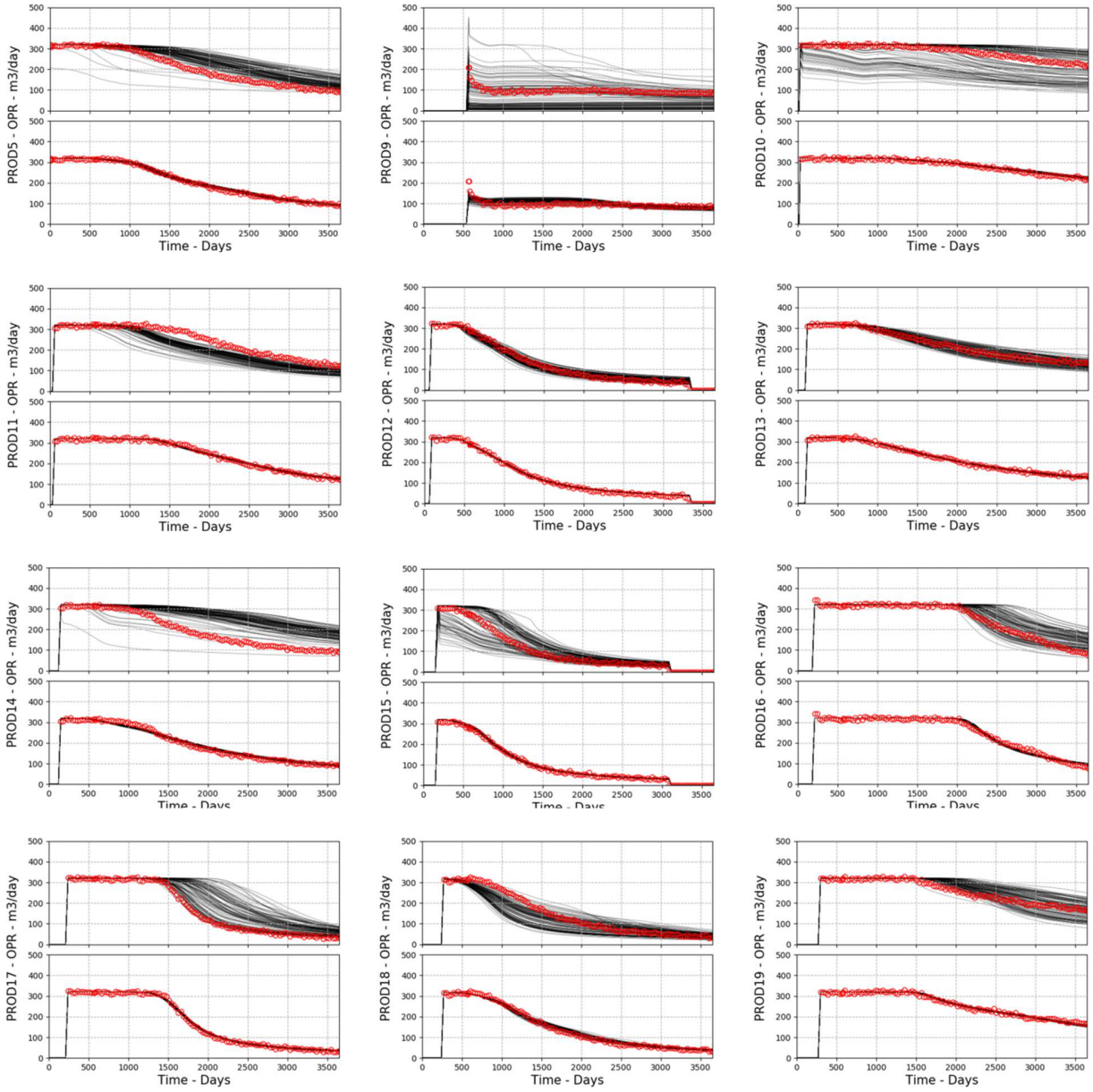

Figure 7.15: The original oil rate curves from some wells, and the matched curves, after ES-MDA method. The historical production data are shown in red.

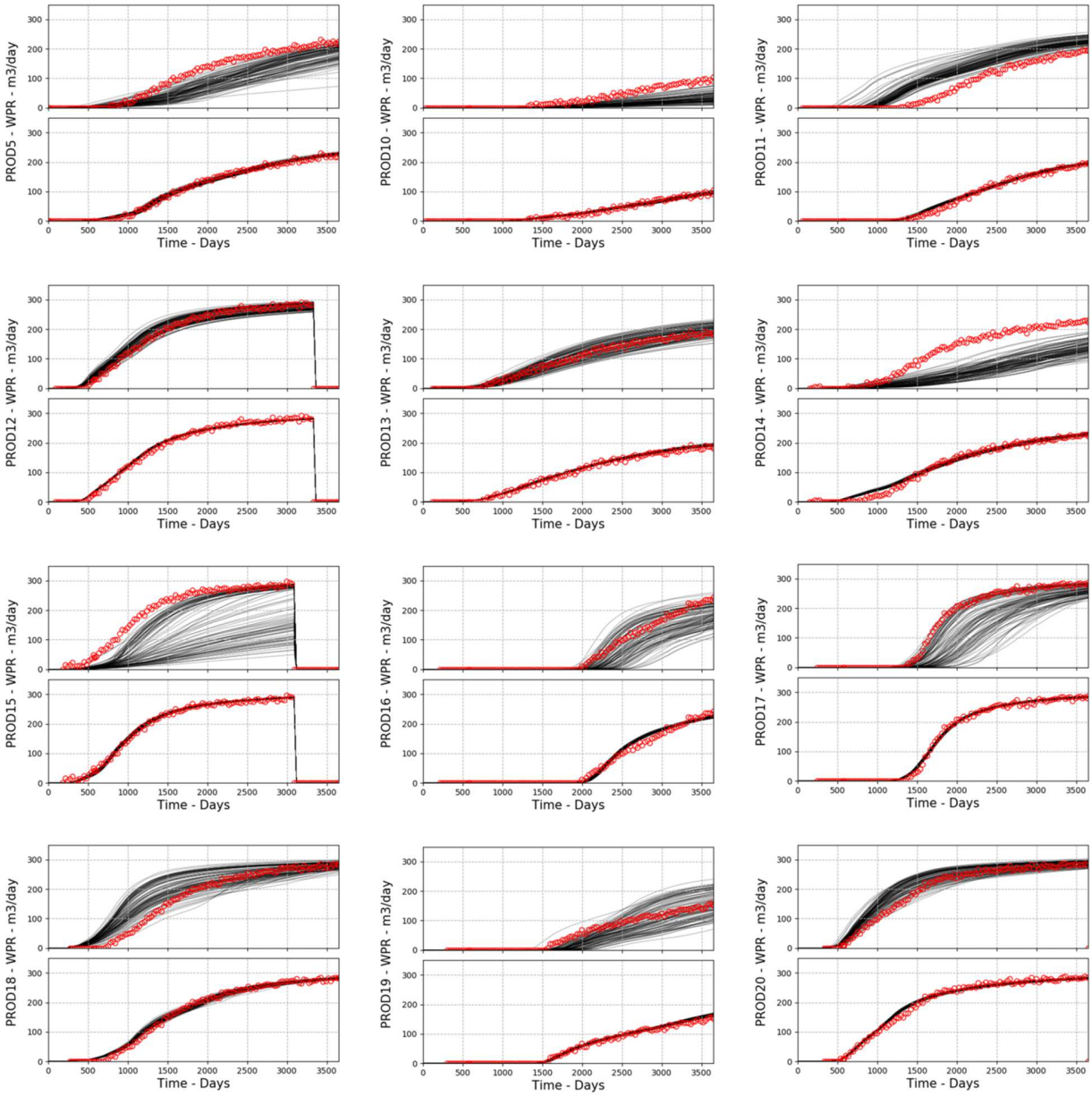

Figure 7.16: The original water rate curves from some wells, and the matched curves, after ES-MDA method. The historical production data are shown in red.

It is also possible to quantify the differences in flow predictions over the observed production data. A simple objective function (OF) that represents the mismatch between the observed and simulated production data is defined as follows:

$$OF^l = \frac{\sum_{i=1}^{N}(d_i^{obs} - d_i^{sim})}{|\sum_{i=1}^{N}(d_i^{obs} - d_i^{sim})|} * \sum_{i=1}^{N}\left(d_i^{obs} - d_i^{sim}\right)^2 \quad l = 1, \dots, L \tag{7.3}$$

where **N** is the number of observed data and $\boldsymbol{d^{obs}}$ and $\boldsymbol{d^{sim}}$ are observed and simulated data, respectively.

The square error is a common manner to mathematically represent the difference between observed and simulated data. The first term of the equation is used to define the sign of the mismatch. If a simulated production curve (e.g., BHP) is predominantly under the observed data, the sign of the mismatch is positive. Otherwise, the sign is negative. This is important to understand the distribution of the models regarding to the observed data in the uncertainty curve. Figure 7.17 illustrates the mismatch of production data (BHP) using the equation 7.3 for some producer wells. The mismatch has been calculated for each realization, prior (in black) and posterior to the HM (in red). The posterior mismatch should be ideally close to zero.

These results illustrate the viability of using the entire ensemble of realizations in the HM process. The use of an ensemble-based HM method provides a set of multiple geological models consistent with static and dynamic data, resulting in robust and more accurate uncertainty estimates of production forecast.

7.3.5 – Decision-Making

The demonstration of a decision-making process is shown as follows. It is an optimization problem, comparing the P50 model and all realizations. The problem consists to drill a new producer well in the reservoir, as shown in Figure 7.18. Two different zones, A and B, have been defined to drill the well. Five well locations per region have been tested to evaluate the production responses over 10 years of production.

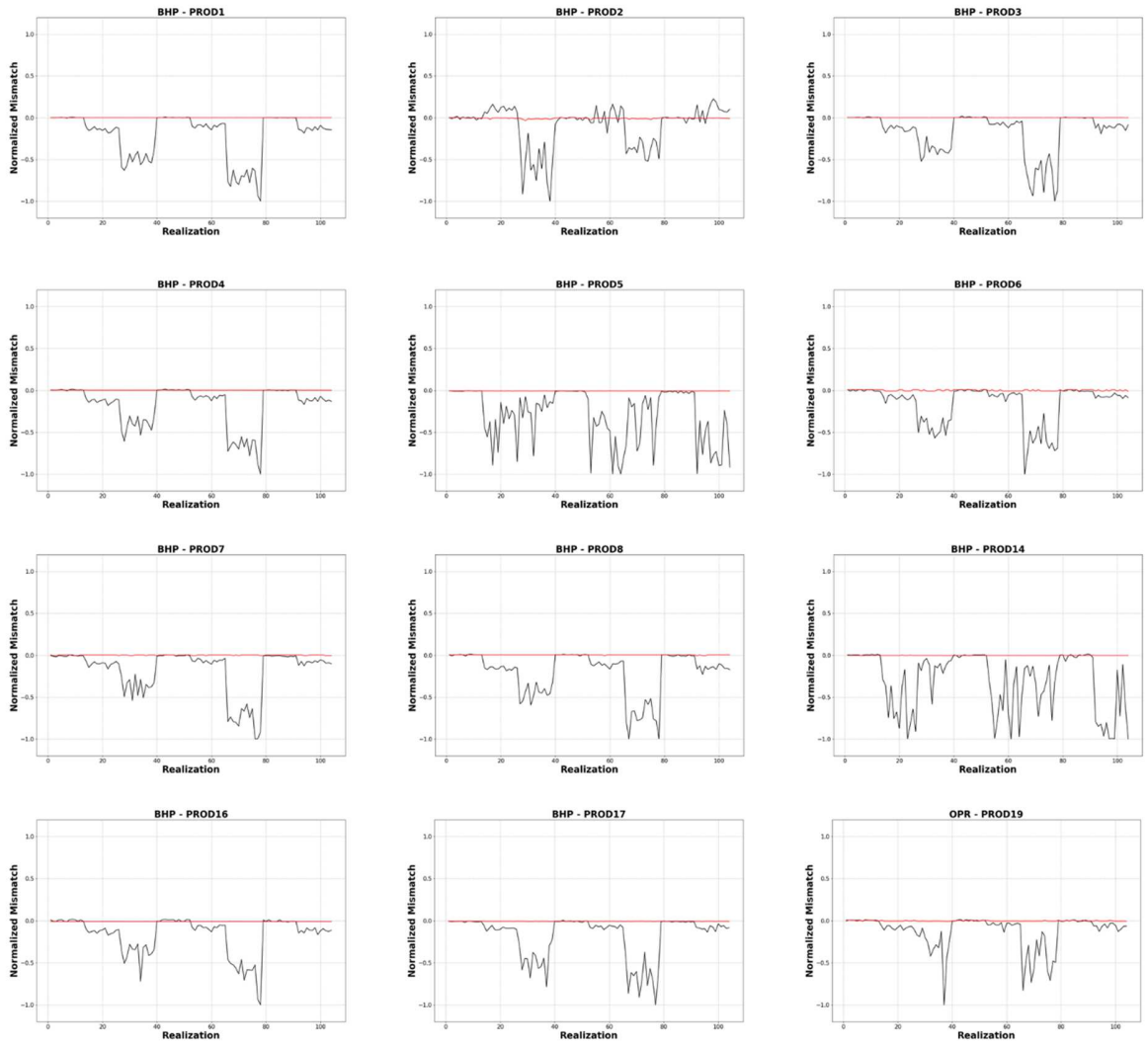

Figure 7.17: Normalized mismatch of BHP for some producer wells, calculated prior (black) and posterior (red) to the HM.

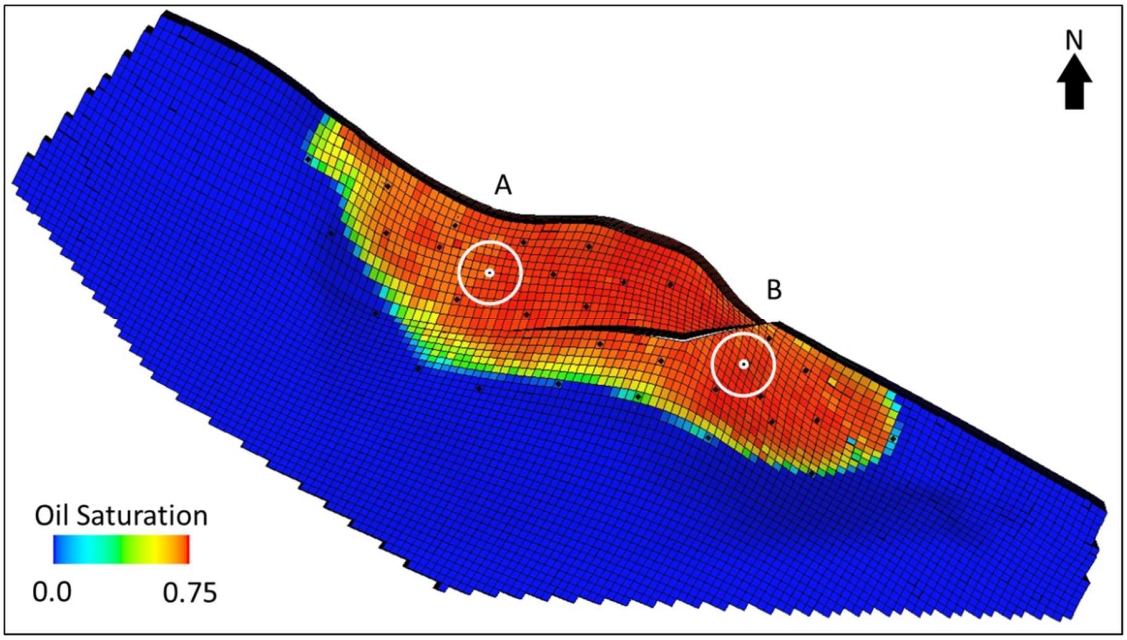

Figure 7.18: Oil saturation of the first layer of the Brugge model, highlighting the regions A and B for drilling a new producer well.

The decision of drilling a new producer well is taken based on the best location based on the P50 model and the best location based on the ensemble of models. The production revenue (PR) is used to compare both decisions. The total oil production at the end of ten years is considered for each realization, as well as the total water production and the total water injection in the same period, according to Equation 7.4:

$$PR_l = Np_l * 60\ USD - Wp_l * 3.5\ USD - Wi_l * 3.5\ USD \tag{7.4}$$

where: Np is the volume of produced oil, Wp is the volume of produced water, and Wi is the volume of injected water (all in barrels), for l = 1,…, L realizations.

The following economic parameters have been considered: oil price equal 60 USD/STB; water price (both injection and production) equal 3.5 USD/STB. Other production and operation costs, such as drilling costs and taxes, have not been considered.

The selection of the optimum well location follows the approach shown in Figure 3.5. The optimum well location is defined according to the maximum PR after 10 years of production from the P50 realization. The optimum well location from the ensemble of realizations is defined according to the expected value of PR, calculated over all realizations. Results from both approaches are shown in Table 7.3.

Table 7.3: PR (in MM USD) according to the best location based on the P50 model and based on all realizations.

Region	Decision-based on	PR (MM USD)	Difference (MM USD)	Difference (%)
A	P50 model	5,728	135	2.4
	All realizations	5,863		
B	P50 model	5,642	142	2.5
	All realizations	5,784		

The results show an improvement of 2.5% in the production revenue taking into account all realizations instead of considering the P50 model. Although the percentage is not impressive at first glance, the absolute value between 135 to 142 MM USD has an economic impact in the reservoir project. Moreover, the costs for managing all realizations are related to CPU time.

7.4 - Discussion

The proposed approach of using all realizations in a decision-making process is demonstrated for a realistic example of Brugge Field.

Although the decisions in reservoir management are often based on a single reference case (usually the P50 model), these decisions do not consider geological uncertainty. A single realization is one outcome out of an ensemble of possible realizations describing the true reservoir.

The restrictions of using all realizations in reservoir development plan are discussed in this chapter based on the Brugge Field. The computational demands of running flow simulation are

presented and overcome. Alternatives for performing history matching using ensemble-based techniques are presented with feasible estimates of the production forecast.

Finally, the economic improvement based on the decision of drilling a new well is presented. The proposed approach is compared with the traditional P50 model approach. The optimum well location presented in this case study is consistent with all realizations. The improvement of the production revenue considering all realizations supports the statement of this research.

7.5 - Summary

- The proposed methodology of considering all realizations is applied to a realistic case study, the Brugge Field;
- The production responses based on the reference model are compared with the production responses based on all realizations;
- Viability of considering all realizations in a reservoir management plan;
- The computational performance for flow simulation and HM are presented and discussed concerning of multiple models
- The visualization of all realizations is also presented using the proposed algorithm.

Chapter 8

Concluding Remarks

Understanding and managing reservoir uncertainties throughout the lifecycle of a reservoir will lead to improved production. Reservoir decision-making requires a conscious irrevocable allocation of resources to achieve desired objectives. Development decisions need to be taken despite an imperfect knowledge of the subsurface.

A methodology to facilitate the transfer of subsurface uncertainty through reservoir management has been developed and demonstrated in this thesis. 2-D synthetic examples and a real case study are considered. Using a single model for flow simulation and for planning the development of a hydrocarbon field can lead to decisions without the full benefit of the modeling work. Considering an ensemble of reservoir models is a better basis for decision support instead of a single or a few models. The contributions, limitations and future work for the research are summarized in this chapter.

8.1 – Summary of Contributions

The main contribution of this thesis is the incorporation of uncertainty analysis for improving the quality of decisions taken to explore and develop hydrocarbon fields. This thesis contributes to an integrated assessment of geological uncertainty in order to provide a rational basis for the management of uncertainties in the reservoir development plan and, therefore, supporting the decision-making process.

An efficient reservoir management plan requires a reliable uncertainty assessment. Reservoir predictions are used in reservoir management to optimize costs and revenues of producing a reservoir. The uncertainty should be taken into account when deciding on an optimal

production strategy. There are also important contributions concerning reservoir geological uncertainty.

8.1.1 – Considering all realizations for uncertainty management

The first main objective of this thesis is improving the understanding and management of uncertainty in reservoir performance forecasting. Alternatives to facilitate the transfer of the subsurface uncertainty through reservoir management are presented and discussed in this research.

Understanding the uncertainties related to reservoir production is crucial to making development and management decisions. The single model paradigm produces a single response with no understanding of uncertainty in production forecasts. Considering an ensemble of reservoir models is a better basis for decision support, rather than just one or a few models.

Multiple equiprobable reservoirs models are generated by geostatistical simulation to characterize the heterogeneity and geological uncertainty. Dealing with multiple realizations provides an assessment of the uncertainty space to be used in the decision-making processes.

As shown in 2-D synthetic examples in Chapter 3 and in the 3-D case study in Chapter 7, making decisions based on a single reference case disregards geological uncertainty. Multiple realizations are generated to capture some of the uncertainties associated with the reservoir model. The results of the reference model (P50) may not represent the response of the ensemble of models. A single reference case is ranked close to the center of all results and chosen/modified to match historical production data. However, different realizations are able to match historical data equally well.

Alternatives for managing multiples realizations are presented in Chapter 3. The ensemble of realizations may be used to assess measures of performance such as OOIP, production forecasts and breakthrough. Outcomes based on all realizations can be represented as distributions or expected values. Any other statistic can be calculated and used as summaries for supporting the decision-making process. The use of multiple realizations may also be useful in an optimization approach. Some decisions should be based on optimized responses, such as defining

the optimal number of wells or choosing the location for drilling a new well. The optimization approach considering all realizations supports the reservoir team to make robust decisions for maximizing the value of the reservoir project.

8.1.2 – Uncertainty visualization

A new method for sequentially displaying multiple geostatistical realizations is developed in Chapter 4. Methods from animation and the distance between realizations are considered. The emphasis is on the visualization aspect of post-processing.

Although the number of geostatistical realizations could be large and has been automated, human inspection is still necessary for quality control and the analysis of results. Tools are required for processing and analyzing the ensemble of realizations qualitatively and productively. Advances in speed and computational storage have made it possible to study the development of complex and dynamic systems and to represent results accordingly.

Since all realizations should be considered in reservoir management, a visualization methodology has been presented in Chapter 4 to facilitate the understanding of the space of uncertainty, such as visualizing all realizations in a way to communicate the regions of high or low uncertainty to the reservoir management team.

8.1.3 – Computational requirements

The current level of detail and complexity of reservoir models requires a high computational cost. The computational requirements for history matching and flow simulation are the main reason to avoid dealing with all realizations all the time. The high demand for computers is one of the main reasons to avoid correct management of the set of geological realizations.

To overcome the limitations and to promote the transfer of geological uncertainty over reservoir management, some alternatives are presented in Chapter 5. Parallel architecture with multiple cores and GPUs has been recently applied in reservoir simulation. Recent advances in computational performance support the premise of managing multiple realizations.

Chapter 5 shows that there is no reason to restrict flow simulation to a single model since computational performance has grown exponentially over the past 30 years through faster processors, multiple cores, parallelism, and GPUs. Such growth in computational capacities makes it possible to generate and handle multiple reservoir models with hundreds of parameters.

High-performance computing has had a significant impact on the evolution of numerical predictive methods over the past 50 years. Petroleum engineering applications have had a significant increase in reservoir simulation capabilities. The execution time of the simulation remains stable over the years, despite the increase in computational performance. The transfer of geological uncertainty through the decision-making process has been neglected by increasing the complexity of the models. The new technologies discussed in this thesis present potential to achieve practical computational improvements.

Computational performance has increased by five orders of magnitude over the past 20 years. The emergence of massively parallel computing platforms has opened new pathways for efficient processing. Simulation of reservoirs on massively parallel computers can reduce simulation time by 3 to 4 orders of magnitude. Parallelism offers a solution to make computationally intensive methods practical to be applied to routine field studies. New reservoir management scenarios can be considered, including all geological realizations.

8.1.4 – Integration of geological and production data

A large number of realizations permit capturing uncertainty in the underlying geologic model that should be used for predicting different hydrocarbon production scenarios. However, the excessive computational requirements to perform the history matching for each reservoir model restricts the number of flow simulation models that can be used for future predictions. The recent advances in computational performance as shown in Chapter 5, and the developments in the ensemble-based history matching techniques, encourage the use of a large number of reservoir models to improve the production forecasts.

As discussed in Chapter 6, ensemble-based techniques, such as EnKF, provide an ensemble of matched models. This creates the opportunity of considering all reservoir geostatistical

realizations for forecasting and decision-making processes. An alternative approach to integrate well test analysis data into the geological modeling workflow is also developed in Chapter 6. The proposed methodology is able to condition an ensemble of reservoir models to the available static and dynamic data while preserving the geological consistency. Consistent integration of geological and dynamic data provides a more accurate uncertainty quantification, supporting reservoir management decisions.

Considering all realizations is challenging for reservoir management. Since many practitioners believe that HM is so laborious that only one realization can be used, this thesis presents a simple and practical approach to ensure that all realizations approximately match historical production data. Changes required on one realization are likely similar to other realizations and having multiple realizations that approximately match history is likely better than having one realization with a false sense of certainty.

8.2 – Limitations

The methodology presented in this thesis has some limitations as discussed as follows.

8.2.1 – Selection of a reference or P50 case

The methodology presented in this thesis is strongly focused on static in-place volumes to select a reference model. Although Chapter 2 have discussed several static and dynamic-based ranking techniques, all numerical examples used in this thesis have considered hydrocarbon volumes for ranking and selecting a reference case or the P50 model. As mentioned before, static ranking techniques are commonly used in industry. However, different advanced ranking approaches should be applied for a more robust validation of the proposed methodology.

Although decisions are based on a single reference case, sometimes a low and a high cases are somehow selected for further production responses assessment. The impact of selecting more than a reference case has not been considered in this research.

8.2.2 - Computational resources optimization

The growth of computational performance have been discussed in Chapter 5 as well as the increasing in reservoir model complexity and flow simulation techniques over time. However, there is a limitation in this chapter concerning the optimal computational resources required for managing multiple realizations. This should be a function of many factors, such as the reservoir model complexity, number of wells, history production data and number of realizations. A detailed analysis is also required to define the more sensitive computer resource for managing multiple realizations.

8.2.3 – Deterministic optimization approach

The optimization examples presented in Chapter 3 and Chapter 7 are limited in a deterministic approach. A few limited potential well locations have been evaluated in order to optimize the production outcomes. Moreover, the presented examples have restricted to drill additional wells. Different types of production optimization should be considered to validate the using of all realizations, such as well spacing, alternative production options and timing of injection.

8.2.4 – Uncertainty Visualization

The current implementation for visualizing the uncertainty of the ensemble of models is limited to a simple 2-D approach. Selecting a cross-section from the 3-D reservoir model is still a manual process, as well as the preparation of input data file for running `uncert_viz`. Moreover, the process for ordering realizations should be optimized. The suitable moving window and the number of intermediate images should be defined automatically in order to optimize the computational performance.

8.2.5 - Validation of uncertainty

The methodology presented in this thesis for considering all realizations in the reservoir decisions has been compared with the conventional methodology of using a reference model.

Chapter 3 has shown the impact of both approaches considering a true model. In practice, however, the true model is not known.

The validation of the uncertainty is a limitation of this research. The improvement of performance from a decision based on all realizations over a single reference case should be computed on the true model. A decision is a choice made from available alternatives, such as the effectiveness of infill drilling locations and trajectories. However, checking the uncertainty model in real circumstances remains a challenge, since the true model is not accessible.

8.3 – Future Work

Despite the developments made in this dissertation, the research presents several avenues for future research.

8.3.1 - Optimization of decision using utility function

A more robust optimization approach should be considered as future work. Determining the best well location for new wells is a complex problem that depends on the reservoir and fluid properties, well and surface equipment specifications, and economic criteria. The uncertainties in the model are transferred to the outcomes of well configuration decisions. Given the probabilistic approach presented in this thesis, the goal is to estimate the expected outcome of any proposed decision and the risks associated with it. A utility function should be used to quantify the risks associated with the decision. The expected outcome of a given decision is dependent on the risk attitude of the decision maker.

The usefulness of the utility function allows a clear definition of the otherwise arbitrary notion of an optimum solution to an uncertain problem. Decision makers who decide not to use a utility function will have difficulty in case of uncertainty. The use of utility function enables the decision makers to balance the risks and outcomes according to their specific risk attitude.

8.3.2 - Practical implementation of visualization

Some challenging problems remain in the field of uncertainty visualization. Commercial 3-D software can potentially order the ensemble of realizations automatically, every time the user modifies the view of the model. Additional work is also necessary to store all geostatistical realizations in the computer memory, optimizing the process for ordering realizations in the selected view.

8.3.3 - Disclosure of results

Transferring the geological uncertainty throughout the reservoir management plan requires a probabilistic approach for describing the full range of possible production outcomes. Moreover, the correct assessment of geological uncertainties is an important step for improving the quality of decisions made in the presence of risk.

The proposed methodology in this thesis highlights the importance of considering the ensemble of realizations for a correct uncertainty assessment. However, consistent disclosure of results based on the probabilistic approach should be considered. Considering all realizations permits a continuous distribution of outcomes to be used to represent the inherent reservoir uncertainty. The low estimate (P90), base estimate (P50) and high estimate (P10) are improved, but the realizations that provide those estimates changes when resource calculation is changed.

Regardless of the methodology, it is important that hydrocarbon companies communicate as explicit and intelligible as possible how reported estimates have been derived and calculated.

8.3.4 - Scenarios vs Realizations

It is important to point out that there is a difference between scenarios and realizations. Scenarios represent cases with singular variations without any continuum linking them. Realizations represent a variation of parameters from a specific scenario. It implies the generation of probability distributions to represent uncertainty.

The methodology presented in this thesis considers essentially a large number of independent realizations of reservoir models. The conventional approach to characterizing and

communicating uncertainty is to build a variety of models that are parametrically quite different, but considering similar geological concepts. A broad range of models can be created by varying these parameters while keeping the underlying structure, environment of deposition, etc. unchanged. These models can be simulated with different depletion concepts, such as the number and position of wells or production management strategies, to yield the desired business metric for each model.

However, there are no restrictions on considering different geological scenarios into the proposed methodology. Anything that can be computed on one model can be computed on hundreds ones, regardless of which concepts have been used. The decision response should be computed on all realizations and the expected response determines the optimal decision. A case study based on different scenarios should be evaluated in the future to demonstrate the applicability of this approach.

8.3.5 - History matching

HM is a very large topic and it has not been deeply investigated in this research. Some ensemble-based techniques have been presented in this thesis for supporting the claim of using all realizations in the uncertainty assessment.

However, there are different complexity levels concerning history matching. The number of model parameters significantly increases the dimensionality of the inverse problem according to the number of wells, the length and the type of historical data. In the history matching, the model is calibrated to field observations, such as production data; pressure data, such as well-test analysis and formation test; and time-lapse data. The type of data that must be matched influences the choice of parameterization.

As future work, it is important to demonstrate the applicability of the ensemble-based techniques incorporating different historical data. Transferring the uncertainty space from the geological model will enhance the accuracy of predicted future reservoir performance.

8.3.6 – Value of Information

Reservoir decisions must be made considering uncertainty since the uncertainties cannot be completely eliminated. Regardless of the methodology used, uncertainties will always exist in reservoir characterization. How much uncertainties should be mitigated depends on the needs of decision analysis for reservoir management and the cost of information. The potential benefits of acquiring additional data (such as a new seismic acquisition, drilling a new well or the execution of pressure tests) must be considered to gain sufficient information and knowledge to make critical decisions.

In future work, the proposed methodology considering all realizations through the reservoir development plan should be applied to evaluate the value of information (VOI). The decision-making process becoming more difficult to make the best decisions for reservoir developments as reservoir projects becoming more challenging. Considering all realizations in the process should be tested to support the VOI analysis and to facilitate the decision-making process.

References

Aanonsen, S.I.; Naevdal, G.; Reynolds, A.C. (2009). The Ensemble Kalman Filter in Reservoir Engineering – a Review. SPE J. 14(3): pp.393-412.

Abadpour, A.; Adejare, M.; Chugunova, T.; Mathieu, H.; Haller, N. (2018). Integrated Geo-Modeling and Ensemble History Matching of Complex Fractured Carbonate and Deep Offshore Turbidite Fields, Generation of Several Geologically Coherent Solutions Using Ensemble Methods. Abu Dhabi International Petroleum Exhibition & Conference, Abu Dhabi, UAE, 12-15 Nov. SPE-193028-MS.

Abdollahzadeh, A.; Reynolds, A.; Christie, M.; Corne, D.W.; Williams, G.J.; Davies, B.J. (2013). Estimation of Distribution Algorithms Applied to History Matching. SPE Journal, 18(03), pp.508-517.

Ahn, J.; Hong, S.; Yoo, S.; Mutlu, O.; Choi, K. (2016). A scalable processing-in-memory accelerator for parallel graph processing. ACM SIGARCH Computer Architecture News, 43(3), pp.105-117.

Alabert, F.G.; Modot, V. (1992). Stochastic Models of Reservoir Heterogeneity: Impact on Connectivity and Average Permeabilities. Paper SPE-24893 presented at the SPE/ATCE, Washington, D.C., 4-7 Oct 1992.

Al-Samhan, A.M.; Gurpinar, O.M.; Ansarizadeh, M.; Wang, J.T.; Moreno, J.O.; Sinha, S. (2017). Challenges and Solutions of History Matching a Giant Reservoir Model: An Example from the greater Burgan Field, Kuwait. SPE Reservoir Characterization and Simulation Conference, Abu Dhabi, UAE, 8-10 May. SPE-186065.

Ani, M.; Oluyemi, G.; Petrovski, A. (2016). Reservoir Uncertainty Analysis: The Trends from Probability to Algorithms and Machine Learning. Paper presented at the SPE Intelligent Energy International Conference and Exhibition, Aberdeen, UK, 6-8 Sep 2016. SPE-181049-MS.

Ani, M.; Oluyemi, G.; Petrovski, A.; Rezaei-Gomari, S. (2018). Ranking of geostatistical models and uncertainty quantification using Signal Detection Principle (SDP). Journal of Petroleum Science and Engineering, 174, pp.833-843.

Aronofsky, J. (1988). Computer Applications in Oil Production: A Viewpoint. Society of Petroleum Engineers. SPE-17645-PA.

Ates, H.; Bahar, A.; El-Abd, S. (2005). Ranking and Upscaling of Geostatistical Reservoir Models Using Streamline Simulation: A Field Case Study. *SPE Res Eval. & Eng.* 8(1): pp.22-32, SPE-81497-PA.

Avansi, G.D.; Maschio, C.; Schiozer, D.J. (2016). Simultaneous history-matching approach by use of reservoir-characterization and reservoir-simulation studies. SPE Reservoir Evaluation & Engineering, 19(04), pp.694-712.

Baker, M. (2015). Use of Cluster Analysis to Improve Representative Model Selection: A Case Study. Society of Petroleum Engineers. SPE-176408-MS.

Ballin, P.R. (1992). Approximation of Flow Simulation for Uncertainty Assessment. PhD Thesis, Stanford University.

Ballin, P.R.; Aziz, K.; Journel, A.G. (1992). Prediction of Uncertainty in Reservoir Performance Forecast. *J Can Pet Technol* 31(4):52-62. PETSOC-92-04-05.

Batycky, R.; Forster, M.; Thiele, M.R.; Stuben, K. (2010). Parallelization of a commercial streamline simulator and performance on practical models, SPE Reservoir Eval. Eng. 13 (03). SPE-118684-PA.

Bayat, M.; Killough, J.E. (2013). An Experimental Study of GPU Acceleration for Reservoir Simulation. SPE Reservoir Simulation Symposium, Woodlands, Texas, 18-20 Feb. SPE-163628.

Becerra, G.G.; Modenesi, A.P.; Lisboa, E. (2012). Uncertainty History Matching and Forecasting, a Field Application. Paper presented at SPE Latin American & Caribbean Petroleum Engineering Conference in Mexico City, Mexico, 16-18 Apr. SPE-153176.

Beckner, B.L.; Haugen, K.B.; Maliassov, S.; Dyadechko, V.; Wiegand, K.D. (2015). General Parallel Reservoir Simulation. Paper presented at Abu Dhabi International Petroleum Exhibition and Conference, Abu Dhabi, 9-12 Nov 2015. SPE-177532.

Beier T.; Neely, S. (1992). Feature-based image metamorphosis. In: Proc. SIGRAPH 92 Computer Graphics (2272), pp. 35-102.

Bickel, J.E.; Bratvold, R.B. (2007). Decision Making in the Oil and Gas Industry: From Blissful Ignorance to Uncertainty-Induced Confusion. Society of Petroleum Engineers. SPE-109610.

Bocquet, M.; Sakov, P. (2014). An Iterative Ensemble Kalman Smoother. Quarterly Journal of the Royal Meteorological Society, 140(682), pp.1521-1535.

Bouffin, N.; Jensen, J.L. (2010). Efficient Detection of Productive Intervals in Oil and Gas Reservoirs. Journal of Canadian Petroleum Technology, Vol. 49, (3), pp. 58-63. SPE-135660-PA.

Bourdet, D. (2002). Well Test Analysis: The Use of Advanced Interpretation Models, Handbook of Petroleum Exploration and Production, Vol 3, Elsevier, 426p.

Bourdet, D.; Ayoub, J.A.; Pirard, Y.M. (1989). Use of pressure derivative in well test interpretation. SPE Formation Evaluation 4(02):293-302.

Brashear, J.P.; Becker, A.B.; Faulder, D.D. (2001). Where Have All the Profits Gone? Society of Petroleum Engineers – SPE-73141-JPT.

Caers, J. (2011). Modeling Uncertainty in the Earth Sciences. John Wiley & Sons, 246pp.

Campozana, F.P.; Backheuser, Y.; Antunes, R.F.; Camoleze, Z. (2007). Stochastic Modeling and Uncertainty Analysis of Mature Fields. Paper presented at the SPE Latin American and Caribbean Petroleum Engineering Conference, Buenos Aires, Argentina, 15-18 Apr 2007. SPE-108274.

Cancelliere, M.; Verga, F.; Viberti, D. (2011). Benefits and limitations of assisted history matching. SPE Offshore Europe Oil and Gas, Aberdeen, UK, 6-8 Sep. SPE-146278-MS.

Canchumuni, S.A.; Emerick, A.A.; Pacheco, M.A. (2017). Integration of Ensemble Data Assimilation and Deep Learning for History Matching Facies Models. Offshore Technology Conference, Rio de Janeiro, Brazil, 24-26 Oct. OTC-28015-MS.

Cao, H. (2002). Development of Techniques for General Purpose Simulators, Ph.D. Thesis, Stanford University, Stanford, CA.

Cardoso, M.A. (2009). Development and Application of Reduced-Order Modeling Procedures for Reservoir Simulation. PhD Thesis, Stanford University, Stanford, CA.

Carlson, M.R. (2006). Practical Reservoir Simulation - Using, Assessing, and Developing Results. PennWell.

Cedilnik, A.; Rheingans, P. (2000). Procedural annotation of uncertain information. In: Proceedings of the 11th IEEE Visualization 2000 Conference (VIS 2000).

Chen, Y.; Oliver, D.S. (2014). History matching of the Norne full-field model with an iterative ensemble smoother. SPE Reservoir Evaluation & Engineering, 17(02), pp.244-256. SPE-164902-PA.

Chen, Y.; Oliver, D.S. (2012). Ensemble Randomized Maximum Likelihood Method as an Iterative Ensemble Smoother. Mathematical Geosciences 44(1): pp.1-26.

Chen, Y.; Oliver, D.S. (2010). Ensemble-based closed-loop optimization applied to Brugge field. SPE Reservoir Evaluation & Engineering, 13(01), pp.56-71. SPE-118926.

Chien, M.; Tchelepi, H.A; Yardumian, H.E; Chen, W.H. (1997). A Scalable Parallel Multi-Purpose Reservoir Simulator. SPE Symposium on Reservoir Simulation, 8-11 June, Dallas. SPE-37976.

Chien, M.; Wasserman, M.; Yardumian, H.; Chung, E.; Nguyen, T.; Larson, J. (1987). The Use of Vectorization and Parallel Processing for Reservoir Simulation. SPE-16025-MS.

Chiles, J.; Delfiner, P. (2012). Geostatistics: modeling spatial uncertainty. 2nd ed. John Wiley & Sons.

Cominelli, A.; Dovera, L.; Vimercati, S.; Nævdal, G. (2009). Benchmark study of ensemble Kalman filter methodology: History matching and uncertainty quantification for a deep-water oil reservoir. In International Petroleum Technology Conference. IPTC-13748.

Corbett, P.W. (2009). Petroleum Geoengineering: Integration of Static and Dynamic Models: 2009 Distinguished Instructor Short Course. SEG Books.

Corre, B.; Thore, P.; Feraudy, V.D.; Vincent, G.; Elf, T. (2000). Integrated Uncertainty Assessment for Project Evaluation and Risk Analysis. Paper presented at the SPE European Petroleum Conference, Paris, France, 24-25 Oct 2000. SPE-65205.

Cox, T.F.; Cox, M.A.A. (1994). Multidimensional Scaling. Chapman and Hall, London, 213p.

da Cruz, P.S. (2000). Reservoir Management Decision-Making in the Presence of Geological Uncertainty. PhD thesis, Stanford University, Stanford, CA.

da Cruz, P.; Horne, R.; Deutsch, C. (2004). The Quality Map: A Tool for Reservoir Uncertainty Quantification and Decision Making. *SPE Reservoir Evaluation & Engineering*, 7:3–6.

Damsleth, E.; Hauge, A.; Volden, R. (1992). Maximum information at minimum cost: A North Sea field development study using experimental design". *Journal of Petroleum Technology*, pp. 1350-1356.

Davis, T.; Keller, C. (1997). Modelling and visualizing multiple spatial uncertainties. Computers and Geosciences 23 (4), pp.397–408.

de Barros, G.; Deutsch, C.V. (2018). Using All Realizations in Reservoir Management. Centre for Computational Geostatistics (CCG). Paper 209, CCG Annual Report 20.

de Barros, G.; Deutsch, C.V. (2017a). Optimal ordering of realizations for visualization and presentation. Computers & Geosciences 103(2017): pp.51-58.

de Barros, G.; Deutsch, C.V. (2017b). Management of Multiple Realizations through the Lifecycle of Reservoir. Centre for Computational Geostatistics (CCG). Paper 201, CCG Annual Report 19.

de Barros, G.; Deutsch, C.V. (2016). Some thoughts on using all realizations for reservoir management. Centre for Computational Geostatistics Annual Report 18, Paper 202.

Dejean, J.P.; Blanc, G. (1999). Managing uncertainties on production predictions using integrated statistical methods. Paper presented at the SPE annual technical conference and exhibition held in Houston, Texas, 3–6 October 1999. SPE 56696.

Deutsch, C.V. (2015). All Realizations all the Time. Centre for Computational Geostatistics Annual Report 17, Paper 101.

Deutsch, C.V. (1998). Fortran Programs for Calculating Connectivity of Three-Dimensional Numerical Models and for Ranking Multiple Realizations. Computers & Geosciences 24(1):69-76.

Deutsch, C.V. (1993). Conditioning Reservoir Models to Well Test Information. In: Geostatistics Tróia ’92, ed A. Soares, vol. 5, Quantitative Geology and Geostatistics, Kluwer Academic Publishers, pp. 505-518.

Deutsch, C.V. (1992). Annealing Techniques Applied to Reservoir Modeling and the Integration of Geological and Engineering (Well Test) Data. PhD Thesis, Stanford University, 304p.

Deutsch, C.V.; Journel, A.G. (1998). GSLIB: geostatistical library and users guide. Oxford University Press, New York.

Deutsch, C.V.; Journel, A.G. (1994). Integrating Well Test--Derived Effective Absolute Permeabilities in Geostatistical Reservoir Modeling, pp. 131-142.

Deutsch, C.V.; Srinivasan, S. (1996). Improved Reservoir Management Through Ranking Stochastic Reservoir Models. Paper presented at the SPE/DOE Improved Oil Recovery Symposium, Tulsa, Oklahoma, 21-24 Apr 1996. SPE-35411.

Djurcilov, S.; Kim, K.; Lermusiaux, P.; Pang, A. (2001). Volume rendering data with uncertainty information. In: Proceedings of the EG+IEEE VisSym on Data Visualization, pp. 243–252.

Dogru, A.H.; Li, K.G.; Sunaidi, H.A.; Habiballah, W.A.; Fung, L.; Al-Zamil, N.; Srivastava, N.K. (1999). A Massively Parallel Reservoir Simulator for Large Scale Reservoir Simulation. SPE Reservoir Simulation Symposium, 14-17 Feb, Houston, Texas. SPE-51886-MS.

Dongarra, J. (1996). Performance of Various Computers Using Standard Linear Equations Software. 19 December 1996 version, available as a Postscript file from http://www.netlib.org/benchmark/performance.ps

Dooley, M.; Lavin, S. (2007). Visualizing method-produced uncertainty in isometric mapping. Cartographic Perspectives 56, pp.17–36.

Dromgoole, P. & Speers, R. (1997). Geoscore: a method for quantify uncertainty in field reserve estimates. Petroleum Geoscience, 3:1-12.

Durlofsky, L.J. (2005). Upscaling and Gridding of Fine Scale Geological Models for Flow Simulation. In: Paper Presented at the 8th International Forum on Reservoir Simulation, Stresa, Italy, 20–24 Jun.

Durlofsky, L.J.; Jones, R.C.; Milliken, W.J. (1997). A Nonuniform Coarsening Approach for the Scale-Up of Displacement Processes in Heterogeneous Porous Media. Adv. Water Resour. 20, pp.335–347.

Ehlschlaeger, C.; Shortridge, A.; Goodchild, M. (1997). Visualizing spatial data uncertainty using animation. Computers & Geosciences 23 (4), pp.387–395.

Emerick, A.A. (2016). Analysis of the performance of ensemble-based assimilation of production and seismic data. Journal of Petroleum Science and Engineering, 139, pp.219-239.

Emerick, A.A.; Reynolds, A.C. (2013). History-matching production and seismic data in a real field case using the ensemble smoother with multiple data assimilation. SPE Reservoir Simulation Symposium, The Woodlands, Texas, 18-20 Feb. SPE-163675.

Emerick, A.A.; Reynolds, A.C. (2011). History matching a field case using the ensemble Kalman filter with covariance localization. SPE Reservoir Evaluation & Engineering, 14(04), pp.423-432.

Emerick, A.A.; Reynolds, A.C. (2010). EnKF-MCMC. In SPE EUROPEC/EAGE Annual Conference and Exhibition, Barcelona, Spain, 14-17 Jun. SPE-13175.

Engels, M. (2004). Portfolio Optimization: Beyond Markowitz. Master of Science Thesis, University of Leiden.

Erbas, D.; Christie, M.A. (2007). Effect of sampling strategies on prediction uncertainty estimation. In SPE Reservoir Simulation Symposium, Houston, Texas, 26-28 Feb. SPE-106229-MS.

Ertekin, T.; Abou-Kassem, J.H.; King, G.R. (2001). Basic Applied Reservoir Simulation. SPE, 406p.

Esler, K.P. et al. (2014). Realizing the Potential of GPUs for Reservoir Simulation. In: ECMOR XIV-14th European Conference on the Mathematics of Oil Recovery.

Esler, K.P.; Atan, S.; Ramirez, B.; Natoli, V. (2011). Accelerating reservoir simulation with GPUs. In Proceedings of the 73rd EAGE Conference & Exhibition.

Evensen, G.; Hove, J.; Meisingset, H.; Reiso, E.; Seim, K. S.; Espelid, O. (2007). Using the EnKF for assisted history matching of a North Sea reservoir model. In SPE Reservoir Simulation Symposium, Houston, Texas, 26-28 Feb. SPE-106184.

Farah, N.; Ding, D.Y.; Wu, Y.S. (2015). Simulation of the Impact of Fracturing Fluid Induced Formation Damage in Shale Gas Reservoirs. Society of Petroleum Engineers. SPE-173264-MS.

Fei, J.; Yarus, J.M.; Chambers, R. (2016). Apply Two-Way Cluster Analysis to Select Candidate Reservoir Models from Multiple Realizations. Paper presented at the SPE/IAEE Hydrocarbon Economics and Evaluation Symposium, Houston, Texas, USA, 17-18 May 2016. SPE-179955.

Fetel, E.; Caumon, G. (2008). Reservoir flow uncertainty assessment using response surface constrained by secondary information. J Petrol Sci Eng 60:170–182.

Fisher, P. (1993). Visualizing uncertainty in soil maps by animation. Cartographica: The International Journal for Geographic Information and Geovisualization 30 (2), 20–27.

Fjerstad, P.A.; Sikandar, A.S.; Cao, H.; Liu, J. (2005). Next Generation Parallel Computing for Large-Scale Reservoir Simulation. SPE-97358.

Flood, M.M. (1956). The Traveling-Salesman Problem. Operations Research 4 (1), 61–75.

Gallardo, E.; Deutsch, C.V. (2017). A Decision-Making Model for Active Geological Risk Management (AGRM) in Petroleum Reservoir Operations. Centre for Computational Geostatistics (CCG). Paper 213, CCG Annual Report 19.

Gao, G.; Vink, J.C.; Chen, C.; Tarrahi, M.; El Khamra, Y. (2016). Uncertainty quantification for history matching problems with multiple best matches using a distributed Gauss-Newton method. In SPE Annual Technical Conference and Exhibition. Society of Petroleum Engineers. SPE-181611-MS.

Gautier Y.; Noetinger, B. (2004). Geostatistical Parameters Estimation using Well Test Data. Oil & Gas Science and Technology – Rev. IFP, Vol 59, No 2, pp. 167-183.

Gilman, J.R.; Ozgen, C. (2013). Reservoir simulation: history matching and forecasting. Richardson, TX: Society of Petroleum Engineers, 109p.

Gomes-Hernandez, J.J.; Carrera, J. (1994). Using Linear Approximations to Rank Realizations in Groundwater Modeling: Application to Worst Case Selection. Water Resources Research 20(7), 2065.

Goovaerts, P. (1997). Geostatistics for natural resources evaluation. Oxford University Press, New York.

Gorbovskaia, O.A. (2017). Probabilistic Geological Uncertainties Assessment: Lessons Learned. Paper presented at the SPE Annual Caspian Technical Conference and Exhibition, Baku, Azerbaijan, 1-3 Nov 2017. SPE-189015.

Gross, H.; Honarkhah, M.; Chen, Y. (2011). Offshore Gas Condensate Field History-Matching and Predictions: Ensuring Probabilistic Forecasts Are Built with Diversity in Mind. Paper

presented at the SPE Asia Pacific Oil and Gas Conference and Exhibition, Jakarta, Indonesia, 20-22 Sep 2011. SPE-147848.

Hamdi H.; Jamiolahmady, M.; Corbertt, P.W.M. (2011). Modeling the Interfering Effects of Gas Condensate and Geological Heterogeneities on Transient Pressure Response. Society of Petroleum Engineers Annual Conference and Exhibition, Vienna – SPE-143613, 16p.

Hamdi, H. (2014). Well-test response in stochastic permeable media. Journal of Petroleum Science and Engineering, Volume 119, July 2014, pp. 169-184.

Haugen, V.E.J.; Natvik, L.J.; Evensen, G.; Berg, A.M.; Flornes, K.M.; Naevdal, G. (2006). History matching using the ensemble Kalman filter on a North Sea field case. In SPE Annual Technical Conference and Exhibition, San Antonio, Texas, 24-27 Sep. SPE-102430-MS.

Hawick, K.; Leist, A.; Playne, D. (2010). Parallel Graph Component Labelling with GPUs and CUDA. Parallel Computing 36(12):655-678.

Hegstad, B.K.; Saetrom, J. (2014). Using Multiple Realizations from an Integrated Uncertainty Analysis to Make More Robust Decisions in Field Development. Abu Dhabi International Petroleum Exhibition and Conference, Abu Dhabi, UAE, Society of Petroleum Engineers, 10-13 November, 2014. SPE-171831-MS.

Hird, K.B.; Durbrule, O. (1995). Quantification of Reservoir Connectivity for Reservoir Description Applications. Paper presented at the SPE/ATCE, Dallas, Texas, 22-25 Oct, 1995. SPE-30751.

Holden, L.; Madsen, R.; Skorstad, A.; Jakobsen, K.A.; Tjolsen, C.B.; Vik, S. (1995). Use of Well Test Data in Stochastic Reservoir Modelling. Society of Petroleum Engineers, SPE Annual Technical Conference and Exhibition, Dallas – SPE 30591.

Höllt, T.; Magdy, A.; Zhan, P.; Chen, G.; Gopalakrishnan, G.; Hoteit, I.; Hansen, C.D.; Hadwiger, M. (2014). Ovis: A Framework for Visual Analysis of Ocean Forecast Ensembles. In: IEEE Transactions on Visualization and Computer Graphics, vol. 20, no. 8, pp. 1114-1126.

Horne, R.N. (1995). Modern well test analysis. Petroway Inc, 259p.

Hu, L.Y.; Ravalec, M.L.; Blanc, G. (2001). Gradual deformation and iterative calibration of truncated Gaussian simulations. Pet. Geosci. 7, 25–30.

Idrobo, E.A.; Choudhary, M.K.; Datta-Gupta, A. (2000). Swept Volume Calculations and Ranking of Geostatistical Reservoir Models Using Streamline Simulation. Paper presented at SPE/AAPG Western Regional Meeting, Long Beach, USA, 19-23 Jun 2000. SPE-62557.

Interrante, V. (2000). Harnessing natural textures for multivariate visualization. IEEE Computer Graphics and Applications 20 (6), 6–11.

Isaaks, E. H.; Srivastava, R. M. (1989). Applied geostatistics. Oxford University Press, New York.

Jensen, J.; Lake, L.W.; Corbett, P.W.; Goggin, D. (2000). Statistics for petroleum engineers and geoscientists (Vol. 2). Gulf Professional Publishing.

Jia, L.; John, A.; Kumar, N.; Bialas, R.; Lanson, T.P.; Jing, X.D. (2016). Novel Benchmark and Analogue Method to Evaluate Heavy Oil Projects. Society of Petroleum Engineers – SPE-184101-MS.

Johnson, P.W. (1988). The relationship between radius of drainage and cumulative production. SPE Formation Evaluation, pages 267–270, March 1988.

Johnstone, D.; Lindley, D. (2013). Mean-Variance and Expected Utility: The Borch Paradox. Statist. Sci. 28 (2013), 2, 223-237.

Jones, A.D.W.; Al-Qabandi, S.; Reddick, C.E.; Anderson, S.A. (1997). Rapid assessment of pattern waterflooding uncertainty in a giant oil reservoir. Paper presented at the 1997 Annual Technical Conference and Exhibition, San Antonio, TX. SPE-38890.

Journel, A.G. (1989). Fundamentals of Geostatistics in Five Lessons. *In* Short Course in Geology, volume 8, American Geophysical Union, Washington, D.C.

Journel, A.G. (1986). Geostatistics: models and tools for the earth sciences. *Mathematical Geology*, 18(1):119-140.

Kaarstad T.; Frauen, J.; Bjorstad, P.; Espedal, M. (1995). A massively Parallel Reservoir Simulator. SPE Symposium on Reservoir Simulation. San Antonio. SPE-29139.

Kao, D.; Dungan, J.; Pang, A. (2001). Visualizing 2D Probability Distributions from Eos Satellite Image-Derived Data Sets: A Case Study. In: Proceedings of the IEEE Visualization Conference, pp. 457–560.

Kao, D.; Kramer, M.; Love, A.; Dungan, J.; Pang, A. (2005). Visualizing Distributions from Multi-Return Lidar Data to Understand Forest Structure. 42(1):35–47.

Kelkar, M.G.; Pochampally, S.; Bahar, A.; Sharifi, M. (2014). Dynamic vs. Static Ranking: Comparison and Contrast in Application to Geo-cellular Models. Society of Petroleum Engineers. SPE-170682-MS.

Khait, M.; Voskov, D. (2017). GPU-Offloaded General Purpose Simulator for Multiphase Flow in Porous Media. Society of Petroleum Engineers. SPE-182663-MS.

Killough, J.E.; Bhogeswara, R. (1991). Simulation of Compositional Reservoir Phenomena on a Distributed Memory Parallel Computer. J. Pet. Tech. 43(11): pp.1-368.

Killough, J.E.; Wheller, M.F. (1991). Parallel Iterative Linear Equation Solvers: An Investigation of Domain Decomposition Algorithms for Reservoir Simulation. SPE Symposium on Reservoir Simulation, 1-4 Feb, San Antonio, Texas. SPE-6021.

Kilough J.E.; Camilleri, D.; Harlow B. (1997). A Parallel Simulator on Local Grid Refinement. SPE Symposium on Reservoir Simulation, 8-11 June, Dallas. SPE-37978.

Kirkpatrick, S.; Gelatt Jr, C.; Vecchi, M. (1983). Optimization by simulated annealing. Science, 220(4598):671–680.

Klie, H. (2015). Physics-Based and data-Driven Surrogates for Production Forecasting. Society of Petroleum Engineers. SPE-173206-MS.

Klie, H.M.; Sudan, H.H.; Li, R.; Saad, Y. (2011). Exploiting capabilities of many core platforms in reservoir simulation. In Proceedings of the 21st SPE Reservoir Simulation Symposium, The Woodlands, Texas, 21-23 February 2011. SPE-141265-MS.

Kloosterman, H.J.; Herring, T.R.; Tull, S.J.; Van der Lee, J.W. (2007). From test tube to value generator: effective use of Experimental Design for uncertainty analysis and development concept optimisation. In: Paper presented at the SPE Europec/EAGE annual conference and exhibition held in London, United Kingdom, 11–14 June 2007. SPE 106893.

Kochenderfer, M.J. (2015). Decision making under uncertainty: theory and application. MIT Press. 323p.

Kosara, R.; Miksch, S.; Hauser, H. (2001). Semantic depth of field. In: Proceedings of the IEEE Symposium on Information Visualization, pp. 97–104.

Lajevardi, S.; Deutsch, C.V. (2014). A New Approach to Reservoir Modeling with Facies Mixing and Distance to Transitions. Proceeding of 16th Annual Meeting of Centre for Computational Geostatistics (CCG), University of Alberta, Edmonton, Canada, Paper No 204.

Lamigueiro, O.P. (2014). Displaying time series, spatial, and space-time with R (The R Series). CRC Press, Chapman & Hall, 197p.

Le Ravalec, M.; Noetinger, B. (2002). Optimization with the gradual deformation method. Math. Geol. 34(2), 125–142.

Lee, B.O. (1982). Evaluation of Devonian shale reservoirs using multiwell pressure transient testing data. In SPE/DOE Unconventional Gas Recovery Symposium, Pittsburgh, PA, May 1982. Society of Petroleum Engineers. SPE/DOE Paper Number 10838.

Levy, H. (2016). Stochastic dominance: investment decision making under uncertainty, 3rd ed. Springer.

Li, G.; Reynolds, A.C. (2009). An iterative ensemble Kalman filter for data assimilation. SPE Journal 14(3): 496-505.

Lie, K.A.; Moyner, O.; Natvig, J.R. (2016). Successful Application of Multiscale Methods in a Real Reservoir Simulator Environment. 15th European Conference on the Mathematics of Oil Recovery, Amsterdam, Netherlands.

Lisboa, E.; Duarte, R. (2010). Uncertainty Analysis Considering the Production History: Evaluation of a Real Field. Paper presented at SPE Latin American & Caribbean Petroleum Engineering Conference in Lima, Peru, 1-3 Dec 2010. SPE-136681.

Liu, N.; Oliver, D.S. (2003). Evaluation of Monte Carlo Methods for Assessing Uncertainty. SPE Journal 8(2): 188-195.

Love, A.; Pang, A.; Kao, D. (2005). Visualizing Spatial Multivalue Data. In: IEEE Computer Graphics and Applications, 25(3):69–79.

Lu, P.; Shaw, J.S.; Eccles, T.K.; Mishev, I.D.; Usadi, A.K.; Beckner, B.L. (2008). Adaptive Parallel Reservoir Simulation. Paper presented at the International Petroleum Technology Conference in Kuala Lumpur, Malaysia, 3-5 Dec 2008. IPTC-12199.

Luo, A.; Kao, D.; Pang, A. (2003). Visualizing Spatial Distribution Data Sets. In: Proceedings of the Symposium on Data Visualisation, pp. 29–38.

Ma, Y.; Chen, A. (2004). Parallel computation for reservoir thermal simulation of multicomponent and multiphase fluid flow. J. Comput. Phys. 201 (1).

MacEachren, A. (1992). Visualizing uncertain information. Cartographic Perspective 13, 10–19.

Manea, A.M.; Tchelepi, H.A. (2017). A Massively Parallel Semicoarsening Multigrid Linear Solver on Multi-Core and Multi-GPU Architectures. SPE Reservoir Simulation Conference. Montgomery, TX, 20-22 Feb. SPE-182718.

Manea, A.M. (2015). Parallel Multigrid and Multiscale Flow Solvers for High-Performance-Computing Architectures. Ph.D. Thesis, Stanford University, Stanford, CA.

Markowitz, H. (1952). Portfolio selection. The Journal of Finance, 7(1), 77–91.

Mattax, C.C.; Dalton, R.L. (1990). Reservoir Simulation (includes associated papers 21606 and 21620). Journal of Petroleum Technology, 42(06), 692-695.

Mattson, T.G. (2003). How good is OpenMP, Sci. Program. 11 (2).

McLennan, J.A.; Deutsch, C.V. (2005). Selecting Geostatistical Realizations by Measures of Discounted Connected Bitumen. Paper presented at the SPE International Thermal Operations and Heavy Oil Symposium, Calgary, Alberta, CA, 1-3 Nov 2005. SPE-98168.

McVay, D.A.; Dossary, M.N. (2014). The Value of Assessing Uncertainty. Society of Petroleum Engineers – SPE-160189-PA.

Meira, L.A.; Coelho, G.P.; Silva, C.G; Schiozer, D.J. (2017). RMFinder 2.0: An Improved Interactive Multi-Criteria Scenario Reduction Methodology. Paper presented at SPE Latin America and Caribbean Engineering Conference, Buenos Aires, Argentina, 18-19 May 2017. SPE-185502-MS.

Mesbah, M.; Vatani, A.; Siavashi, M.; Doranehgard, M.H. (2019). Parallel processing of numerical simulation of two-phase flow in fractured reservoirs considering the effect of natural flow barriers using the streamline simulation method. International Journal of Heat and Mass Transfer, Volume 131, Pages 574-583.

Meuer, H.W.; Gietl, H. (2013). Supercomputers–Prestige objects or crucial tools for science and industry? PIK-Praxis der Informationsverarbeitung und Kommunikation, 36(2), 117-128.

Mirzayev, M.; Jensen, J.L. (2016). Measuring Interwell Communication using the Capacitance Model in Tight Reservoirs. SPE Western Regional Meeting, 23-26 May, Anchorage, Alaska, USA. SPE-180429-MS.

Mohajeri, S.; Eslahi, R.; Bakhtiari, M.; Zeinali, M.; Rajabi, H.; Alizadeh, A.; Mortezazadeh, E. (2018). Advances in Parallel Reservoir Simulation Technology, using Multi-Threaded Algorithms. SPE International Petroleum Exhibition & Conference, 12-15 Nov, Abu Dhabi, UAE. SPE-193218-MS.

Nair, R. (2015). Evolution of memory Architecture. Proceedings of the IEEE, Vol. 103, No 8, August 2015.

Nishikori, N.; Sugai, K.; Normann, C.; Onstein, A.; Melberg, O. (2008). Na integrated workflow for Gas Injection EOR and a Successful Application to a Heterogeneous Sandstone Reservoir in the Southern North Sea. International Petroleum Technology Conference, Kuala Lumpur, Malaysia, 2-5 Dec - Paper IPTC-12025.

Obermaier, H.; Joy, K.I. (2014). Future Challenges for Ensemble Visualization. In: IEEE Computer Graphics and Applications, vol. 34, no. 3, pp. 8-11.

Oliver, D.S.; Chen, Y. (2011). Recent Progress on Reservoir History Matching: a Review, Computational Geosciences, 15(1), 185-221.

Oliver, D.S.; Reynolds, A.C.; Liu, N. (2008). Inverse theory for petroleum reservoir characterization and history matching. Cambridge University Press.

Pang, A.T.; Wittenbrink, C.M.; Lodha, S.K. (1997). Approaches to Uncertainty Visualization. The Visual Computer, 13:370–390.

Perrone, A.; Pennadoro, F.; Tiani, A.; Della Rossa, E.; Saetrom, J. (2017). Enhancing the Geological Models Consistency in Ensemble Based History Matching an Integrated Approach. In SPE Reservoir Characterisation and Simulation Conference and Exhibition, Abu Dhabi, UAE, 08-10 May. SPE-186049-MS.

Peters, L.; Arts, R.; Brouwer, G.; Geel, C.; Cullick, S.; Lorentzen, R.J.; Sarma, P. (2010). Results of the Brugge benchmark study for flooding optimization and history matching. SPE Reservoir Evaluation & Engineering, 13(03), 391-405. SPE-119094.

Phadke, M.N.; Pinto, L.; Alabi, F.; Harter, J.; Taylor, R.M.; Wu, X.; Petersen, H.; Bass, S.A.; Healey, C.G. (2012). Exploring Ensemble Visualization. In: Proceedings of SPIE, 8294(82940B).

Poollen, H.K. (1964). A hard look at radius of drainage and stabilization-time equations. Oil and Gas Journal, pages 139–147, September 1964.

Potter, K.; Rosen, P.E.; Johnson, C.R. (2012). From quantification to visualization: a taxonomy of uncertainty visualization approaches. In: Uncertainty Quantification in Scientific Computing, IFIP Advances in Information and Communication Technology Series, 377:226-249. 2012.

Praetor M.; Wheeler, J.A.; Pope, G.; Wang, K.; Wang, P. (1997). A New Compositional EOS Reservoir Simulator: Part II - Framework and Multiprocessing. SPE Symposium on Reservoir Simulation, 8-11 June, Dallas. SPE-37977.

Pyrcz, M. J.; Deutsch, C. V. (2014). Geostatistical reservoir modeling. Oxford University Press, NewYork.

Rhodes, P.; Laramee, R.; Bergeron, R.; Sparr, T. (2003). Uncertainty visualization methods in isosurface rendering. In: EUROGRAPHICS 2003 Short Papers, pp. 83–88.

Robinson, A. (2006). Highlighting techniques to support geovisualization. In: Proceedings of the ICA Workshop on Geovisualization and Visual Analytics.

Romero, C.E.; Carter, J.N.; Gringarten, A.C.; Zimmerman, R.W. (2000). A modified genetic algorithm for reservoir characterisation. In International Oil and Gas Conference and Exhibition in China. Society of Petroleum Engineers.

Rossi, M.E.; Deutsch, C.V. (2014). Mineral Resource Estimation. Springer Science Business Media.

Rutledge, J.M.; Jones, D.R.; Chen, W.H.; Chung, E.Y. (1991). The Use of Massively Parallel SIMD Computer for Reservoir Simulation. SPE Symposium on Reservoir Simulation, Anaheim. SPE-21213.

Saad, N.; Maroongroge, V.; Kalkomey, C.T. (1996). Ranking Geostatistical Models using Tracer Production Data. Paper presented at the 1996 European 3-D Reservoir Modeling Conference, Stavanger, Norway, 16-17 Apr 1996. SPE-35494.

Saetrom, J.; Katterbauer, K.; Munck, T. (2015). Improved Reservoir Management Decisions using Ensemble Based Methods. SPE Reservoir Characterization and Simulation Conference, Abu Dhabi, UAE, 14-16 Sep. SPE-175668-MS.

Sakov, P.; Oliver, D.S.; Bertino, L. (2012). An iterative EnKF for strongly nonlinear systems. Monthly Weather Review, 140(6), 1988-2004.

Sarma, P.; Chen, W.H.; Xie, J. (2013). Selecting Representative Models from a Large Set of Models. Society of Petroleum Engineers. SPE-163671-MS

Satter, A.; Iqbal, G.M. (2015). Reservoir Engineering: The Fundamentals, Simulation, and Management of Conventional and Unconventional Recoveries. Gulf Professional Publishing.

Sawyer, D.N.; Cobb, W.M.; Stalkup, F.I.; Braun, P.H. (1974). Factorial Design Analysis of the Wet Combustion Drive. Paper presented at the SPE Annual Meeting, San Antonio, Oct. 8-11. SPE-4140.

Scheidt, C.; Caers, J. (2009a). Representing Spatial Uncertainty Using Distances and Kernels. Mathematical Geosciences 41 (4):397-419.

Scheidt, C.; Caers, J. (2009b). Uncertainty Quantification in Reservoir Performance Using Distances and Kernel Methods – Application to a West Africa Deepwater Turbidite Reservoir. Society of Petroleum Engineers. SPE-118740-PA.

Scott, S.L.; Wainwright, R.L.; Raghavan, R.; Demuth, H. (1987). Application of Parallel (MIMD) Computers to Reservoir Simulation. SPE Symposium on Reservoir Simulation, San Antonio. SPE-16020.

Shamsuddin, S.M.; Razali, N.H.; Salehuddin, R. (2012). Review of Image Morphing Methods and Techniques. In: Multimedia Data Processing - Review of Image Morphing Technique: Sem1-2012-2013.

Sharifi, M.; Kelkar, M.; Bahar, A.; Slettebo, T. (2014). Dynamic Ranking of Multiple Realizations by Use of the Fast-Marching Method. *SPE Journal* SPE-169900.

Shiralkar, G.S.; Stephenson, R.E.; Joubert, W.; Lubeck, O.; van Bloemen, B. (1997). A Production Quality Distributed Memory Reservoir Simulator. SPE Symposium on Reservoir Simulation, 8-11 June, Dallas. SPE-37975.

Shirangi, M.G.; Durlofsky, L.J. (2016). A general method to select representative models for decision making and optimization under uncertainty. Computers & Geosciences (96):109-123.

Singh, G.; Chelini, L.; Corda, S.; Awan, A.J.; Stuijk, S.; Jordans, R.; Boonstra, A.J. (2018). A Review of Near-Memory Computing Architectures: Opportunities and Challenges. In Proceedings of the 21st Euromicro Conference on Digital System Design (DSD).

Själander, M.; Martonosi, M.; Kaxiras, S. (2014). Power-Efficient Computer Architectures: Recent Advances. In Synthesis Lectures on Computer Architecture., San Rafael, CA, USA:Morgan & Calypool, 2014.

Srivastava, R.M. (1994). The interactive visualization of spatial uncertainty. SPE 27965, pp. 87–95.

Steagall, D.E.; Schiozer, D.J. (2001). Uncertainty Analysis in Reservoir Production Forecasts During Appraisal and Pilot Production Phases. Paper presented at the SPE Reservoir Simulation Symposium, Houston, USA, 11-14 Feb 2001. SPE-66399.

Subbey, S.; Mike, C.; Sambridge, M. (2003). A strategy for rapid quantification of uncertainty in reservoir performance prediction. In SPE Reservoir Simulation Symposium, Houston, Texas, 03-05 Feb. SPE-79678-MS.

Suslick, S.B.; Schiozer, D.; Rodriguez, M.R. (2009). Uncertainty and risk analysis in petroleum exploration and production. Terrae, 6(1), 2009.

Telishev, A.; Bogachev, K.; Shelkov, V.; Eydinov, D.; Tran, H. (2017). Hybrid Approach to Reservoir Modeling Based on Modern CPU and GPU Computational Platforms. Society of Petroleum Engineers. SPE-187797-MS

Thiele, M.R.; Batycky, R.P. (2016). Evolve: A Linear Workflow for Quantifying Reservoir Uncertainty. Paper presented at SPE Annual Technical Conference and Exhibition, Dubai, UAE, 26-28 Sep 2016. SPE-181374-MS.

Thiele, M.R.; Batycky, R.P.; Fenwick, D.H. (2010). Streamline Simulation for Modern Reservoir-Engineering Workflows. Journal Petroleum Technology, Vol 62, No 1, pp. 64-70.

Tleukhabyluly, O.; Dallorto, M.; Porcelli, F.; Tarantini, V. (2016). Speeding Up a Reservoir Simulation – Case Study on Giant Carbonate Reservoirs. SPE Annual Caspian Technical Conference & Exhibition, 1-3 Nov, Astana, Kazakhstan. SPE-182560-MS.

Vakili-Ghahani, S.A.; Jansen, J.D. (2012). A System-Theoretical Approach to Selective Grid Coarsening of Reservoir Models. Comput Geosci (2012) 16:159-176.

Vallhs, B.; Naevdal, G. (2009). Revisiting Brugge case study using a hierarchical ensemble Kalman filter. In International Petroleum Technology Conference. International Petroleum Technology Conference, Doha, Qatar, 7-9 Dec. IPTC-14074-MS.

Viard, T.; Caumon, G.; Levy, B. (2011). Adjacent versus Coincident Representations of Geospatial Uncertainty: Which Promote Better Decisions? In: Computers & Geosciences, 37 (4), pp. 511-520.

Walls, M. (2005a). Corporate risk-taking and performance: A 20 years look at the petroleum industry. Journal of Petroleum Science and Engineering 48(2005) 127-140.

Walls, M. (2005b). Measuring and Utilizing Corporate Risk Tolerance to Improve Investment Decision Making. The Engineering Economist, 50(4), 361–376.

Watts, J.W. (1997). Reservoir Simulation: Past, Present, and Future. SPE Reservoir Simulation Symposium, Dallas, 8-11 June. SPE-38441-PA.

Wen, X.H.; Deutsch, C.V.; Cullick, A.S.; Reza, Z.A. (2005). Integration of Production Data in Generating Reservoir Models, CCG Monograph Volume 1, Centre for Computational Geostatistics, University of Alberta, Edmonton, Canada.

Wickens, L.M. & Kelly, R. (2010). Rapid Assessment of Potential Recovery Factor: A New Correlation Demonstrated on UK and USA Fields. Society of Petroleum Engineers, SPE Annual Technical Conference and Exhibition, Florence, Italy, 19-22 Sep - Paper SPE-134450.

Yadavalli, S.K.; Roadifer, R.D.; Jones, J.R.; Krase, L.D.; Yeh, N.S. (1994). Use of pressure transient data to obtain geostatistical parameters for reservoir characterization. Society of Petroleum Engineers, SPE Annual Technical Conference and Exhibition, New Orleans, SPE 28432, pp. 719-732.

Yazdi, M.M.; Jensen, J.L. (2014). Fast screening of geostatistical realizations for SAGD reservoir simulation. Journal of Petroleum Science and Engineering, Vol. 124, pp. 264-274.

Yong, L.; Chunxia, J.; Benbiao, S.; Baozhu, L.; Yixiang, Z.; Qihao, Q.; Chenji, W. (2017). Geological Models Comparison and Selection for Multi-layered Sandstone Reservoirs. Society of Petroleum Engineers. SPE-183812-MS.

Yousef, A.A.; Gentil, P.; Jensen, J.L.; Lake, L.W. (2006). A Capacitance Model to Infer Interwell Conectivity from Production- and Injection-Rate Fluctuations. SPE Annual Technical Conference and Exhibition, 9-12 Oct, Dallas, SPE-95322, pp. 630-646.

Zhang, Y.; Lorentzen, R.J.; Stordal, A.S. (2018). Practical Use of the Ensemble-Based Conjugate Gradient Method for Production Optimization in the Brugge Benchmark Study. In SPE Norway One Day Seminar. Society of Petroleum Engineers. SPE-191314.

Zhang, Y.; Oliver, D.S. (2011). History matching using the ensemble Kalman filter with multiscale parameterization: A field case study. SPE Journal, 16(02), 307-317.

Zheng, S.Y.; Legrand, V.M.; Corbertt, P.W. (2007). Geological Model Evaluation through Well Test Simulation: A Case Study from the Wytch Farm Oilfield, Southern England. Journal of Petroleum Geology, Vol. 30(1), pp. 41-58.

Zhou, Y.; Jiang, Y.; Tchelepi, H.A. (2013). A Scalable Multistage Linear Solver for Reservoir Models with Multisegment Wells. Computational Geosciences, 17(2): 197-216.

Appendix A

Production Data Integration

HM refers to the adjustment of model variables in a numerical simulator so that the model is calibrated to field observations, for example production data or time-lapse seismic data. Core and well log measurements reflect reservoir properties at the vicinity of the wellbore. They are usually referred to as hard data and are commonly used to condition reservoir models prior to matching dynamic data. Production data are the most widely used data for HM.

WTA is a standard measurement technique of recording pressure and rate data from a reservoir (Hamdi, 2014). In this process, a transient pressure response is created by a temporary change in production rate. The well response is usually monitored during a relatively short period compared to the life of the reservoir.

In most cases, the flow rate is measured at surface while the pressure is recorded downhole. Before starting the test, the initial pressure is often constant and uniform in the reservoir. During the flowing period, the drawdown pressure response is calculated by the difference between the initial and current reservoir pressure.

The type of test performed is related to the test objectives or is governed by practical limitations. Among the various types of well tests, the two main types are (Figure A.1):

Drawdown test: this type of test is a sequence of bottom-hole pressure (BHP) observations in a well with a constant flow rate. It is a good method of reservoir limit testing, since the time to observe a boundary response is long. It may be difficult to make the well flow at constant rate, even after it has stabilized.

Buildup test: this type of test is the most commonly used method. A well flowing at a constant rate is shut-in and the BHP pressure is measured as the pressure build up. The practical advantage of a buildup test is that the constant flow rate condition is more easily achieved (Horne, 1995). On the other hand, it may be difficult to achieve the constant rate production prior to the shut in. Besides, the well production is lost while the test is performed.

Unlike geological and log data, WTA provides a description of the reservoir in dynamic conditions. As the investigated reservoir volume is relatively large, the estimated parameters are

average values. Interpreted results from WTA give important information about reservoir properties such as fluids, initial and average pressures, reservoir boundaries, heterogeneities (natural fractures, layering), horizontal and vertical permeability, etc. Properties related to the well can also be determined such as productivity index and skin factor.

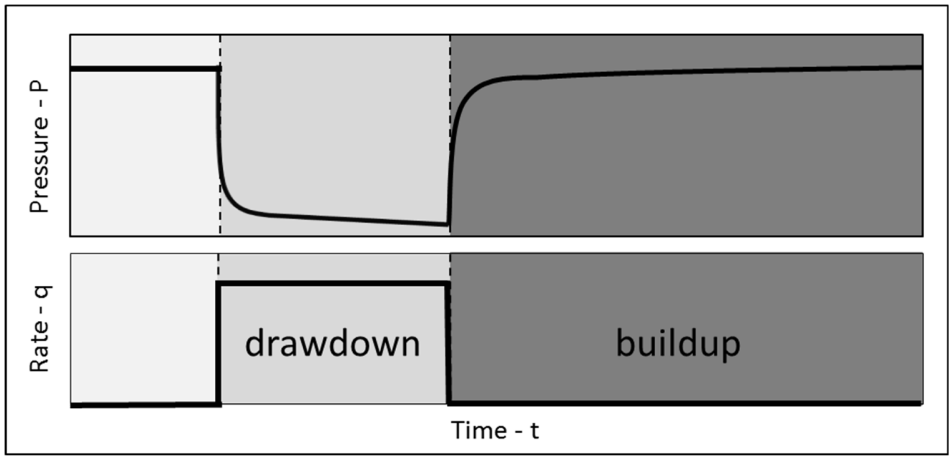

Figure A.1: Bottom-hole pressure and flow rate responses during drawdown and buildup tests.

Some diagnostic plots are used to aid the interpretation of recorded pressure. The most common is a log-log plot of pressure drop and pressure derivative versus time (Figure A.2). The effects of reservoir properties can be observed on the derivative curve in terms of distinct slopes and stabilizations (Hamdi, 2014). The average well test permeability is estimated from the radial flow regime, where the derivative curve plateaus off over a definite value. This is an average permeability of a region around the wellbore with a larger scale than the core measurements (Corbett, 2009).

A.1 – Wellbore Storage and Infinite-Acting Radial Flow

While flow rates in a well test are measured at the wellhead valve or flow line, pressure response of the reservoir is taken within the wellbore itself, close to the production zone. When a well is opened, the production at surface is initially due to the expansion of the fluid stored in the wellbore. This effect is called wellbore storage and according to Bourdet (2002) can last from

a few seconds to a few minutes. The reservoir properties cannot be estimated during this flow regime. Then the reservoir production starts and the sand face rate becomes the same as the surface rate - Infinite-Acting Radial Flow. In this condition, pressure response describes in effect the reservoir behavior.

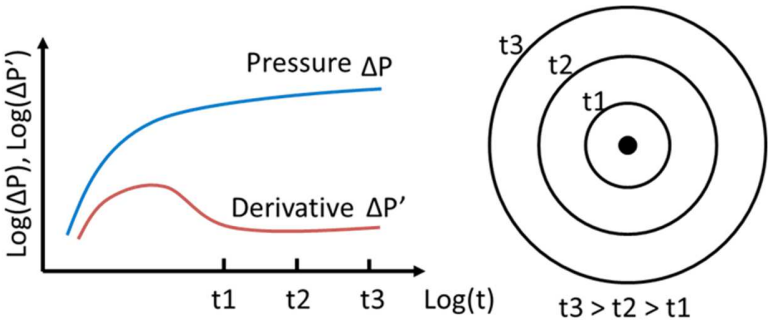

Figure A.2: Diagnostic plot showing change of pressure (blue line) and pressure derivative (red line) versus time (both in log scale). On the right: plan view sketch of the radius of well test investigation increasing over time.

The diagnostic plot is used to identify the pure wellbore regime. With a constant surface rate condition, the pressure changes linearly with time. At early time, the response follows a straight line of unit slope (Bourdet et al., 1989), as shown in Figure A.3.

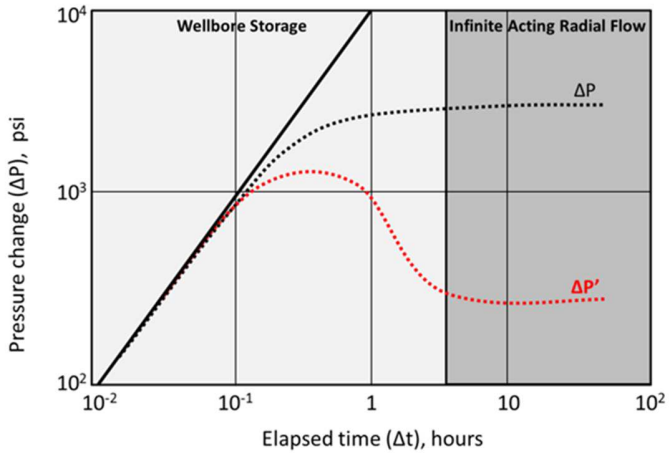

Figure A.3: Pressure change and pressure derivative during wellbore storage and in the infinite acting regime. After a period of time, when the fluid stored in the wellbore, the reservoir production starts, describing the infinite acting radial flow.

A.2 – Average Permeability

The average permeability (K_{avg}) is a property derived from WTA valid within an annular region of investigation. This property is based on the pressure response during the infinite-acting radial flow. Considering a typical pressure response shown on Figure 6.4, a plot of pressure versus the log of time (Miller-Dyes-Hutchinson Plot), the slope **m** on the straight line is linearly related to the permeability as follows:

$$K_{avg} = 162.6 * \frac{qB\mu}{mh} \quad \text{(Eq. A.1)}$$

where K_{avg} is the average permeability (mD), **q** is the flow rate (STB/d), **B** is formation volume factor (RB/STB), μ is the fluid viscosity (cp) and **h** is the formation thickness (feet).

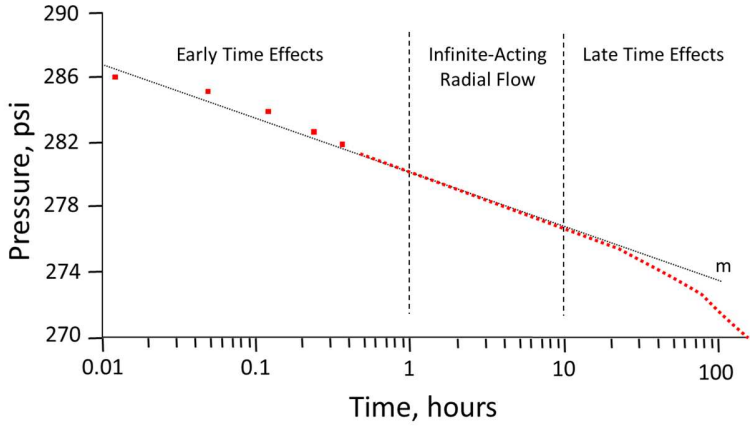

Figure A.4: A Miller-Dyes-Hutchinson (MDH) semilog plot showing the pressure against the logarithm of time. Average permeability can be calculated by the slope m from the plot during the infinite acting radial flow regime (modified from Wen et al., 2005).

A.3 – Radius of investigation

The pressure response is conventionally based on analytical solutions of the radial diffusivity equation (e.g., Deutsch, 1992; Zheng et al., 2007; Hamdi, 2014). In theory, a pressure change at the well would be felt at least infinitesimally everywhere in the reservoir. However, in

practice, there is some point distant from the well at which the pressure response is small and can be neglected. This point defines the region of the reservoir that has been tested during WTA and corresponds to the radius of investigation.

The radius of investigation (r_i) can be defined as the reservoir volume during the infinite-acting radial flow period in a specified period of time (t_{min} and t_{max}). According to several definitions (Poolen, 1964; Lee, 1982; Johnson, 1988; Horne, 1995; Bourdet, 2002), r_i can be written as:

$$r_i = A * \sqrt{\frac{K_{avg} * \Delta t}{\emptyset * \mu * c_t}} \qquad \text{(Eq. A.2)}$$

where $\mathbf{r_i}$ is radius (feet), **A** is a constant (traditionally 0.03), $\mathbf{K_{avg}}$ is the average permeability (mD), $\mathbf{\Delta t}$ is the well test period (hours), ϕ is porosity (pore vol / bulk vol), μ is viscosity (cp) and $\mathbf{c_t}$ is fluid compressibility (psi^{-1}).

Equation A.2 assumes that the horizontal permeability near the well is isotropic. For an anisotropic permeability field, an equivalent isotropic reservoir model of average radial permeability can describe the pressure response of the well (Bourdet, 2002). In this equivalent isotropic system, the original wellbore is changed into an ellipse whose major and minor axis ratio corresponds to the square root of the of permeability anisotropy ratio (Figure A.5). Although the area around the well is the same compared with the original system, the perimeter of the equivalent system is increased (Bourdet, 2002).

Both properties, K_{avg} and r_i, obtained from WTA, are important information that could improve geological modeling.

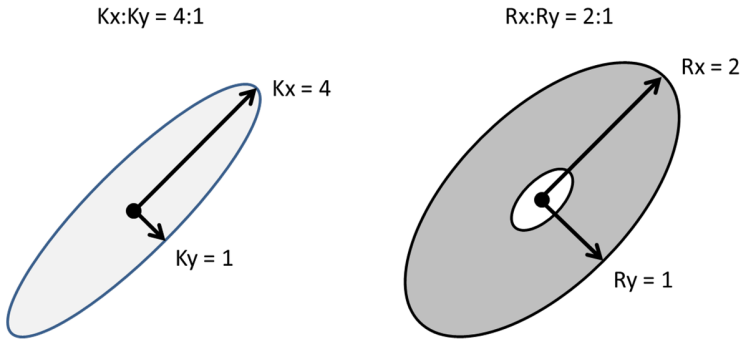

Figure A.5: Considering an anisotropic permeability field, the radius of investigation of the well test is not circular but elliptical. The ratio of major and minor axis corresponds to the square root of the permeability anisotropy ratio.

A.4 – Numerical Examples

A synthetic 2-D model is represented by 256 x 256 x 1 regular grid blocks with 10m dimensions in X and Y directions and 5m dimension in Z direction. The synthetic reservoir is produced by a single well near to the center of the model. Porosity is assumed equal to 0.2 in the whole model. Reservoir dynamic properties used in the examples are listed in Table A.1.

Table A.1: Dynamic properties used in this example.

Property	Value
Initial pressure (kPa)	20000
Oil volume factor (RB/STB)	1.12
Total compressibility (kPa^{-1})	7.25E-6
Oil viscosity(cP)	2.0
Initial Water Saturation	0.1

The first example considers a deterministic permeability field equal to 1000mD in the whole grid. A 24 hours drawdown production is simulated considering a constant flow rate equal to 30 m^3/day. BHP has been measured and the diagnostic plot has been created to calculate K_{avg} and r_i from the WTA.

The second example considers 100 realizations of stochastic permeability maps. A 24 hours drawdown production is simulated considering a constraint flow rate equal to 30 m^3/day for each permeability realization map.

Figure A.6 shows the deterministic case, illustrated by the grid with a 1000md constant permeability and a central well. The figure also shows the pressure field at the end of the drawdown test and the bottom-hole pressure variation during the test.

Figure A.7 shows the standard log-log diagnostic plot of pressure and pressure derivative of the observed pressure drawdown data. r_i and K_{avg} are calculated using Equations A.1 and A.2, as shown on the semi-log plot in the Figure A.8. Early times of the diagnostic plot correspond to the wellbore storage period. As mentioned before, data of that period are not considered for the permeability and drainage area accounts. As expected, average permeability based on well test is consistent with the input permeability model.

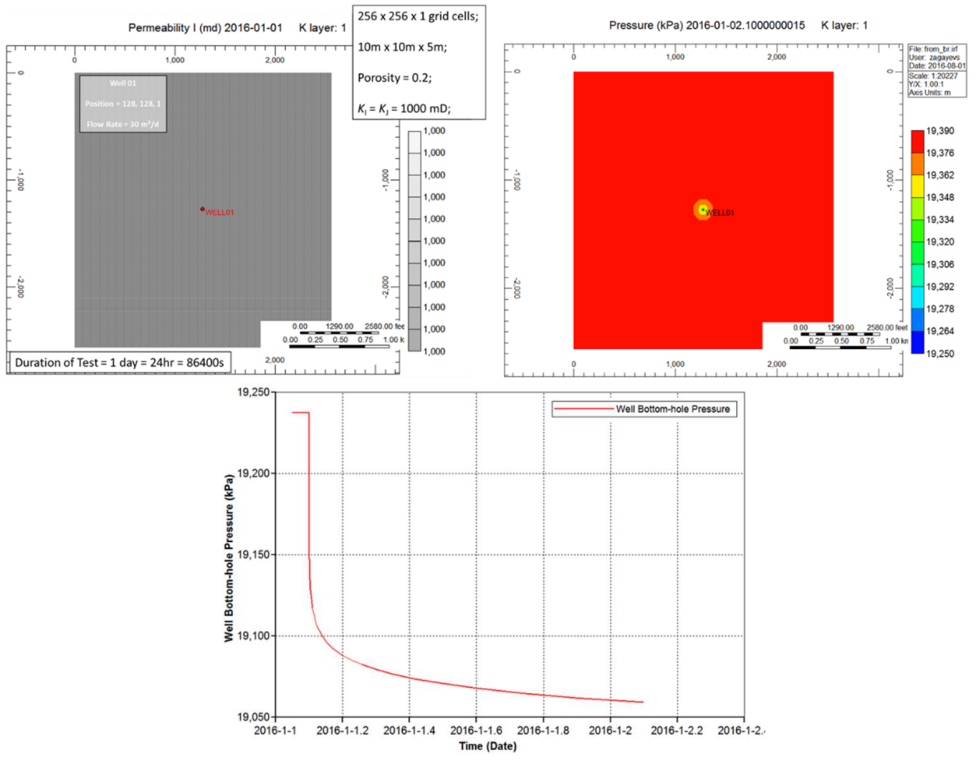

Figure A.6: Deterministic example considering a 1000mD permeability field and the resultant pressure map after 24 hours of a drawdown test. The variation of BHP through the time is shown on bottom.

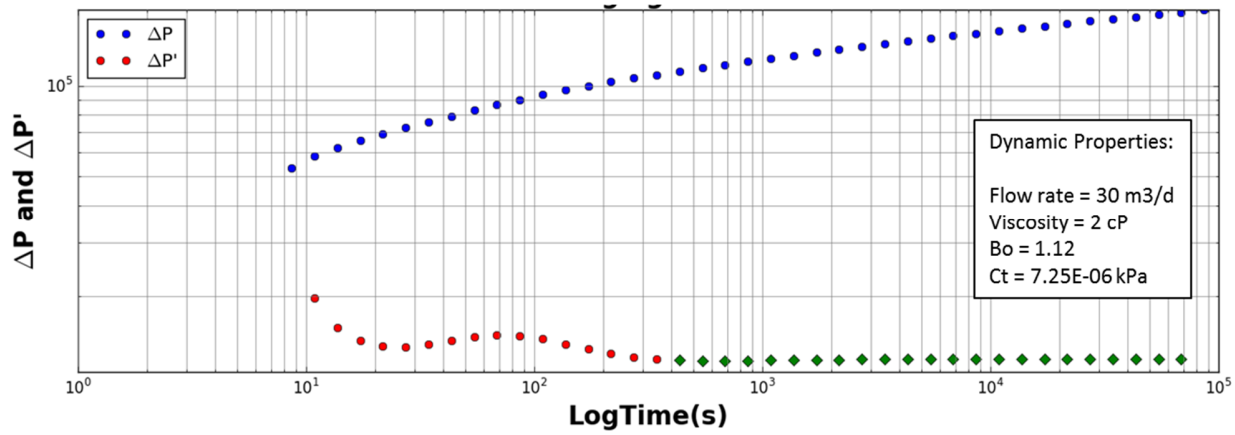

Figure A.7: Diagnostic plot from the deterministic example. Delta pressure is shown in blue dots and its derivative is shown in red dots. Green dots correspond to the infinite-acting radial flow.

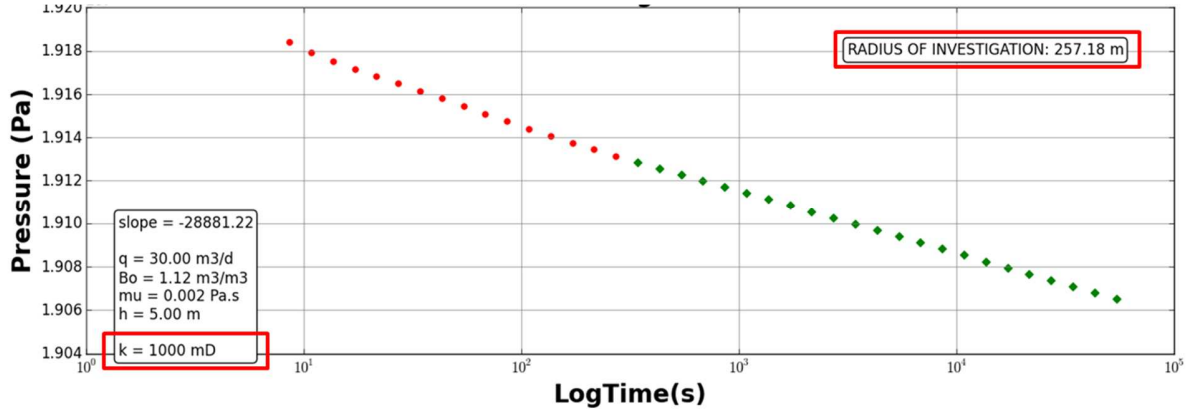

Figure A.8: Semi-log plot used to compute the average permeability and the drainage area detected by the drawdown well test. Green dots correspond to the infinite-acting radial flow.

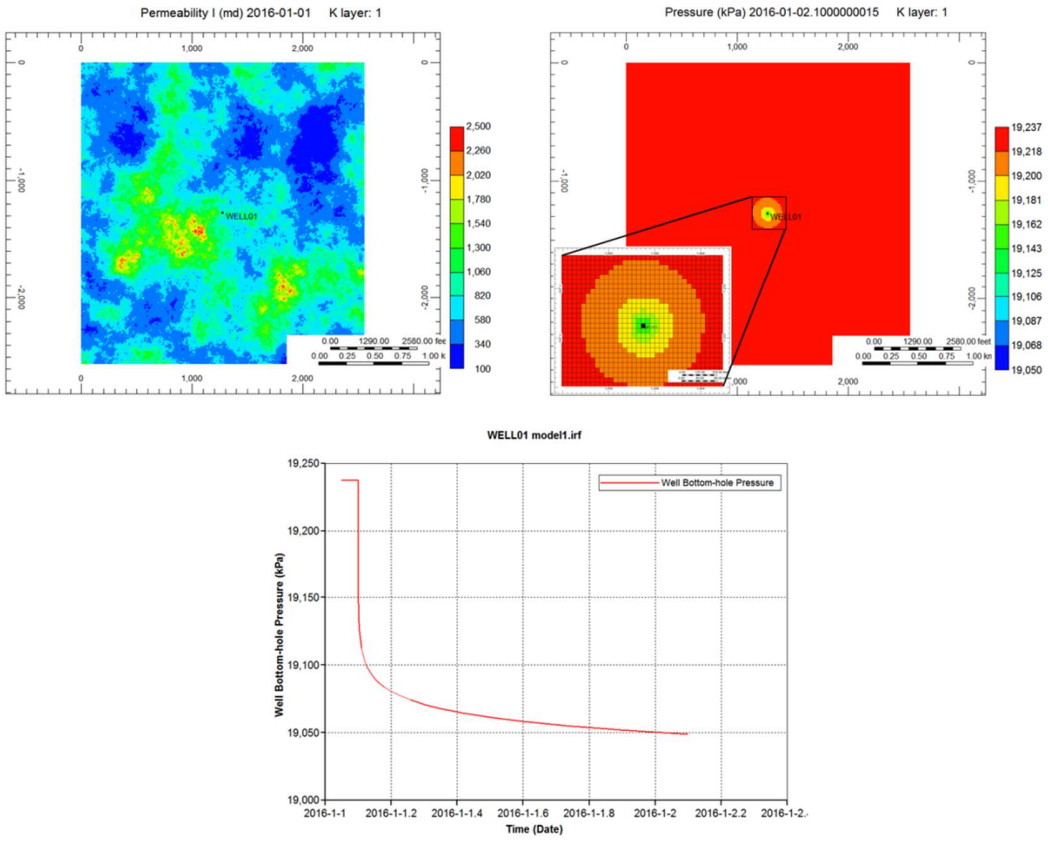

Figure A.9: Stochastic example considers 100 realizations of permeability map. Figure shows one realization and the resultant pressure map after 24 hours of a drawdown test. The well bottom-hole pressure is shown on bottom.

According to the Figures A.7 and A.8, the K_{avg} calculated from WTA is consistent with the model permeability (1000mD) and r_i corresponds to 257m.

In the second example, the drawdown test is performed for each of the 100 permeability realizations (Figures A.9 and A.10).

The K_{avg} and the respective r_i are calculated for each realization using Equations A.1 and A.2. Figure A.11 compares K_{avg} from WTA and the average permeability calculated from realizations.

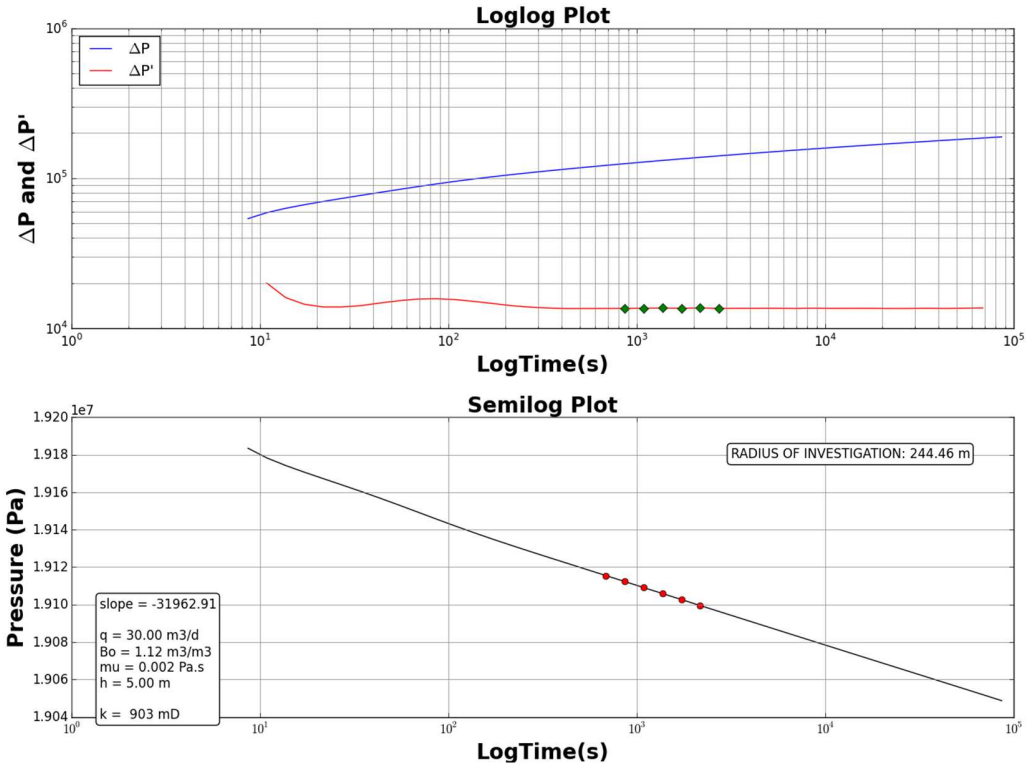

Figure A.10: Diagnostic plot from the one realization of stochastic example. Delta pressure is shown in blue line and its derivative is shown in red line. Green dots correspond to the infinite-acting radial flow (on top). Semi-log plot used to compute the average permeability and the drainage area in that realization (on bottom).

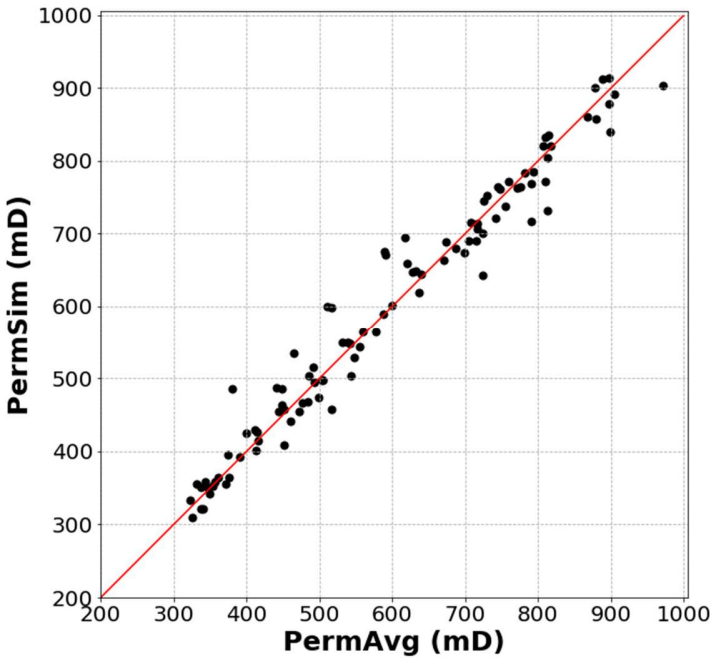

Figure A.11: Crossplot between permeability from well test (PermAvg) and permeability calculated directly from simulated data (PermSim).

Appendix B

Uncertainty Visualization Software: uncert_viz

This program assists geostatisticians and other users with uncertainty visualization. The program shows the sequence of random or ordered realizations. For this last option, it is calculated some intermediate images in order to perform the morphing process, according to the number of previous defined intervals. Finally, it is possible show the sequence of images on screen or save an animation. The code has been developed in Python as following:

Load Parameter File

```
filepar = 'uncertvis.par'
file, vartype, window, interv, show, order, min, max, incr = read_par(filepar)
filemovie = str(file[:len(file)-4])+'.mp4'
```

Load Datafile

```
params = lc.getline(file, 2)
temp = params.split()
NX = int(temp[1])
NY = int(temp[2])
nreal = int(temp[10])
data1 = np.loadtxt(file,skiprows=3,unpack=True)
data = np.empty((nreal,NX*NY))
for j in range(nreal):
    for i in range(NX*NY):
        data[j,i] = data1[i+j*(NX*NY)]
data_flt = []
```

Window Moving Filter

```
for i in range(nreal):
    if window != 1:
        data_flt.append(ndimage.median_filter(np.reshape(np.array(data[i]),\
((NY,NX))),window))
    else:
        data_flt = data
```

Calculating Distances

```
dist_mat = distance(nreal,data_flt
```

Calculating Simulated Annealing

```
city1 = run_SA(dist_mat)
ordem1 = city1          #ordering from SA
ordem0 = range(nreal)   #random ordering
```

Defining Ordering

WITH ORDERING

```
diff = []
for i in range(nreal-1):
    diff.append(data[ordem1[i]] - data[ordem1[i+1]])
diff.append(data[ordem1[nreal-1]] - data[ordem1[0]])
dif_rows = nreal*interv
difext = []
for k in range(nreal):
    for i in range(interv):
            difext.append(data[ordem1[k]] - i * (diff[k]/interv))
deltaext = np.array(difext)
```

WITHOUT ORDERING

```
ord_orig = []
for j in range(interv):
    for i in ordem0:
        ord_orig.append(i)
```

Defining Colormap

```
if max <= min:
    min  = deltaext.min()
    max  = deltaext.max()
    incr = (max - min) / 5.0

crg = max - min
num_incr = int(crg / incr)

# number of categories
ncat = int(max - min) + 1

leg = []
for i in range(ncat):
    leg.append(int(min+i))

legend = []
for i in range(num_incr + 1):
    legend.append(round((min + i * incr),2))
```

Recording Animation / Saving Figures

```
fig = plt.figure()
ax1 = fig.add_subplot(1,1,1)
axins1 = inset_axes(ax1,width = '3%',
                        height = '100%',
                        loc = 3,
                        bbox_to_anchor = (1.05,0.,1,1),
                        bbox_transform = ax1.transAxes,
                        borderpad = 0.1,)
```

```
cmap = colors.ListedColormap(['red','yellow','orange','blue'])
img=[]
for i in range(dif_rows):
    if order==1:
        im = np.reshape(np.array(deltaext[i]),((NY,NX)))
    else:
        im = np.reshape(np.array(data[ord_orig[i]]),((NY,NX)))
    if vartype==0:
        IMG=ax1.imshow(im,extent=[0,NX,NY,0],interpolation='none',cmap='jet',vmin=min,\
            vmax=max)
    else:
        IMG=ax1.imshow(im,extent=[0,NX,NY,0],interpolation='none',cmap=cmap,vmin=min,\
            vmax=max)
    img.append([IMG])
    if vartype==0:
        plt.colorbar(IMG,cax=axins1,ticks = legend,)
    else:
        plt.colorbar(IMG,cax=axins1,ticks = leg,)
    ax1.set_xlim(0,NX)
    ax1.set_ylim(0,NY)
    ax1.set_aspect('auto')
    ax1.set_title('UNCERTAINTY VISUALIZATION',fontsize=20,fontweight='bold')
if order==0:
    frame_rate = float(400/interv)
else:
    frame_rate = 150
img_ani = animation.ArtistAnimation(fig,img,interval=frame_rate,blit=True)
if show == 1:
    img_ani.save(filemovie, dpi=200)
else:
    plt.show()
```

Functions

Import libraries:

```
import numpy as np
import linecache as lc
import matplotlib.pyplot as plt
from numpy.random import rand
import matplotlib.animation as animation
from mpl_toolkits.axes_grid1.inset_locator import inset_axes
from scipy import ndimage
from matplotlib import colors
```

Read Parameters:

```
def read_par(file):
    par_file   = lc.getline(file,5).split()[0]
    par_vartype     = int(lc.getline(file,6).split()[0])
    if par_vartype==0:
        par_window = int(lc.getline(file,7).split()[0])
    else: par_window = 1
    par_interv = int(lc.getline(file,8).split()[0])
    par_show   = int(lc.getline(file,9).split()[0])
    par_order  = int(lc.getline(file,10).split()[0])
    par_min    = float(lc.getline(file,11).split()[0])
```

```
    par_max    = float(lc.getline(file,11).split()[1])
    par_incr   = float(lc.getline(file,11).split()[2])
    if par_vartype==1:
        par_min    = int(par_min)
        par_max    = int(par_max)
        par_incr   = int(par_incr)
    return par_file, par_vartype, par_window, par_interv, \
                par_show, par_order, par_min, par_max, par_incr
```

Distance Function

```
 def distance(nreal,data):
    data1 = np.reshape(np.array(data),((nreal,NX*NY)))
    cell = int(data1.shape[1])
    dist = np.ones((nreal,nreal))
    for i in range(nreal):
        for k in range(nreal):
            if i == k:
                dist[i,k] = 0.0
            elif i < k:
                dif = 0.0
                for j in range(0,cell,window):
                    dif = dif + ((data1[i,j] - data1[k,j]) * (data1[i,j] - data1[k,j]))
                dist[i,k] = np.sqrt(dif)
                dist[k,i] = dist[i,k]
            else:
                continue
    return dist
```

Simulated Annealing

```
def TotalDistance(city, matdist):
    dist=0
    for i in range(len(city)-1):
        dist += matdist[i,i+1]
    dist += matdist[-1,0]
    return dist


def reverse(city, n):
    nct = len(city)
    nn = int((1+ ((n[1]-n[0]) % nct))/2)
    for j in range(nn):
        k = (n[0]+j) % nct
        l = (n[1]-j) % nct
        (city[k],city[l]) = (city[l],city[k])


def transpt(city, n):
    nct = len(city)
    newcity=[]
    # Segment in the range n[0]...n[1]
    for j in range( (n[1]-n[0])%nct + 1):
        newcity.append(city[ (j+n[0])%nct ])
    # is followed by segment n[5]...n[2]
    for j in range( (n[2]-n[5])%nct + 1):
        newcity.append(city[ (j+n[5])%nct ])
    # is followed by segment n[3]...n[4]
    for j in range( (n[4]-n[3])%nct + 1):
        newcity.append(city[ (j+n[3])%nct ])
```

```
    return newcity

def run_SA(matdist):
    ncity = nreal          # Number of cities to visit
    maxTsteps = 100        # Temperature is lowered not more than maxTsteps
    Tstart = 0.2           # Starting temperature - has to be high enough
    fCool = 0.01           # Factor to multiply temperature at each cooling step
    maxSteps = 25*ncity    # Number of steps at constant temperature
    maxAccepted = 10*ncity# Number of accepted steps at constant temperature
    Preverse = 0.5         # How often to choose reverse/transpose trial move
    ndim = 2               # number of dimensions to calculate the distances-2D,3D,etc.
    # The index table -- the order the cities are visited.
    city = range(nreal)    # Distance of the travel at the beginning
    dist = TotalDistance(city, matdist)  # Stores points of a move
    n = np.zeros(6, dtype=int)
    nct = ncity # number of cities
    T = Tstart # temperature
    for t in range(maxTsteps):  # Over temperature
        accepted = 0
        for i in range(maxSteps): # At each temperature, many Monte Carlo steps
            while True: # Will find two random cities sufficiently close by
                # Two cities n[0] and n[1] are chosen at random
                n[0] = int((nct)*rand())     # select one city
                n[1] = int((nct-1)*rand())   # select another city, but not the same
                if (n[1] >= n[0]): n[1] += 1
                if (n[1]<n[0]):(n[0],n[1])=(n[1],n[0])
                nn = (n[0]+nct -n[1]-1) % nct
                if nn>=3: break
            n[2] = (n[0]-1) % nct
            n[3] = (n[1]+1) % nct
            if Preverse > rand():
                de = matdist[city[n[2]],city[n[1]]] + matdist[city[n[3]],\
                    city[n[0]]] - matdist[city[n[2]],city[n[0]]] - matdist[city[n[3]],\
                    city[n[1]]]
                if de<0 or np.exp(-de/T)>rand():
                    accepted += 1
                    dist += de
                    reverse(city, n)
            else:
                # Here we transpose a segment
                nc = (n[1]+1+ int(rand()*(nn-1)))%nct
                n[4] = nc
                n[5] = (nc+1) % nct
                # Cost to transpose a segment
                de = -matdist[city[n[1]],city[n[3]]] - matdist[city[n[0]],\
                        city[n[2]]] - matdist[city[n[4]],city[n[5]]]
                de += matdist[city[n[0]],city[n[4]]] + matdist[city[n[1]],\
                        city[n[5]]] + matdist[city[n[2]],city[n[3]]]
                if de<0 or np.exp(-de/T)>rand():
                    accepted += 1
                    dist += de
                    city = transpt(city, n)
            if accepted > maxAccepted: break
        T *= fCool   # The system is cooled down
        if accepted == 0: break
    return city
```